

Nearby Supernova Rates from the Lick Observatory Supernova Search. III. The Rate-Size Relation, and the Rates as a Function of Galaxy Hubble Type and Colour

Weidong Li^{1*}, Ryan Chornock^{1,2}, Jesse Leaman^{1,3}, Alexei V. Filippenko¹, Dovi Poznanski^{1,4,5}, Xiaofeng Wang^{1,6,7}, Mohan Ganeshalingam¹, and Filippo Mannucci⁸

¹Department of Astronomy, University of California, Berkeley, CA 94720-3411, USA

²Harvard-Smithsonian Center for Astrophysics, 60 Garden Street, Cambridge, MA 02138, USA

³NASA Ames Research Center, Mountain View, CA 94043, USA

⁴Computational Cosmology Center, Lawrence Berkeley National Laboratory, 1 Cyclotron Road, Berkeley, CA 94720, USA

⁵Einstein Fellow

⁶Department of Physics, Texas A&M University, College Station, TX 77843-4242, USA

⁷Physics Department and Tsinghua Center for Astrophysics (THCA), Tsinghua University, Beijing, 100084, China

⁸INAF – Osservatorio Astrofisico di Arcetri, Largo E. Fermi 5, I-50125, Firenze, Italy

8 December 2010

ABSTRACT

This is the third paper of a series in which we present new measurements of the observed rates of supernovae (SNe) in the local Universe, determined from the Lick Observatory Supernova Search (LOSS). We have considered a sample of ~ 1000 SNe and used an optimal subsample of 726 SNe (274 SNe Ia, 116 SNe IbC, and 324 SNe II) to determine our rates. We study the trend of the rates as a function of a few quantities available for our galaxy sample, such as luminosity in the B and K bands, stellar mass, and morphological class. We discuss different choices (SN samples, input SN luminosity functions, inclination correction factors) and their effect on the rates and their uncertainties. A comparison between our SN rates and the published measurements shows that they are consistent with each other to within the uncertainties when the rate calculations are done in the same manner. Nevertheless, our data demonstrate that the rates cannot be adequately described by a single parameter using either galaxy Hubble types or $B - K$ colours. A secondary parameter in galaxy “size,” expressed by luminosity or stellar mass, is needed to adequately describe the rates in the rate-size relation: the galaxies of smaller sizes have higher SN rates per unit mass or per unit luminosity. The trends of the SN rates in galaxies of different Hubble types and colours are discussed. We examine possible causes for the rate-size relation. Physically, such a relation for the core-collapse SNe is probably linked to the correlation between the specific star-formation rate and the galaxy sizes, but it is not clear whether the same link can be established for SNe Ia. We discuss the two-component (“tardy” and “prompt”) model for SN Ia rates, and find that the SN Ia rates in young stellar populations might have a strong correlation with the core-collapse SN rates. We derive volumetric rates for the different SN types (e.g., for SNe Ia, a rate of $(0.301 \pm 0.062) \times 10^{-4}$ SN Mpc $^{-3}$ yr $^{-1}$ at redshift 0) and compare them to the measurements at different redshifts. Finally, we estimate the SN rate for the Milky Way Galaxy to be 2.84 ± 0.60 SNe per century (with a systematic uncertainty of a factor of ~ 2), consistent with published SN rates based on several different techniques.

Key words: supernovae: general — supernovae: rates

1 INTRODUCTION

The Lick Observatory Supernova Search (LOSS; Li et al. 2000; Filippenko et al. 2001; Filippenko et al. 2011) has been

* Email: wli@astro.berkeley.edu

the most successful nearby supernova search engine in the past 12 years. During the period from March 1998 through the end of 2008 (on which the data from this study are based), LOSS found 732 SNe, easily exceeding any other searches for nearby SNe and accounting for more than 40% of all SNe with redshift $z < 0.05$ reported to the Central Bureau for Astronomical Telegrams. It found an even larger fraction of the reported young SNe, discovered close to or before maximum brightness. One major goal of LOSS is to improve our understanding of the statistics of SNe — in particular, the SN rates in galaxies of different types and colours. Here, in Paper III of this series on LOSS SN rates in the local Universe, the goal is to put all of the ingredients together to derive the SN rates.

In this section, we first summarise what we have learned from Paper I (Leaman et al. 2011) and Paper II (Li et al. 2011) *that is relevant to the rate calculations*, and then discuss the details of the control-time and rate calculations. The rest of the paper is organised as follows. Section 2 discusses an observed correlation between the normalised SN rates and the host-galaxy sizes¹ (the “rate-size relation”), while §3 reports the SN rates for a fiducial galaxy size. Section 4 discusses comparisons with the published SN rates, the possible causes of the rate-size relation, the two-component model for SN Ia rates, and the volumetric rates; it also provides an estimate of the SN rate in the Milky Way Galaxy. Our conclusions and possible future improvements are summarised in §5. In the Appendix, we offer additional discussion of the rate-size relation, including its discovery and an alternative description using the rate-colour relation. We adopt a Hubble constant of $H_0 = 73 \text{ km s}^{-1} \text{ Mpc}^{-1}$ (Spergel et al. 2007) in our study, consistent with the recent direct determination based on Cepheid variables and SNe Ia by Riess et al. (2009).

1.1 Summary of Papers I and II

Paper I of this series discusses the construction of the galaxy and SN samples. Two galaxy samples are heavily used here, in Paper III: the “full” sample with a total of 14,882 galaxies, and the “optimal” sample with a total of 10,121 galaxies. The “optimal” sample excludes all of the small (major axis $< 1'$) E and S0 galaxies, as well as highly inclined ($i > 75^\circ$) spirals, in the “full” sample to avoid the uncertainties in the detection efficiencies and inclination correction factors (see Paper I for details). Four SN subsamples (out of the 7 discussed in Paper I) are used throughout this paper,

- (i) The “full” SN sample with a total of 929 SNe, which include all of the SNe that occurred in the “full” galaxy sample.
- (ii) The “full-optimal” SN sample with a total of 726 SNe, which are all of the SNe that occurred in the “optimal” galaxy sample.

¹ Hereafter, “the galaxy size” refers to the magnitude of both the luminosity and stellar mass, unless otherwise specified, because the mass is directly calculated from the luminosity, with a small dependence on $B - K$ colour (Paper I; Mannucci et al. 2005).

(iii) The “season” SN sample with a total of 656 SNe, which include all of the SNe discovered “in season”² and that occurred in the “full” galaxy sample.

(iv) The “season-optimal” sample with a total of 499 SNe, which are all of the SNe discovered “in season” and that occurred in the “optimal” galaxy sample.

Paper I also shows that for each individual epoch of imaging in our database, the limiting magnitude can be calculated from several parameters (flux ratio, seeing conditions, and sky background) recorded in the log files, to a precision of 0.2–0.3 mag. The detection efficiency (DE) for SNe with different significance is also determined through Monte Carlo simulations, and reaches a limit of about 90% because some of the SNe are missed near the centres of galaxies.

Paper II discusses the construction of a complete SN sample. A total of 175 SNe are selected from the “season” SN sample with a cutoff distance of 80 Mpc for SNe Ia and 60 Mpc for SNe Ibc and II. Photometry is collected for every SN to derive the light-curve shape and peak absolute magnitude, and the incompleteness of each SN is studied and corrected.³ The peak absolute magnitudes are corrected only for the Galactic extinction in the direction of each SN. Because of this, we do not need to consider the host-galaxy extinction (which is poorly known) toward each SN, as it is naturally included in these “pseudo-observed” luminosity functions (LFs). The LFs also show significant dependence on the host-galaxy Hubble types. To alleviate the effect of small-number statistics, the LFs are constructed in two broad Hubble-type bins: E–Sa and Sb–Irr for SNe Ia, and S0–Sbc and Sc–Irr for SNe Ibc and II.

We note that for the control-time calculations, it is important to match the different SN subsamples with the proper subsets of SNe in the LFs, as long as there is a sufficient number of objects in the LFs. As discussed in Paper II, the LFs do not change significantly regardless of whether the SNe discovered in small (major axis $< 1'$) early-type (E/S0) galaxies are considered, so the “full,” “full-nosmall,” “season,” and “season-nosmall” SN samples can use the full set of SNe in the LFs. On the other hand, the “full-optimal” and “season-optimal” SN samples exclude all of the SNe that occurred in highly inclined spiral galaxies, so the rate calculations for these samples should compute the control times using the subset of SNe in the LFs that are not in highly inclined spiral galaxies as well. Fortunately, only 40 out of the 175 SNe (23%) in the full LF sample occurred in highly inclined spiral galaxies, leaving a reasonable number of SNe in the LFs when they are excluded.

² An “in-season” SN is one that explodes during the active monitoring period of its host galaxy. The active monitoring period refers to the time when the galaxy emerges from being too close to the Sun in the sky to the time when it once again becomes unobservable, a period during which the galaxy is actively monitored in our survey with a short observation interval. In other words, a SN discovered in the first image of a galaxy after a long break when the galaxy was too close to the Sun was not counted as an “in-season SN.” See Paper I for further discussion.

³ The completeness of a SN is defined as the ratio between the total control time for the SN and the total season time. In other words, for a SN that in our survey has 100% completeness, we should have discovered all such SNe during our monitoring period.

1.2 The Control-Time Calculation

Section 3 and the Appendix of Paper I provide the mathematical details of the control-time method. Here we provide the numerical details regarding how the control-time calculation is performed.

As discussed in Paper II, each SN in the LF sample is a discrete point, with its own light-curve shape and peak absolute magnitude, and a fractional contribution proportional to the completeness correction factor. We first calculate the control time for a single SN from the LF. The uncertainty of the peak absolute magnitude is used to generate a random correction (according to Gaussian statistics). This correction, together with the Galactic extinction toward a specific galaxy in a galaxy sample, is applied to the peak absolute magnitude of the SN. The light curve with the derived peak absolute magnitude is then converted to the apparent light curve according to the distance of the galaxy.

For a single image recorded in the log files of this galaxy, the limiting magnitude is calculated from the parameters in the log files, as detailed in Paper I. The difference between the apparent light curve and the limiting magnitude is then converted to a control-time curve using the DE curves for the Hubble type of the galaxy, as reported in Paper I. This process is demonstrated in Figure 1; SN 2002fk is used as an example, in a galaxy with a distance of 100 Mpc and an extinction of $A_V(\text{Galactic}) = 0$ mag. The apparent light curve is shown in the upper panel, with the limiting mag also marked (assumed to be 19; dashed line). The middle panel shows the DE curve (as derived in Paper I) for the Sb–Sbc bin, the Hubble type we assume for the galaxy. The offset between the apparent light curve and the limiting magnitude can then be converted to the control-time curve shown in the lower panel. Depending on the apparent light-curve shape and the offset between the peak and the limiting magnitudes, the control-time curve can have different shapes, but generally has a rising, a constant, and a declining portion, and is different from a step function (i.e., 0 when the SN is fainter than the limiting magnitude, and 1 when it is brighter). The total integration for the curve marks the maximum possible contribution to the control time from this single epoch.

Next, the total control time for all of the epochs of images for this galaxy is computed. As each epoch can have different control-time curves, it is difficult to compute the total control time analytically. Instead, the problem is solved numerically. We use a large array with each cell corresponding to a single day in the survey period. The maximum allowable control time for each day is the limit of the DE at the bright end plus a random correction according to the uncertainty of the DE. For any given epoch of image, the control-time curve is calculated, and is allowed to shift along the time axis to compute the total contribution to the control time at or before the epoch (as the image cannot “control” any SNe that occurred after the observation). The shift that gives the maximum contribution is then used. Our control-time algorithm follows the simple philosophy of maximizing the contribution to the control time from any given epoch, which is the principle of the control-time method.

We also note that because of the small observation intervals in our survey, the contribution to the total control time from each epoch is typically the DE multiplied by the

observation interval; in other words, the constant portion of the control-time curve is used most of the time. Consequently, our rates are relatively insensitive to the input SN LF (see more discussion in §3.2), especially for SNe Ia which are very luminous.

Following the same procedure, the control time is calculated for the SN for all of the galaxies in the galaxy sample, and then for all of the SNe in the LF sample. For each galaxy, the total control time for each SN type (Ia, Ibc, and II) is then calculated according to Equation (A11) of Paper I — that is, the sum of the control time of each SN component weighted by its fractional contribution to the luminosity function.

The adopted light-curve shapes are important for the control-time calculation, so in Figure 2 we compare our light curves as constructed in Paper II with those used by Cappellaro et al. (1999; hereafter, C99). The differences between the two sets of light curves are significant, with the C99 light curves in general evolving faster than our light curves. This is not surprising, since the C99 light curves are in the B band while ours are in the R band.

1.3 The Rate Calculation

The total control time calculated for the galaxy sample can be normalised by a chosen factor to generate the total normalised control time, which is then used to calculate the rate, as described by Equations (A3) and (A4) of Paper I. The normalisation factors we choose to use are the B -band luminosity (L_B), the K -band luminosity (L_K), and the stellar mass. The resulting rates are labeled SNuB, SNuK, and SNuM, which have units of one SN per 100 yr per $10^{10} L_\odot(B)$, $10^{10} L_\odot(K)$, and $10^{10} M_\odot$, respectively.

However, before we proceed with the rate calculations, we need to discuss a strong observed correlation between the SN rates and the sizes of the host galaxies, which fundamentally changes the way our SN rates are determined. The details are described in the next section.

2 THE RATE-SIZE RELATION

In this section, to compute the SN rates we use the “full-optimal” SN sample with 726 objects that occurred in the “optimal” galaxy sample. As discussed later in the paper, we also adopt this combination of the SN and galaxy samples for the final rate calculations.

An important step in the rate calculations is to find an ideal method to divide the galaxies into different groups so that galaxies within each group have the same rate. As the specific star-formation rate (SSFR, the star-formation rate per unit mass) is often considered to be intimately connected to the (mass-normalised) SN rates, especially for core-collapse supernovae (CC SNe), a galaxy sequence that also represents a SSFR sequence could be used to describe the SN rates. Historically, the SN rates have been published in galaxies of different Hubble types or $B - K$ colour. The underlying assumption is that the galaxy Hubble type or $B - K$ colour is a good proxy for SSFR, and the SN rate is a constant in galaxies having the same Hubble type or $B - K$ colour.

In the process of checking the robustness of our rate-calculation pipeline, however, we found that the SN rates cannot be adequately described by a single parameter, either the galaxy Hubble type or galaxy $B-K$ colour (see §A of the Appendix for more details). Instead, a secondary parameter of galaxy size, expressed in either luminosity (in the B or K bands) or stellar mass, is needed to quantify the rates. One would normally expect the SN rates to be constant for galaxies of different sizes, since the rates have been *linearly* normalised by the galaxy size as indicated by Equations (A3) and (A4) in Paper I. But in fact, below we show that there is a strong correlation between SN rates and galaxy sizes, for the rates in galaxies of different Hubble types (§2.1) or $B-K$ colours (§2.2).

2.1 The Rate-Size Relation for the Hubble-Type Rates

We first consider whether there is a correlation between galaxy sizes and CC SN rates in galaxies of different Hubble types. The results for the SNuM rates are shown in Figure 3. Only galaxy Hubble types 3–7 (Sab–Scd) are considered because of the small number of CC SNe discoveries in E, S0, and Irr galaxies. For each Hubble type, the galaxies are sorted in order of their masses, and then divided into several bins from the least massive to the most massive, with roughly the same number of discovered SNe in each bin because small-number statistics are often the dominant source of uncertainty. The SN Ibc and SN II rates are then calculated for each mass bin. Only the statistical errors are considered here.

For the SN II rates (Figure 3, top panel), we find that *there is a strong correlation between SNuM and galaxy mass, with smaller galaxies having a higher SNuM*. A χ^2 -minimizing technique is used to fit a power law of $\text{SNuM} \propto M^{-0.55}$ (solid line, the final adopted relation in our calculations), using the rates in the Sbc galaxy bins as the anchor points and scaling the rates in the other Hubble types by a multiplicative constant (with proper error propagation). The reduced χ^2 (i.e., χ^2/DOF [degree of freedom]) of the fit is ~ 0.7 , suggesting a good fit to the data.

For the SN Ibc rates (Figure 3, bottom panel), there is more scatter due to small-number statistics, but they can be well fit ($\chi^2/\text{DOF} \approx 1.0$) by the same relation as determined for the SN II rates after scaling the rates in each Hubble type. The power-law indexes between the rates and masses, which we call the rate-size slopes (RSSs) hereafter, are also measured for the SN II rates in each Hubble-type bin and are listed in the third column of Table 1. The RSSs in different Hubble types have individual statistical significances of 3– 5σ and are consistent with each other. The significance of the RSS after combining the rates in Sab–Scd galaxies (i.e., the linear fit in the top panel of Figure 3) is $\sim 10.7\sigma$.

The results for the SNuM rates of SNe Ia are shown in Figure 4 and the RSSs are listed in the second column of Table 1. Here the rates in the Sb galaxies are used as the anchor points, and the power-law index of -0.50 as plotted is the final adopted value in our rate calculations. The reduced χ^2 of the fit is ~ 0.6 , suggesting a good fit to the data. The RSSs in different Hubble-type bins are significant at the 2– 3σ level and are generally consistent with each other. The combined significance (i.e., the linear fit in Figure 4) is

$\sim 7.4\sigma$. More discussion of the RSSs and their significance can be found in §4.2.

We investigate the dependence of the RSSs on the normalisation (L_B , L_K , or mass), different SN types (Ia, Ibc, and II), various Hubble types, and distinct SN samples. The RSSs have a relatively strong dependence on the normalisation, increasing from SNuB to SNuK to SNuM. The RSSs for the two types of CC SNe are generally consistent with each other and are thus not discriminated from each other hereafter. There are some differences (with low significance due to uncertainties) between the RSSs for SNe Ia and those for CC SNe. Different SN samples yield consistent RSSs for the same SN type and normalisation. For each type of SN, no significant difference is found in the RSSs in various galaxy Hubble types, though the uncertainties for some RSSs are relatively large (e.g., as shown in Table 1).

The power-law correlation between the SN rate and the sizes of the galaxies is called the *rate-size relation* hereafter. The rate-size relation can be explicitly expressed as

$$\text{SNuB}(L_B) = \text{SNuB}(L_{B0}) \left(\frac{L_B}{L_{B0}} \right)^{\text{RSS}_B}, \quad (1)$$

$$\text{SNuK}(L_K) = \text{SNuK}(L_{K0}) \left(\frac{L_K}{L_{K0}} \right)^{\text{RSS}_K}, \text{ and} \quad (2)$$

$$\text{SNuM}(M) = \text{SNuM}(M_0) \left(\frac{M}{M_0} \right)^{\text{RSS}_M}, \quad (3)$$

where L_{B0} , L_{K0} , and M_0 are the fiducial galaxy sizes, and RSS_B , RSS_K , and RSS_M are the rate-size slopes for the different normalisations.

2.2 The Rate-Size Relation for the $B-K$ Colour Rates

Historically, SN rates have also been parameterised by the $B-K$ colours of the host galaxies (e.g., Mannucci et al. 2005; hereafter M05). Unlike the galaxy Hubble types, which are discrete points in parameter space, the galaxy $B-K$ colours span a wide range and follow a continuous distribution, so it is impractical to group the galaxies in *constant* $B-K$ colours and then study the SN rates in different galaxy sizes.

We adopt the following procedure to investigate whether there is a rate-size relation (i.e., Eqs. 1–3) in the $B-K$ SN rates. The SNuK rates of SNe II are used as an example (Figure 5; the SNuB and SNuM rates of SNe II, and the SN Ia rates, all show a similar relation). As illustrated in the top-left panel, the galaxies are first sorted according to their $B-K$ colours, and then divided into four colour groups from the bluest to the reddest (the same symbol, left to right). For each colour group, the galaxies are subsequently sorted by L_K , and divided into seven L_K bins (the different symbols). For clarity, only three size bins are shown: the smallest (size bin 1, open circles), the intermediate (size bin 4, half-solid circles), and the largest (size bin 7, solid circles). Next, for each bin the SNuK rate, the average $B-K$ colour, and the average L_K are calculated and plotted. The size of the symbol is proportional to the logarithm of the average L_K . The dashed line is the average rate for the different $B-K$ groups (i.e., all galaxies are used in the rate calculations without considering the differences in L_K). A systematic trend is observed in this panel: the rates for the bins with the intermediate L_K (half-solid circles)

closely follow the average rates (dashed line), while the bins with the smallest L_K (open circles) are higher, and the bins with the largest L_K (solid circles) are lower than the average rates. This trend becomes more obvious after the rates are normalised by the average curve (the bottom-left panel).

At face value, this trend suggests that there is a rate-size relation for the $B - K$ SN rates. To further investigate this, we study the SNuK – L_K correlation in two narrow ranges of galaxy $B - K$ colours. As can be seen in the bottom-left panel of Figure 5, there are only minimal colour changes in the different L_K bins for the groups of galaxies at $B - K \approx 2.9$ and 3.3 mag. Thus, for each of these two colour groups, any correlation between SNuK and L_K (i.e., the rate-size relation) is not significantly affected by the rate changes due to colour variation within the group. The results are shown in Figure 6, using the rates for the $B - K \approx 2.9$ mag galaxies as the anchor points and scaling the rates for the $B - K \approx 3.2$ mag galaxies. The linear fit has a power-law index of -0.38 , the final adopted RSS in our analysis. The existence of a rate-size relation is verified at $\sim 3.5\sigma$ using these two colour groups alone.

To quantify the RSSs for the rate-size relation for the $B - K$ SN rates, we use two numerical methods. The first employs a multi-variate linear regression model to fit the rates as a function of both galaxy $B - K$ colours and L_K , so that

$$\log(\text{SNuK}) = c_1 + c_2 \log\left(\frac{L_K}{L_{K0}}\right) + c_3(B-K) + c_4(B-K)^2, \quad (4)$$

where c_1 , c_2 , c_3 , and c_4 are the coefficients to be evaluated during the fitting process. It can be seen that $c_2 = \text{RSS}_K$ in this equation. Here we also assume that the logarithm of the rates for a fiducial galaxy can be adequately fit by a second-order polynomial function of $B - K$ colour, an assumption that is verified by the discussion in §3.6.

The second method employs a χ^2 -minimizing technique and is demonstrated by the right-hand panels in Figure 5. A wide range of RSS values is tested to convert the rates in all of the L_K bins as well as the average rates to a fiducial galaxy size using Equation (2), and the optimal RSS is the one that yields the minimum χ^2 when the rates in different L_K bins are compared to the average rates. As the right-hand panels of Figure 5 show, after the rate-size relation is considered and all of the rates are converted to the same fiducial galaxy size, the systematic trend presented in the left panels is gone, and the rates in different L_K bins are consistent with the average rates to within $\sim 1\sigma$.

The RSSs derived from these two methods are fully consistent with each other, so we average them as our adopted values. We derived the RSSs for the SN Ia and SN II rates, but not for the SN Ibc rates due to the relatively large uncertainties. Instead, we assume that the SN Ibc rates have the same RSSs as the SN II rates.⁴ Unlike the RSSs for the SN rates in galaxies of different Hubble types, which exhibit a significant dependence on the normalisations (L_B , L_K , or mass), the RSSs for the rates in galaxies of different $B - K$ colours are within a narrow range and consistent with each

other for the different normalisations (for the same SN type), so only two RSSs are needed.

Our final adopted RSSs, which are the averages for the different SN types and normalisations, are reported in Table 2. We adopt an uncertainty of 0.10 for most RSSs, roughly the value of adding the scatter of the RSSs from different SN samples and the uncertainty of an individual RSS measurement in quadrature. Somewhat larger errors of 0.20 and 0.15 are adopted for the SN Ia SNuB Hubble-type rates and all $B - K$ rates due to larger RSS measurement scatter or uncertainties.

2.3 The Effect of the Rate-Size Relation on the Rate Calculations

The existence of the rate-size relation has two implications. First, the SN rate before the normalisation by the sizes of the galaxies (i.e., the SN frequency, or number of SNe per year) is not linearly proportional to the galaxy size, but to a power law of size $^{(1+\text{RSS})}$, where size can be L_B , L_K , or mass. For example, for the B -band normalisation, the SN frequency for SNe II is proportional to $L_B^{0.73}$ instead of to $L_B^{1.00}$. Second, since the rate varies with galaxy size, we need to choose a fiducial galaxy size to compute the rate, so that the rates for the other galaxy sizes can be evaluated using the RSSs. As the exact value of the fiducial size is not of great importance, we use a value that is close to the average galaxy size in each normalisation for this purpose: $L_{B0} = 2 \times 10^{10} L_\odot$ for SNuB, $L_{K0} = 7 \times 10^{10} L_\odot$ for SNuK, and $M_0 = 4 \times 10^{10} M_\odot$ for SNuM. These values are listed in the last column of Table 2.

Using SNuM as an example, here we show how the rates are computed for a fiducial galaxy size. Let M_0 be the fiducial galaxy size. Then the rate-size relation can be written as

$$\text{SNuM}(M) = \frac{N(\text{SN})}{MC} = \text{SNuM}(M_0) \left(\frac{M}{M_0}\right)^{\text{RSS}_M}, \quad (5)$$

where C is the control time. This can be rewritten as

$$\text{SNuM}(M_0) = \frac{N(\text{SN})}{MC(M/M_0)^{\text{RSS}_M}}. \quad (6)$$

In other words, the rate for each galaxy can be effectively converted to the rate for the galaxy with the fiducial galaxy size (hereafter, the fiducial galaxy) when the control time C is scaled by a factor of $(M/M_0)^{\text{RSS}}$. This is the main modification to the rate calculations discussed in §3 of Paper I and in §1.3 here.

We note that a nonlinear proportionality between the SN frequency and the host-galaxy size has been reported for SN Ia rates in star-forming galaxies by Sullivan et al. (2006), although our results are somewhat different. More detailed discussion of this and the possible causes of the rate-size relation can be found in §4.2.

An alternative parameterisation of the SN rates using Hubble types and colour as the two independent variables is discussed in §B of the Appendix.

⁴ We tested this assumption by adopting the RSSs from the SN II rates in the SN Ibc rate calculations, and found that these RSSs adequately removed any rate-size relation in the SN Ibc rates.

3 THE SN RATE IN A FIDUCIAL GALAXY

3.1 The SN Rates in Different SN Samples

As discussed in Paper I and summarised in §1.1, there are several SN subsamples with different associated galaxy samples. One test to investigate the robustness of our rate-calculation pipeline is to compute the rates using different SN subsamples, and check for their consistency, as shown in Figure 7. Here SNuM for a fiducial galaxy is calculated for SNe Ia, Ibc, and II in different galaxy Hubble types. Only the statistical errors are shown. The solid circles are for the rates of the 929 SNe in the “full” sample, the triangles are for the 726 SNe in the “full-optimal” sample, the open squares are for the 656 SNe in the “season” sample, the solid squares are for the 499 SNe in the “season-optimal” sample, and the open circles are for the 583 SNe in the “full-optimal” sample but only using SNe discovered before the end of the year 2006. As discussed in §1.1, the full set of SNe in the LFs is used to calculate the control times for the galaxy samples for the “full” and “season” SN samples, while the LFs without the SNe occurring in highly inclined spiral galaxies are used for the galaxy samples for the “optimal” SN samples.

Inspection of Figure 7 reveals that the rates from different SN subsamples are consistent with each other to within 1σ . For each Hubble-type bin, we calculate the average and root-mean square (RMS) of the rates, and find that the RMS is about 6% of the average for SNe Ia, 12% for SNe Ibc, and 11% for SNe II. The rates using the SNe in the “full-optimal” sample before the end of the year 2006 are consistent with the rates using the whole “full-optimal” sample. This suggests that our rate-calculation pipeline is robust in terms of the cutoff period for the SN sample.

Our final rates use the 726 SNe in the “full-optimal” sample, which provides a good balance between improving small-number statistics and avoiding systematic biases. We emphasize, however, that using a different SN sample does not significantly affect our discussion in the subsequent sections of this paper. As the different SN samples are not independent of each other, a straight average or median of the rates is not the proper way to proceed.

3.2 The SN Rates with Different LFs

In this section, we investigate how our rates are affected by the choices of the input LFs for the SNe. Three sets of LFs are considered. The first set of LFs splits the LF SNe into two broad Hubble-type bins (hereafter 2LF), which is our choice for the final rate calculations. The second set of LFs combines all of the SNe into a single LF for each SN type (hereafter 1LF). The third set of LFs is actually not a LF at all, but a single light curve with a single peak absolute magnitude as adopted in the C99 rate calculations (hereafter C99-LF).⁵ As shown in Figure 2, the light curves adopted by the C99 study are quite different from those used in our rate calculations, and are only suitable for surveys done in the *B* band. Since our unfiltered survey is more closely matched to

⁵ The C99 rate calculation was performed with a Gaussian LF and *BVR* light curves depending on the specific search. Here only the *B*-band light curve and the average peak absolute magnitude are used.

the *R* band, the calculations using the C99-LF are not very meaningful except to demonstrate the effect of an extreme choice of the input LF.

The results are shown in Figure 8 for the “full-optimal” sample of SNe. For SNe Ia, the rates are remarkably stable with different input LFs, even when the extreme choice of the C99-LF is used. When all three rates are used to calculate the average for each Hubble-type bin, the RMS is about 7% of the average, similar to the scatter found in the previous section for the different SN samples. The reason the SN Ia rates are insensitive to the choice of the input LF is simple. Due to the depth of our SN survey, the short observational intervals, and the luminous nature of SNe Ia, our survey is largely volume-limited for SNe Ia, so the control time is close to the season time for any reasonable choice of the input LFs.

For the CC SNe, the rates are more sensitive to the choice of the input LFs. This is not unexpected, as the CC SNe already suffer some incompleteness within 60 Mpc, as discussed in Paper II. When the 2LF and 1LF rates are used to calculate the average for each Hubble-type bin, the RMS is about 16% of the average for SNe Ibc and 12% for SNe II. Compared to the 2LF rates of SNe Ibc, the 1LF rates are smaller in early-type spirals and bigger in late-type spirals, while it is the opposite for SNe II. This is consistent with the expectations from the LF study of the SNe Ibc and II in Paper II. The average luminosity of SNe Ibc in early-type spirals is fainter than that of SNe Ibc in late-type spirals. Consequently, using a separate LF for the SNe Ibc in the early-type spirals will enhance the rates in these galaxies. The same logic can be applied to the SNe Ibc in late-type spirals and the SNe II.

The C99-LF rates are dramatically different from the other rates for the SNe Ibc and II. These rates, though not very meaningful, do provide information on how our rates and the published C99 results compare when the same sets of light curves and peak absolute magnitudes are used. When the C99-LF is used, our rates are depressed for SNe Ibc (by $\sim 50\%$ and $\sim 20\%$ for the early-type and late-type spirals, respectively). This is because the C99 SN Ibc light curve has a peak absolute magnitude of -17.0 , brighter than more than 60% of the SNe in our SN Ibc LF. As a result, the control time is increased, yielding a lower rate. The SN II rates, on the other hand, are enhanced (by $\sim 60\%$ and $\sim 10\%$ for the early-type and late-type spirals, respectively). This is likely to be mainly caused by the differences in the adopted light-curve shapes. The C99 SN II light curves have a much narrower peak than ours, resulting in a smaller control time and a higher SN rate.

We note that the effect of the light-curve shape is dramatically reduced for the rates in the “season” and “season-optimal” SN samples, as these calculations do not include the control time for the first epoch of each season, which is often the only epoch when the control time from light-curve shape is needed [the other epochs mostly use DE \times (observation interval)]. Accordingly, the SN II rates in the “season” and “season-optimal” SN samples using the C99 light curves do not show a significant difference from those obtained with the 2LF and 1LF LFs.

3.3 The Inclination Correction Factor

The presence of a strong bias in the discovery of SNe in inclined *spiral* galaxies was first reported by Tammann (1974), and subsequently discussed by van den Bergh & Tammann (1991), Cappellaro et al. (1997, hereafter, C97), and C99. Historically, researchers have used an inclination correction factor (ICF), which is the ratio of the SN rate in a face-on galaxy to that in an inclined galaxy, to account for the bias. A significant ICF (on the order of 2–3) has been reported in searches conducted visually or with photographic plates (e.g., C97, C99).

Since our search is conducted with a red-sensitive CCD camera and our SNe are discovered via image subtraction to deal with the bright central regions of galaxies, the ICF is expected to be relatively small in our rates compared with previous studies. To verify this, we divide the “full-nosmall” SN sample into three inclination bins ($0^\circ - 40^\circ$, $40^\circ - 75^\circ$, $75^\circ - 90^\circ$), and calculate the respective rates (r_0 , r_1 , r_2) for different SN types and normalisations. We also divide the spiral galaxies into early-type (Sa–Sbc) and late-type (Sc–Scd) bins (as mentioned previously, the inclination angle is not meaningful for the elliptical or irregular galaxies). Since the goal is to address how our rates are affected by a possible ICF, we used the subset of SNe in the LFs that are not in highly inclined spiral galaxies, which are adopted in the final rate calculations, to calculate the control times. The results are listed in Table 3 and plotted in Figure 9. Only the statistical errors⁶ are considered here.

Inspection of Table 3 and Figure 9 reveals that there may be a sizable ICF in our rates. In particular, for the SN II rates in the late-type spirals, the ICFs between the face-on galaxies (r_0 ; $0^\circ - 40^\circ$) and the highly inclined galaxies (r_2 ; $75^\circ - 90^\circ$) are 3.2–4.7 (the column labeled as $r_0/r_2 - 1$), although their uncertainties are relatively large due to the rate uncertainties.

For our final rate calculations, we elect not to adopt an ICF. Instead, the highly inclined galaxies ($75^\circ - 90^\circ$) and the SNe that occurred in them are not considered. These rates are reported as $r_3(0\text{--}75)$ in Table 3, together with the ratios when compared to the rates in the face-on galaxies ($r_0/r_3 - 1$). We avoid using an ICF for two main reasons, as follows.

(1) The significance of the ICFs for the two bins with small and medium inclinations ($0^\circ - 40^\circ$ and $40^\circ - 75^\circ$) is low. As shown by $r_0/r_1 - 1$ in Table 3, the SN Ia and Ibc rates do not have a significant ICF for all of the normalisations. The SN II rates display differences in the two bins with a significance level of only $\sim 2\sigma$ for all normalisations.

(2) We fail to explain the presence of an ICF for the SN II rates, but not for the SN Ia and SN Ibc rates. Historically, the presence of an ICF is attributed to greater extinction toward the SNe in more highly inclined galaxies. Consequently, the SNe in inclined galaxies are, on average, dimmer than those in face-on galaxies. Using the average LF without considering the inclinations thus overestimates the control time for the inclined galaxies and underestimate the rates. However, as discussed in §5.2 of Paper II, when the LF SNe

are considered, only SNe Ibc are consistent with greater extinction in more highly inclined galaxies, with small-number statistics. Thus, an ICF for the SN II rates, if real, cannot be easily explained by greater extinction in more highly inclined galaxies.

As a further test to investigate whether the differences in the SN II rates are caused by an ICF, we calculate the rates for the SNe II in the late-type spirals in two distance bins, and plot the results in Figure 10. The open circles are for the rates in the galaxies with distance $D < 75$ Mpc, while the solid circles are for the galaxies with $D \geq 75$ Mpc. In theory, the control times for the more nearby galaxies should be less affected by additional extinction in more highly inclined galaxies, because a large fraction of the galaxies are in the volume-limited regime. As Paper II discussed, the SNe II in the LF sample (with $D < 60$ Mpc) have only a small ($\sim 10\%$) incompleteness in our search; hence, a smaller ICF for the rates is expected for the more nearby galaxy bin. Figure 10 does not support such a conclusion, but it does not eliminate the conclusion either because of the relatively large uncertainties.

As described in Paper II, we have host-galaxy inclination information for all of the LF SNe. To investigate whether the discrepancies in the rates are caused by the differences in the LFs in the various inclination bins, we calculate the rate for each inclination bin using the subset of SNe with the same inclination range in the LFs to calculate the control times. The results are shown in Figure 11. The SN Ia rates do not show a significant ICF. The SN Ibc rates, on the other hand, show a negative ICF due to the strong dependence (with small-number statistics) of the SN Ibc LFs on the inclinations. The SN II rates still exhibit a significant ICF for the late-type spiral galaxies. Thus, inclination-dependent LFs, at least with the small-number statistics in our LFs, do not solve the problem for the SN II rates in late-type spiral galaxies.

We have also investigated whether the rates in galaxies having different $B - K$ colours show significant differences at various inclinations. The spiral galaxies (Sa–Scd) are split into two bins with $B - K < 3.1$ mag and $B - K \geq 3.1$ mag. No significant difference is found for the SN Ia and Ibc rates in the smallest and medium-inclination bins, but a $2-3\sigma$ difference is found for the SN II rates in both colour bins.

We note that the inclination effect for the SN II rates in late-type spiral galaxies appears stronger in SNuB than in SNuK or SNuM. As discussed in Paper I, the galaxy B luminosities are corrected for internal extinction due to inclination using the prescription by Bottinelli et al. (1995). It is possible that this prescription overestimated the galaxy luminosity correction, and thus the SNuB rates in the edge-on galaxies are underestimated. However, incorrect internal extinction will not explain the strong inclination effect for the SN II rates in late-type spirals in SNuK, as the K -band luminosities of the galaxies have *not* been corrected for any internal extinction (see Paper I for more details). It should also be noted that any attempt to remove the inclination effect for the SN II rates in late-type spirals by changing the galaxy luminosities will also result in a negative inclination effect for the SN Ibc rates, as the same set of galaxies is used to calculate the rates for both types of SNe.

We conclude that invoking extinction to explain the dif-

⁶ To simplify the rate ratio calculations, the upper and lower uncertainties due to Poisson statistics are averaged to generate the statistical errors reported in Table 3.

ferences in the SN II rates does not present a coherent picture when all of the observational evidence is considered. Rather, the differences may be caused by a combination of several factors, such as small-number statistics, systematic errors (§3.4), errors in the control-time calculation (due to the limitation of the LF and the light-curve shape, as discussed in Paper II), and the presence of an ICF.

Regardless of the reasons for the differences in the SN II rates in the different inclination bins, the differences themselves may be real. If true, our neglect of a correction factor will result in an underestimate of the SN II rates. As the values of $r0/r3 - 1$ in Table 3 show, the average SN II rates in the $0^\circ - 75^\circ$ bin for the late-type spirals are underestimated by about 40–50% when compared to the rates in the face-on galaxy bin. For the galaxies with different $B - K$ colours, the average rates are underestimated by about 30–70%. The ICF (or lack thereof) thus becomes the largest uncertainty in our treatment of the SN rates, especially for SNe II, as discussed in the next section. We also note that for the SN Ia and Ibc rates, the presence of an ICF cannot be completely ruled out on statistical grounds because of the relatively large uncertainties in the rate ratios. It is thus important to substantially enlarge the sample size in future SN rate calculations, to further evaluate the rate dependence on the galaxy inclinations.

3.4 Error Budget

It is important to have a reasonable uncertainty estimate for the SN rates before discussing any trends or biases. Here we describe the error budget for our rates, considering the statistical and systematic errors separately.

We emphasise that it is nearly impossible to account for every possible source of uncertainty in the rate calculations because of the large amount of involved data and the complexity of the pipeline. Even though we tried to make use of the best available data in the current astronomical database (see the discussion in Paper I of how our galaxy and SN databases were constructed), many measurements are ultimately limited by our knowledge and/or the precision of the existing astronomical quantities. For example, for the galaxies, the B and K photometry suffers from relatively large uncertainties due to the difficulty of cleanly measuring fluxes of extended objects. For the SNe, the LFs (Paper II) were measured from a sample of nearby objects, whose distances derived from the Hubble law suffer from relatively large uncertainties due to peculiar motions in the local Universe. For the rate-calculation pipeline, the choice of the RSSs and whether an inclination correction factor is adopted have significant effects on the final derived rates.

One positive aspect of the uncertainties, resulting from the sheer number of galaxies and SNe involved in the calculations, is that the uncertainty is determined by the sample as a whole; the effect of the uncertainty for a single galaxy or SN becomes relatively small.

For the statistical errors, we use Poisson statistics. The upper and lower Poisson 1σ uncertainties of the number of SNe involved in a rate calculation are computed and used to derive the errors (Gehrels 1986). For the rates in the Irr galaxies, or the CC SNe in early-type galaxies (E–S0), the statistical errors can be as large as $\sim 100\%$ of the measurements due to small-number statistics. For the other rates

with significant numbers of SNe involved, this value is $\sim 10\text{--}30\%$ (see, e.g., the rates listed in Tables 4 and 5, discussed below).

For the systematic errors, we adopt the following methodology to calculate the contribution from each likely source except those from the ICF. The rates from the “full-optimal” sample are used as the “anchor points.” For a new set of rates with a different choice of parameters, the difference is calculated as a percentage of the anchor point, and its absolute value is used as both the upper and lower uncertainties. For the ICF, an asymmetric error matrix is used, as discussed in detail below. The final upper and lower uncertainties (as percentages of the anchor points) are calculated with the individual components added in quadrature, and then converted to errors by multiplying the values of the anchor points.

We consider the following sources for the systematic errors.

(i) Scatter from using different SN samples. While §3.1 provides a detailed discussion of how the rates are affected by using five different SN samples, the scatter in the rates are not all independent of the other uncertainties discussed below. For example, part of the difference between the “full” sample and the “full-optimal” sample may be caused by an inclination correction factor. For this reason, the contribution to the systematic errors due to the sample selection is calculated from the “full-optimal” and “season-optimal” samples. The sample selection causes an uncertainty in the range $\sim 5\text{--}20\%$, with a median at $\sim 10\%$.

(ii) Scatter from using different input LFs. The change in the rates when using 1LF or 2LF demonstrates the effect of the input LFs. Ideally, a LF should be constructed for each galaxy Hubble type, but our small-number statistics preclude such an exercise. While it is difficult to predict how the rates would change from 2LF to multiple LFs, we can use the differences between the 1LF and 2LF rates as a reasonable estimate of the uncertainty caused by the inadequate precision in the input LFs. The choice of the input LFs causes an uncertainty in the range $\sim 5\text{--}30\%$, with a median of $\sim 10\%$.

(iii) Uncertainty caused by the errors in the RSSs. The errors in the RSSs as reported in Table 2 are used to calculate the resulting uncertainty in the rates, and the two errors from the upper and lower uncertainty of the RSSs are averaged. The RSS errors cause an uncertainty in the rates in the range $\sim 5\text{--}25\%$, with a median of $\sim 10\%$.

(iv) Uncertainty caused by the treatment of the ICF. As discussed in the previous section, the SN II rates show a potential ICF for the late-type spirals or galaxies with different $B - K$ colours. As the adoption of an ICF will only increase the rates, we use the following asymmetric error matrix. For the upper uncertainty, the percentage that the average rate in the $0^\circ - 75^\circ$ bin is underestimated relative to the face-on bin is adopted (40–50% for the late-type spirals, 30–70% for the galaxies with different $B - K$ colours). For the lower uncertainty, a global 10% is assumed. For all of the other rates, a global $\pm 10\%$ uncertainty is adopted.

(v) Uncertainty caused by miscellaneous small factors. As mentioned earlier, it is very difficult to fully assess the uncertainties caused by the errors of the various measurements (such as photometry, hubble types, inclination, and

distance) for a large number of galaxies and SNe. Since the previous several sources all contribute roughly 10% each toward the total systematic error budget, we adopt a global uncertainty of $\pm 10\%$ for all remaining miscellaneous factors.

As discussed in the next several sections, for most of the rates the systematic errors are roughly the same size as the statistical errors. For the SN II rates in the late-type spirals and in galaxies of different $B - K$ colours, the systematic errors are a factor of $\sim 1\text{--}4$ times that of the statistical errors, and can reach $\sim 80\%$ of the measurements. We emphasise that our final systematic errors are quite uncertain due to the rough estimates from several components. Fortunately, for most discussions of the internal trends and comparisons based on one set of chosen parameters, only the statistical errors need to be considered (as we have done in §3.1 and 3.2). The systematic errors become relevant when our rates are compared with other published results, or when the rate-size relation and/or ICF play a significant role. We shall discuss the uncertainties and their significance in the following sections on a case-by-case base.

3.5 The SN Rates as a Function of Galaxy Hubble Type

In the previous sections, we have shown that our rates are stable for different SN subsamples but are sensitive to the choice of the input SN LFs. For the final rate calculations, we elect to use 2LF (for more detailed LFs) and the 726 SNe in the “full-optimal” sample (for a good balance between statistical and systematic uncertainties). The rates for a galaxy with the fiducial size are computed according to the RSSs in Table 2 (also listed in Table 4), and reported in Table 4 for different Hubble types. The statistical errors are given together with the systematic errors (in parentheses). To calculate the rate for a specific galaxy, one simply needs to apply Equations (1) through (3) (assuming the size of the galaxy is known). Table 4 shows that our rates are derived from significant numbers of SNe for most of the SN types and galaxy Hubble types, except for the Irr galaxies (not enough galaxies) and for CC SNe in E–S0 galaxies (CC SNe are intrinsically rare in such galaxies).

These rates, together with the statistical errors, are plotted in Figure 12. To illustrate the effect of adopting a fiducial galaxy size for each normalisation, we also evaluate the rates at the median galaxy size for each Hubble type and plot them as open circles in Figure 12. Inspection of the figure reveals the following.

(i) The SNuK and SNuM rates for the same SN type display very similar trends, so we choose to discuss only SNuM in this section. The results on SNuM generally apply to SNuK, unless explicitly expressed otherwise.

(ii) The SNuB of SNe Ia declines from the early- to the late-type galaxies, with only an upper limit derived for the Irr galaxies. Since the B -band luminosity of a galaxy is heavily influenced by the amount of blue, young, massive stars, L_B is not a good indicator of the total amount of mass that is responsible for the production of SNe Ia, which arise from white dwarfs. This is particularly true for the late-type galaxies having abundant massive stars from recent star formation. Consequently, the SNuB rates in the

late-type galaxies are depressed because their L_B are significantly contaminated by massive stars.

(iii) The SNuM rates of SNe Ia are consistent with being *constant* for the different Hubble-type bins. Without considering the upper limit in the Irr galaxies, the rest of the rates can be fit as a constant ($\text{SNuM} = 0.136 \pm 0.018$) with a reduced $\chi^2 \approx 0.8$.

(iv) The rates of the CC SNe in the early-type galaxies (E and S0) are close to 0 for all of the normalisations. These small rates provide a strong constraint on the amount of recent star formation and/or the delay-time distribution (DTD; a distribution of the delay time between the formation of the progenitor star and the explosion of the SN) in these galaxies, as discussed later in this paper.

(v) The CC SN rates generally *increase* from early- to late-type spiral galaxies for all of the normalisations (except perhaps for the SNuB rates of SNe Ibc which are nearly constant). The SN II rates have a more dramatic change than the SN Ibc rates, especially considering the fact that the SN II rates in Sc/Scd galaxies may be underestimated due to the presence of an ICF. There might be a declining trend from the Sc to the Irr galaxies, but the significance of such a trend hinges on the uncertain rates in the Irr galaxies. For example, when the rates for the Irr galaxies are not considered, such a trend would have a low significance for the SN II rates. For the SN Ibc rates, the decline from the Sc galaxies to the Scd galaxies is more obvious, but the difference is still within 2σ of the uncertainties. We need more SNe to reduce the statistical uncertainties of the rates and verify the presence of such a trend.

(vi) The rates evaluated at the median galaxy size for each Hubble type, nearly identical to those found when not adopting the rate-size relation in the rate calculations (see §4.1 for more discussion), show that the biggest differences from the rates using a single fiducial galaxy size are presented in E (for SNe Ia) and Scd/Irr (for all SN types) galaxies. Not surprisingly, these galaxies are also at the two extreme ends of the luminosity/mass size distribution (most luminous/massive for E, and least luminous/massive for Scd/Irr galaxies).

(vii) Understanding the observed trends in the SN rates requires knowledge of the SSFR and the initial mass function (IMF) in the different Hubble types, DTDs for stars with different masses, and the link between stars of different masses and the different SN types (see Smith et al. 2011).

3.6 The SN Rates as a Function of Galaxy $B - K$ Colour

It is well known that the Hubble-type sequence from E to Irr corresponds to a sequence in the star-formation rate (SFR). The SFR is virtually zero in ellipticals and becomes increasingly larger toward late-type spirals. An alternative indicator of the SFR are the broad-band colours (in particular the optical to near-infrared), with bluer galaxies hosting a younger stellar population having stars that are more massive than those in redder galaxies. For this reason and following the work of M05, we calculate the SN rates for galaxies with different $B - K$ colours. As discussed in Paper I, we have secured the $B - K$ colour measurements for a majority of the LOSS sample galaxies.

We divide the galaxies into different $B - K$ colour bins,

calculate the SN rates for the fiducial galaxy, and report the results in Table 5. To evaluate the rate for a specific galaxy, one needs to know the galaxy size and apply Equations (1) through (3) (with the RSSs listed in both Tables 2 and 5). The rates in Table 5, together with their statistical errors, are plotted in Figure 13. The rates are also evaluated at the median galaxy size for each colour bin, and plotted as open circles. The dashed lines shown in Figure 13 represent the second-order polynomial fits (as a function of $B - K$ colour) for the logarithm of the rates as determined during the multi-variate linear regression model analysis using Equation (4). As mentioned in §2.2, this analysis is not applied to the SN Ibc rates due to their relatively large uncertainties⁷. Inspection of the figure reveals the following.

- (i) As in Figure 12, the SNuK and SNuM rates for the same SN type display very similar trends, and we choose to discuss only SNuM as an example.
- (ii) The SNuB rate of SNe Ia increases from blue to red galaxies, likely due to the increasing influence of massive stars in the total B -band luminosity in the bluer galaxies. The SNuB rate of SNe II, on the other hand, is consistent with a constant for the several bins at the blue colour end, and then declines toward the red colours. This is likely caused by the increasing influence of an old stellar population in the redder galaxies. The SNuB rate of SNe Ibc rises from the bluest galaxies to $B - K = 3.0$ mag, then declines thereafter.
- (iii) The SNuM rate of SNe Ia increases dramatically from red to blue galaxies (by a factor of ~ 6.5). This is different from the Hubble-type rates where the SN Ia rates are consistent with being a constant in different Hubble types for SNuK and SNuM.
- (iv) The CC SN rates are small (but not zero) in the reddest galaxies, and in general become progressively higher for bluer galaxies. However, the SN Ibc rate becomes smaller for the bluest galaxy bin. Aside from small-number statistics, other possible reasons for this change are the metallicity effect on the binary progenitor evolution of SNe Ibc, the progenitor-star mass range, and/or the DTD. More detailed discussion is beyond the scope of the current analysis.
- (v) The dashed lines provide excellent fits to the SN Ia and SN II rates, indicating that we have adopted a reasonable functional form during the multi-variate linear regression model analysis in §2.2.
- (vi) The rates evaluated at the median galaxy size for each colour bin show that the biggest differences from the rates using a single fiducial galaxy size are present in the bluest galaxies, which have the lowest luminosity per unit mass among all of the galaxies.

4 DISCUSSION

4.1 Comparison with Historical Results

In this section, we compare our SN rates with the published results, in particular to the benchmark work of C99 and

⁷ We actually performed the analysis for the SN Ibc rates, and the model provides a reasonable fit to the data. The fits are not shown in Figure 13 in order to be consistent with the discussion in §2.2.

M05. There are many differences in the calculations, as detailed in Papers I and II and the previous sections of this paper, such as the total number of SNe, the survey method, the treatment of the LFs, the light-curve shapes, the host-galaxy extinction, and the ICFs. The biggest difference, however, is our adoption of the rate-size relation and the use of the RSSs. Accordingly, our rates are calculated for a fiducial galaxy size. Since the C99 and M05 results do not consider a RSS, their rates are for the average galaxy sizes. To mimic the calculations performed by C99 and M05, there are two options. One is to evaluate our rates (for the fiducial galaxies) at the average galaxy size for different Hubble types or colours, while the other is to calculate the rates without using the RSSs in the rate-calculation pipeline. The two options are not exactly the same, as the rates without using the RSSs in the pipeline are the average of the rates for the galaxies weighted by their control times. In practice, however, the rates from the two approaches are nearly identical, as there are numerous galaxies involved in the calculations and the effect of the control time is averaged out.

We elect to calculate the rate for the average KAIT galaxies without using the RSSs in the pipeline, exactly the same way the rates were calculated by C99 and M05. The rates are listed in Tables 6 (for different Hubble types) and 7 (for different $B - K$ colours), and they are plotted in Figures 14 and 15. As no RSSs are used to calculate the average SN rates, the systematic errors reported in the tables are the combination of the remaining components discussed in §3.4. The total uncertainties (the statistical and systematic errors added in quadrature) are also plotted in Figures 14 and 15; since our rates are compared to the measurements from another analysis, we need to show the full error matrix.

For the rates as a function of galaxy Hubble type (Figure 14), our results and those published by C99 and M05 are generally in good agreement within the uncertainties, even though nominally our fiducial SN Ibc rates are higher (by a factor of ~ 2), and our fiducial SN II rates are lower (by a factor of ~ 1.5). The only significant difference is the rates in the Irr galaxy bin. As discussed earlier, there is a deficit of Irr galaxies in the LOSS galaxy sample, and only 11 out of the 929 SNe considered in the rate calculations were discovered in the Irr galaxies. Consequently, the SN rates for the Irr galaxies are quite uncertain in our calculations, but we are in the process of remedying this by monitoring more Irr galaxies in our search. Nevertheless, our rates in the Irr galaxies, derived from a small number of SNe for SNe Ibc and II, and the upper limit of our rate for SNe Ia, do not support the dramatic increase of the rates in the Irr galaxies suggested by C99 and M05. We suspect that the true SN rates in the Irr galaxies are in between our rates (or limits) and the C99/M05 results. Obviously, better constraints will be obtained once more SNe are discovered in the galaxies and incorporated into future rate calculations.

For the rates as a function of galaxy $B - K$ colour (Figure 15), the SN Ia rates show good agreement, and exhibit a dramatic increase from the red to the blue galaxies, much more so than the rates for the fiducial galaxies (Figure 13). This is caused by the differences in the average masses of the galaxies with different colours, as discussed in Paper I. Bluer galaxies tend to have smaller masses, and their SNuM becomes higher as indicated by the rate-size relation. Since the CC SN rates are combined together by M05, we also com-

bine our CC SN rates, giving the comparison in the lower panel of Figure 15. Again, our rates agree with the M05 results to within the uncertainties. We also plot the SN Ibc rates (dashed line) and SN II rates (dash-dotted line). The SN II rates show a more dramatic increase from the red to the blue galaxies than the SN Ibc rates.

The good agreement between our rates and those reported by C99 and M05, though with different approaches to treat the various aspects of the rate calculations, suggests that both analyses employed reasonable assumptions and corrections to deal with the observational biases and uncertainties involved. However, we note that the agreement is only achieved when the rates are calculated in the same manner, without considering the important rate-size relation that we discovered during the course of our research.

4.2 The Rate-Size Relation

In this section, we offer more discussion of the rate-size relation. We emphasise that this relation is empirically derived from the data; finding the exact causes of the relation is not critical for the rate calculations, but may shed light on the correlation between the SFR and the galaxy properties, and on the DTD for the various types of SNe. As also discussed in the next section, the rate-size relation has a significant effect on the study of the two-component model fit to the SN Ia rates.

We first attempt to quantify the effect of adopting the rate-size relation in our rate calculations. Figures 12 and 14 show our rates in different Hubble types with and without the adoption of the rate-size relation, respectively. The differences are significant. For example, the SNuM rate of SNe Ia exhibits only a weak increasing trend from the early-type to the late-type galaxies, and is consistent with a constant in Figure 12, but a much more prominent increasing trend is seen in Figure 14. The ratio of the rates between Figures 12 and 14 for the same Hubble-type bin reflects the corrections caused by the rate-size relation.

Numerically, the existence of the rate-size relation indicates that the rates cannot be adequately described by a single parameter using either galaxy Hubble type or $B - K$ colour. The galaxy size (L_B , L_K , mass) is thus used as a second parameter to quantify the rates (in the form of the rate-size relation). We have considered other combinations of parameters to describe the rates — that is, to replace the rate-size relation with some other empirical correlations. One combination that merits more discussion is to parameterise the rates as a function of both galaxy Hubble type and $B - K$ colour; see §B of the Appendix.

Physically, what could possibly cause the SN rates to be sensitive to the sizes of the galaxies? For the CC SNe, which come from massive stars and are intimately connected to the recent SFR, the rate-size relation might be explained by the correlation between the SSFR and the galaxy mass recently reported by Noeske et al. (2007a, 2007b), Salim et al. (2007), and Schiminovich et al. (2007). Using the ultraviolet-optical colour-magnitude diagram in conjunction with spectroscopic and photometric measurements derived from the Sloan Digital Sky Survey spectroscopic sample, Schiminovich et al. (2007) studied the physical properties of the galaxies as a function of SSFR and stellar mass. As demonstrated in the rightmost panel of their Figure 7, the SSFR of the galax-

ies has an apparent dependence on the stellar mass of the galaxies, with $\text{SFR}/M \propto M^{-0.36}$ for star-forming galaxies, and $\text{SFR}/M \propto M^{-0.16}$ for non-star-forming galaxies. The main cause of this correlation is likely the higher gas mass fractions and surface densities in the low-mass galaxies.

The average SSFR for all of the galaxies, weighted by the intensity of the contour map (Table 3 of Schiminovich et al.), is shown in Figure 16 as a function of galaxy mass. Due to the mix of the star-forming and non-star-forming galaxies and their loci on the SFR/M vs. M diagram, the average SSFR for all of the galaxies is proportional to $M^{-0.55 \pm 0.09}$, as shown by the solid line in Figure 16. Note that our CC SN SNuM rate is proportional to $M^{-0.55 \pm 0.10}$ (Table 2). The correlations thus have an essentially identical dependence on galaxy mass, indicating the consistency of these two tracers of star-formation activity.

While the SN Ia SNuM rate shows a dependence of $M^{-0.50 \pm 0.10}$, similar to the correlation between the SSFR and galaxy mass, a link between the two correlations is more difficult to understand. First, SNe Ia are believed to come from the thermonuclear explosion of a white dwarf in a binary system, so they are often associated with the old population of their host galaxies, although recently a component of SNe Ia that is associated with the intermediate-age population, or perhaps even the young/star-forming population, has been proposed (i.e., the “prompt” component in the SN Ia rates; see, however, the discussion in the next section). Still, a direct link between the SN Ia rate and the SSFR is not to be expected. Rather, the DTD needs to be considered.

Perhaps more troubling is the fact that the SN Ia rates in the E-S0 galaxies, or even in the E galaxies, show the same rate-size correlation as in the spiral galaxies. While there is some observational evidence for a widespread, low-level presence of star formation in the early-type E and S0 galaxies (see Mannucci et al. 2008, and the references therein), the SNe Ia in these early-type galaxies should be dominated by the “tardy” component (the component that is associated with the old population), as demonstrated in the next section. We further argue against the influence of the SSFR in the early-type galaxies as being the main cause of the rate-size relation, because the near-zero rate of CC SNe in these galaxies suggests that their SSFR is low.

Possible reasons for the rate-size relation for the SN Ia rates are as follows. (a) The DTD and the age of the stellar populations. Maoz et al. (2011, Paper IV in this series) developed a method to recover the DTD for SNe Ia, and found that the SN Ia rate decreases monotonically with the age of the stellar population, with the relatively “young” (age < 420 Myr) stellar populations having a rate that is at least an order of magnitude higher than the “old” (age > 2.4 Gyr) stellar populations. If smaller galaxies have a younger average age for the stellar populations, they would have a higher rate. (b) The probability of a white dwarf in a binary system exploding as a SN Ia. If the less massive galaxies affect the binary evolution of the white dwarf in such a way as to boost the probability of a SN Ia explosion (due to metallicity or other factors), the SN Ia rate can be enhanced. We consider reason (a) to be more likely, and reason (b) to be a secondary, more speculative possibility.

We emphasise that the above discussion of the rate-size relation of SNe Ia hinges on the existence of the rate-size

relation for the galaxies having different Hubble types or $B - K$ colours. We note the relatively large uncertainties in some of our RSS measurements due to small-number statistics. For example, the significance of the rate-size relation is only 1.6σ for the SN Ia SNUM rate in the E galaxies. It is thus conceivable that the SN Ia rates do *not* depend on the mass of these galaxies, and that the rate-size relation of the SN Ia rates in the star-forming galaxies is indeed related to the dependence of the SSFR on the galaxy mass. Sullivan et al. (2006) reported a nonlinear proportionality between the SN Ia frequency and the galaxy mass for the star-forming galaxies, with a RSS of $\sim -0.30 \pm 0.08$, while for the non-star-forming (“passive”) galaxies, the SN Ia frequency is consistent with a linear relation with the galaxy mass (i.e., no RSS is required). While the discrepancy between our results and those reported by Sullivan et al. (2006) does not have high significance due to the large uncertainties involved in both studies, the different results nonetheless highlight the need to further increase the sample sizes and reduce the uncertainties of the RSSs.

We note that Sullivan et al. used the SFR to split the galaxies into different bins, while we use the galaxy Hubble types and colours. Even though the galaxy Hubble type or colour sequence reflects a sequence in the SFR, there is not a one-to-one association. As discussed in §2.1 and §2.2, the rate-size relation shows a dependence on how the galaxies are grouped to calculate the rates: the RSSs depend on the normalisation for the Hubble-type rates, while they are insensitive to the normalisation for the $B - K$ colour rates. The different behaviour of the rate-size relation with the two different grouping methods for the galaxies leaves the possibility that the rate-size relation may not be needed for certain galaxy grouping methods. We plan to perform a rate calculation using the SFR for the galaxies in a future paper, when the SFRs for the LOSS sample galaxies are derived. One test, for example, is to investigate whether there is a rate-size relation when the galaxies are binned according to the SSFR. The expectation is that the rate-size relation should still be present if it is universal and not related to the SSFR and galaxy-mass relation. Otherwise, no such rate-size relation should be present.

We also note that while studying the SN rates in galaxies of different SFRs is a different and valuable approach, our measurements for galaxies of different Hubble types and $B - K$ colours have their own merits. In particular, the Hubble type and $B - K$ colour of a galaxy are *observed* quantities and widely available for the nearby galaxies, while the SFR of a galaxy is an *inferred* quantity based on synthetic models of the integrated broad-band fluxes or spectra. Moreover, when SFR measurements are derived from spectral energy distribution (SED) fitting, a strong degeneracy with dust extinction (which, in general, is relatively poorly known) is usually found, reducing the precision of the derived values. The SFR measurements of the nearby galaxies also suffer from the difficulty of properly measuring fluxes of extended objects (especially when there are Galactic stars along their lines of sight), and could introduce systematic uncertainties into the rate calculations. The situation is improved at moderate to high redshift, where galaxies become more like a point source and Galactic contamination is minimal, so photometry can be more accurately conducted and modeled.

4.3 The Two-Component Model for the SN Ia Rates

Based on the fact that the SN Ia rate per unit mass (SNUM) in late-type or blue galaxies is approximately an order of magnitude higher than in early-type or red galaxies, a trend similar to that seen for CC SNe, M05 and Scannapieco & Bildsten (2005) suggested that the overall SN Ia rate could be described as the sum of two components. One, denoted the “young” or “prompt” component, is proportional to the ongoing SFR (and thus to the CC SN SNUM) and has a relatively short DTD. The other, called the “old” or “tardy” component, is proportional to the mass of the galaxies (and thus a constant SNUM) and has a relatively long DTD. The so-called “two-component model” for the SN Ia rates, with its limitation as a simplified analytic model, has been discussed in numerous subsequent studies of SN rates (e.g., Neill et al. 2006; Sullivan et al. 2006; Mannucci et al. 2006; Dahlen et al. 2008; Pritchett et al. 2008; see also Bartunov, Tsvetkov, & Filimonova 1994, who over a decade earlier found that SNe Ia occur in spiral arms with a frequency similar to that of SNe II).⁸

As discussed in §4.2, the rates used to derive the two-component model by M05 and Scannapieco & Bildsten (2005) have not been corrected for the rate-size relation, and thus are for the average galaxy sizes. We perform a similar analysis and display the results in the left panel of Figure 17. We also apply the model to the rates for the fiducial galaxy (i.e., after the rate-size relation is considered); the results are shown in the right-hand panel. For both cases, we confirm that the SN Ia rates in galaxies of different $B - K$ colours (the solid circles) can be well fit by a constant plus a fraction of the CC SN rate (the dashed line; the error bars of the fit are not shown but are comparable to those of the SN Ia rates), as follows:

$$\text{SNUM(Ia)} = (0.036 \pm 0.022) + (0.220 \pm 0.067) \text{SNUM(CC)}, \quad \text{and} \quad (7)$$

$$\text{SNUM(Ia, } M_0) = (0.046 \pm 0.019) + (0.248 \pm 0.071) \text{SNUM(CC, } M_0). \quad (8)$$

Compared with the fit parameters reported by M05, the constant (the tardy component) is in good agreement, while the fraction of the CC SN rate (the prompt component) is somewhat different. Our fractions (0.220 ± 0.067 , 0.248 ± 0.071) are smaller than those reported by M05 (0.35 ± 0.08), but the differences are not significant once the uncertainties are considered.

To further investigate the correlation between the SN Ia and CC SN rates, we adopt an approach to visualise the correlation without using the galaxy Hubble type or colour as the platform. We first create $(X, Y) = (\text{CC SN rate}, \text{SN Ia rate})$ pairs for the galaxies with the same Hubble type or colour range, and then fit a linear correlation $Y = a + bX$ to quantify the coefficients and the significance of the correlation. For each correlation, we also calculate the χ^2/DOF

⁸ Note that the idea that some SNe I come from a relatively young stellar population was first proposed long ago by Dallaporta (1973) and Oemler & Tinsley (1979). However, at the time these papers were published, SNe Ib and SNe Ic were still not recognized as separate classes from SNe Ia, so there was potential contamination of the SN Ia sample by SNe Ibc.

for a constant fit to the SN Ia rates (i.e., no correlation with the CC SN rate).

We demonstrate how the two-component model for the SN Ia rates is affected by the choices of the RSSs and the sizes of the galaxies in Table 8 and Figure 18. The rates in galaxies of different $B - K$ colours are used to construct the (X, Y) pairs. The first three entries of Table 8 and the top panel of Figure 18 show the results for the different RSSs for the SN Ia rates (the fiducial RSS and its 1σ upper and lower errors). For the CC SN rates, the RSS is fixed at the adopted fiducial value (-0.38). One can see that the choice of the RSS has a significant effect on the two-component model. As the RSS for the SN Ia rates becomes bigger, the correlation between the SN Ia rates and the CC SN rates becomes weaker, as indicated by the larger tardy component (“ a ”), the smaller coefficient and significance for the CC SN rate fraction (“ b ”), and the smaller reduced χ^2 for a constant fit.

The last three entries of Table 8 and the lower panel of Figure 18 show the correlation for the galaxies with different sizes. When the galaxy size becomes bigger, the significance of the correlation does not change (as indicated by the same reduced χ^2 for a constant fit). However, the tardy component becomes smaller, and the coefficient for the CC SN rate fraction becomes bigger. This can be understood by multiplying Eq. (8) by $(M/M_0)^{-0.25}$, which yields the following:

$$\text{SNuM(Ia, } M) = 0.046 (M/M_0)^{-0.25} + 0.248 M^{0.13} \text{SNuM(CC, } M). \quad (9)$$

In other words, the tardy component varies with galaxy mass because of the rate-size relation, while the CC SN rate fraction changes with galaxy mass because the RSSs for the SN Ia and CC SN rates are different (by 0.13, though with a low significance level).

We have investigated how the two-component model fit results are affected by different choices of parameters in the rate calculations, such as the normalisation (SNuB, SNuK, or SNuM), the RSSs (with or without), and the construction of the rate (X, Y) pairs (using rates in the different Hubble types or $B - K$ colours). The results are listed in Table 9 and plotted in Figure 19. For Table 9, Column 1 (“Src”) shows how the rate (X, Y) pairs are constructed: “H-type” means the rates in the different Hubble types are used, while “ $B - K$ ” means the rates in the different $B - K$ colours are used. Column 2 (“Rate”) shows the normalisation. The next two blocks of columns show the fit parameters for the model, with and without RSSs.

Inspection of Table 9 and Figure 19 reveals the following.

(i) The normalisation has a rather significant effect. Using SNuB, for example, yields a reverse trend as expected from the two-component model (the SN Ia rate decreases with increasing CC SN rate), although with a low significance level as indicated by the small reduced χ^2 for a constant fit. This fact serves as a reminder that we have not yet found an ideal normalisation to measure the rates for all types of SNe. The blue luminosity, for example, is dominated by contributions from very massive stars (a small minority of all stars), and is thus a relatively poor gauge of the stellar population responsible for the production of SNe Ia; few, if any, SNe Ia arise from stars having $M \gtrsim 8 M_\odot$. The K -band luminosity, on

the other hand, can be used to derive the mass, especially in conjunction with the $B - K$ colours; it arises from a combination of both young and old populations. The discussion of the two-component model should take into account the limitations of our current knowledge of the ideal normalisation, and the associated pitfalls. It is likely, for example, that the rate cannot be quantified by a single normalisation parameter, as witnessed by the existence of the rate-size relation. Other more subtle effects such as environmental influences (metallicity, active galactic nuclei, radio jets, etc.) may become more obvious in future studies with larger and more complete samples. The SNuB correlations will *not* be considered hereafter unless explicitly expressed otherwise.

(ii) The rate-size relation affects the results of the two-component model fit. The correlation between the SN Ia rates and the CC SN rates in general becomes weaker after the rate-size correction is applied, as indicated by the fit parameters: the tardy component becomes larger (comparing “ a_2 ” to “ a_1 ” in Table 9), the CC SN rate fraction and significance become smaller (compare “ b_2 ” to “ b_1 ”), and the reduced χ^2 for a constant fit becomes smaller (compare “ $\chi^2(c)_2$ ” to “ $\chi^2(c)_1$ ”).

(iii) The construction of the rate (X, Y) pairs has a significant effect on the two-component model, suggesting that there is not a one-to-one correlation between the SN Ia and the CC SN rates. For the cases both with and without the rate-size corrections, the rates from the galaxy $B - K$ colours display a more significant correlation than the rates from the galaxy Hubble types. In particular, we note that after the rate-size relation is considered, the SN Ia rates in different Hubble types are consistent with being a constant (i.e., no correlation with the CC SN rates), as discussed in §3.5 and demonstrated by the small $\chi^2(c)_1$ value in Table 9. This is disconcerting, and suggests that there could be no correlation or a strong correlation, depending on how the galaxies are grouped to calculate the rates. It is of course dangerous to define, *a posteriori*, “optimal” ways to group the galaxies for the purpose of the two-component model analysis.

To further explore the correlation between the SN Ia and the CC SN rates, we attempt to split the SN Ia rates into two components: the contribution from (1) old and (2) young *stellar populations* in galaxies (hereafter, the “old-s” and “young-s” components, respectively). Note that this approach is different from the two-component model for the SN Ia rates by M05 and Scannapieco & Bildsten (2005), where the SNe Ia are split into an old/tardy and a young/prompt component. In other words, the old/tardy component in the two-component model is proportional to the *total mass* of a galaxy, while the “old-s” component in our approach is proportional to the *mass of the old stellar population* in a galaxy. It is generally accepted that early-type galaxies (E/S0) are predominantly made of old stellar populations, while late-type galaxies (Sc/Scd) consist of mostly young stellar populations, so we adopt a toy model in which the fraction of the “old-s” SN Ia component decreases from 100% in E galaxies, to 83.3% in S0, 66.7% in Sab, 50.0% in Sb, 33.3% in Sbc, 16.7% in Sc, and 0% in Scd galaxies⁹. Our goal is to study whether there is a signifi-

⁹ Thus, our toy model naively assumes that the number sequence

cant correlation between the “young-s” SN Ia rate and the CC SN rate.

Figure 20 shows the results for the SNuM rates for a fiducial galaxy. The left panel shows the conventional (M05; Scannapieco & Bildsten 2005) two-component model fit (dashed line) for the total SN Ia rates (solid dots) as follows:

$$\text{SNuM}(\text{Ia}, M_0) = (0.116 \pm 0.012) + (0.051 \pm 0.032) \text{SNuM}(\text{CC}, M_0). \quad (10)$$

As discussed above, the SN Ia rates can be well fit by a constant, and the correlation with the CC SN rates is not significant (at only the $\sim 1.5\sigma$ level). Also shown in the panel is our adopted “old-s” SN Ia component (dash-dotted line): it accounts for 100% of the SNe Ia in E galaxies and 0% in Scd galaxies. The “young-s” component, the difference between the total rate and the “old-s” component, is plotted in the right-hand panel, together with a two-component model fit as follows:

$$\begin{aligned} \text{SNuM}[\text{Ia(young)}, M_0] = & (0.001 \pm 0.005) \\ & + (0.187 \pm 0.027) \text{SNuM}(\text{CC}, M_0). \end{aligned} \quad (11)$$

Not surprisingly, the tardy component is consistent with being zero. There is also a strong correlation between the “young-s” component of the SN Ia rate and the CC SN rate (at the $\sim 7\sigma$ level).

This exercise suggests that the fundamental idea of the two-component model for the SN Ia rates as proposed by M05 and Scannapieco & Bildsten (2005) is correct. The only required modification to the model is that the “tardy/delayed” component is related to the mass of the old stellar population, rather than to the total mass, of the galaxies. However, we caution that the treatment of the young/old stellar populations in our toy model is *ad hoc*; there is clear observational evidence indicating that early-type galaxies do harbor some young stellar populations, and that late-type galaxies do also contain an old component (Mannucci et al. 2008, and references therein).

A more sophisticated analysis will only become possible if methods are developed to properly reconstruct the age distributions of stellar populations in galaxies and identify the SNe Ia associated with different populations (Neill et al. 2009; Brandt et al. 2010; Maoz et al. 2011). While we have some clues (e.g., SN 1991bg-like objects probably come from an old stellar population while SN 1991T-like objects from a young population), we do not have a clear picture for normal SNe Ia, which are two-thirds of the total SN Ia population (Paper II) and occur in galaxies of all Hubble types. It is thus impossible to directly measure the SN Ia rates in stellar populations of different ages. Brandt et al. (2010) and Maoz et al. (2011) developed a recovery method to constrain the DTD of SNe Ia in different stellar populations. In particular, Maoz et al. (2011) found evidence for a population of SNe Ia in both “young” (age < 420 Myr) and “old” (age > 2.4 Gyr) stellar populations, which they called the “prompt” and “delayed” components. We note, however, that their “delayed” component refers to SNe Ia that occur in old (age > 2.4 Gyr) stellar populations, so in essence it is

1–7 for the E–Scd galaxies represents a linear decrease of the fraction of the old stellar population.

the “old-s” component we discussed above, not the delayed component discussed in the original two-component model of M05 and Scannapieco & Bildsten (2005), which is proportional to the total mass (including young stellar populations) of a galaxy.

In summary, the correlation between the SN Ia and the CC SN rates is affected by the normalisation and the way the galaxies are grouped. Whether there is a *physical connection* between the rates hinges on finding the ideal normalisation and an optimal way to group the galaxies. It is also found that the rate-size relation plays a significant role in the two-component model. While the cause of the rate-size relation is not clear (see the discussion in the previous section), the fact remains that for galaxies having the same size, the correlation between the SN Ia and CC SN rates becomes rather weak (e.g., for the rates from different $B - K$ colours), or nonexistent (e.g., for the rates from different Hubble types). We also find that the SN Ia rate for the young stellar population in galaxies might have a significant correlation with the CC SN rate even after applying the rate-size corrections.

While recent studies provide indisputable evidence of a “weak” bimodality (Mannucci 2008) — that SNe Ia come from stellar populations that are both young and old (e.g., M05; Maoz et al. 2011) — it is unclear whether the two progenitor populations are well separated (the so-called “strong” bimodality; e.g., Mannucci et al. 2006; Scannapieco & Bildsten 2005; our toy model above) or form a continuous distribution. Models of binary-star evolution exists that produce both bimodalities (e.g., Greggio 2005; Hachisu et al. 2008; Lipunov et al. 2010). Due to uncertainties in the two-component models, fitting the SN Ia rate evolution with redshift based on the two-component models and the star-formation history becomes highly uncertain until we understand the origin of the rate-size relation and properly parameterise the two-component models.

4.4 The Volumetric SN Rates

Supernova rates at different redshifts provide important information on the evolution of a number of physical processes over cosmic time, such as the cosmic SFR and the DTD for the explosion of SNe Ia. All of the published rates at moderate to high redshifts are expressed as a volumetric rate in units of SNe $\text{Mpc}^{-3} \text{ yr}^{-1}$; thus, in this section, we attempt to derive a volumetric rate in the local Universe from our dataset.

As discussed in Paper I, our galaxy sample is not complete, even for the very nearby volume within $D < 60$ Mpc, so we cannot directly measure a volumetric rate using the control-time method. To convert our rates for galaxies of different Hubble types into a volumetric rate, we require knowledge of the local luminosity density for galaxies of different Hubble types. A further complication is the presence of the rate-size relation; we need to know the distribution of the sizes for the galaxies (i.e., the galaxy luminosity function).

Unfortunately, our combined knowledge of the galaxy luminosity function and local density for different Hubble types and colours is still rather limited. We were only able to find a complete set of measurements in the literature with galaxies split into broad early-type and late-type bins. In our calculation, we make use of the K -band galaxy lumi-

nosity function and density published by Kochanek et al. (2001). In particular, we adopt the standard model in their Table 3 for the early-type and late-type galaxies. With our adopted Hubble constant, this means local K -band luminosity densities of $j_{\text{early}} = (2.25 \pm 0.36) \times 10^8 L_\odot \text{ Mpc}^{-3}$ and $j_{\text{late}} = (2.96 \pm 0.42) \times 10^8 L_\odot \text{ Mpc}^{-3}$.

Our volumetric rates are derived with the following steps. We first calculate SNuK for a fiducial galaxy for the early-type (E-S0) and late-type (Sa–Irr) galaxies using the “full-optimal” SN sample. These rates are reported in the first two rows in Table 10 for the different SN types¹⁰. The Kochanek et al. (2001) luminosity functions for the early- and late-type galaxies are then used to derive the number distribution for the galaxies having different luminosities, and the RSSs as reported in Table 2 are used to calculate the rates for different luminosities according to the rate-size relation. The average values of SNuK, weighted by the number distributions of the LFs, are reported in the third and forth rows in Table 10. These SNuK values are multiplied by the corresponding luminosity densities as reported above, and the contributions from the early- and late-type galaxies are summed to yield the final volumetric rates reported in the last row of Table 10.

The evolution of the volumetric rate versus redshift (up to $z \approx 0.5$) for SNe Ia is shown in Figure 21. The published rates (all converted to our adopted Hubble constant) include those of C99 (Botticella et al. 2008), Hardin et al. (2000), Madgwick et al. (2003), Tonry et al. (2003), Blanc et al. (2004), Dahlen et al. (2004), Barris & Tonry (2006), Neill et al. (2006), Neill et al. (2007), Dilday et al. (2008), Botticella et al. (2008), and Horesh et al. (2008). Our volumetric rate is plotted with the statistical error only (half-solid circle, displaced for clarity at $z = -0.01$), and then with the statistical error and systematic error added in quadrature (solid circle). We note that our measurement with the total uncertainty has roughly the same precision as some of the other measurements, despite the fact that we have used more SNe in our calculations. The explanation is twofold. First, the precision of our volumetric rate is limited by the precision of the local luminosity density. Second, we take an aggressive approach to calculating the systematic errors (as discussed in §3.4), and hence may overestimate the total errors. As can be seen, our measurement including only the statistical error is the most precise among all the points.

Our rate is consistent with the C99 measurement at the same redshift to within the uncertainties¹¹. The SN Ia rates are consistent with being a constant from $z = 0$ to ~ 0.3 , followed by a rise toward higher redshifts; however, a gentle rising behaviour from $z = 0$ to 0.5 cannot be ruled out, as indicated by the lower dash-dotted line, which is evaluated at the 1σ lower error bar of the C99 measurement and follows

¹⁰ We note that our definition of the early-type and late-type galaxies is somewhat different from that adopted by Kochanek et al. (2001), but the ratio of the integrated total K -band luminosity between the early- and late-type galaxies in our sample, 1.27, is consistent with that reported by Kochanek et al. (1.17 ± 0.12).

¹¹ Note that the differences between our volumetric rates and the C99 measurements are caused by a combination of several factors: the difference in the rate numbers, the use of RSSs and galaxy LFs in our calculation (see also Mannucci et al. 2006), and the difference in the adopted luminosity density for the galaxies.

a rate $\propto (1+z)^{3.6}$, a functional form that is the same as the derived SFR history from Hopkins & Beacom (2006). The dashed and the upper dash-dotted lines follow the same functional form but are evaluated at our measurement, and at the 1σ upper error bar of our measurement, respectively, and they do not provide a satisfactory fit to the ensemble of the measurements. We also plot the expected SN Ia rate from the SFR history study by Mannucci et al. (2007; dotted line). Detailed discussions of the redshift evolution of the SN Ia rate, the comparison to SFR history, and constraints on the DTD are beyond the scope of this paper.

Figure 22 shows the redshift evolution of the volumetric rates of the CC SNe. The published rates (all converted to our adopted value of the Hubble constant) include C99, Dahlen et al. (2004), Cappellaro et al. (2005), Botticella et al. (2008), and Bazin et al. (2009). Our volumetric rate, obtained by summing the SN Ibc and SN II rates in Table 10, is plotted with the statistical error only (half-solid circle, displaced at $z = -0.03$ for clarity), and then with the total error (solid circle). Our rate is consistent with the C99 measurement at the same redshift to within uncertainties, though our number is nominally higher (by 65%). The dashed line again gives a rate $\propto (1+z)^{3.6}$, while the dotted line follows the SFR history from Mannucci et al. (2007). Both curves are evaluated at our measurement and offer excellent fits to all of the published results. Taken at face value, it would appear that the CC SN rate closely follows the SFR history, though we caution that most of the measurements have rather large uncertainties. Detailed discussions of the CC SN rate redshift evolution and the various renditions of the SFR are beyond the scope of this paper.

We further note that to investigate the rate evolution at different redshifts, one needs to consider potential galaxy-size evolution (i.e., a luminosity function change) at different redshifts because of the rate-size relation.

4.5 The SN Rates in the Milky Way

From our measured rates reported in Table 4, we can determine the expected SN rates in the Milky Way Galaxy (MW, hereafter) and compare them with values obtained from other sources. To achieve this, we require knowledge of the size and the Hubble type of the MW. We assume the MW to be of Hubble type Sbc (e.g., van den Bergh & McClure 1994). The total B -band luminosity of the MW is quite uncertain; we adopt $(2.0 \pm 0.6) \times 10^{10} L_\odot$ (van der Kruit 1987) and $(2.6 \pm 0.6) \times 10^{10} L_\odot$ (van den Bergh 1988). Alternatively, we can assume that the MW has a size similar to that of the Andromeda galaxy (M31), as they are the largest galaxies in the Local Group and generally thought to be similar in many ways. For M31, the B -band magnitude, 3.36, is adopted from RC3 and is corrected for both internal (due to inclination) and Milky Way extinction. The K -band magnitude (0.875) is adopted from the 2MASS extended source catalog and corrected for extinction as well. The distance to M31 ($D = 0.778 \pm 0.017$ Mpc) is calculated from 17 Cepheid measurements archived in NED. Finally, we assume that the MW has the average size of the Sbc galaxies in the “optimal” LOSS galaxy sample.

Table 11 lists all of our rate estimates (in SNe per century). The rates for a fiducial Sbc galaxy in Table 4 are corrected by the rate-size relation according to the size of

the MW (with the RSSs in Table 2). The uncertainties for the individual measurements are not reported, as they are much smaller than the scatter among the different measurements. The average rates are given in the last row together with the 1σ scatter. Considering the uncertainties for the Hubble type and size of the MW, these rates may have a systematic uncertainty of a factor of ~ 2 . In particular, we note that the MW rate in SNe per century is proportional to size $^{1+{\rm RSS}}$ (§2.2), so even if the MW size is off by a factor of 10, the SN rate is erroneous only by a factor of 2.8–5.9 (depending on the SN type and the normalisation).

Our fiducial estimate of 2.84 ± 0.60 SNe per century is in good agreement with published results of 1.4–5.8 SNe per century based on different techniques, including direct star counting, pulsar birth rates, the number of radio SN remnants, and historical SN records (van den Bergh 1991; van den Bergh & Tammann 1991; Cappellaro et al. 1993; van den Bergh & McClure 1994). Our CC SN rate estimate of 2.30 ± 0.48 SNe per century is also consistent with published values (1.9–2.6 per century) based on observations of gamma-ray emission from radioactive ^{26}Al within the MW (Timmes et al. 1997; Diehl et al. 2006).

4.6 The Rate Ratio as a Function of Galaxy Mass

We report the rate-size relation in §2.2 and offer more discussion of the possible causes in §4.2. One interesting question is whether the relative fractions of SNe also change with galaxy size. To investigate this, we divide the galaxies into different size bins for the “full-optimal” sample, calculate the SNuM rate ratios relative to the CC SN rates, and show them in Figure 23. We have included only spiral galaxies (Hubble type = 3–7) in this analysis because CC SN rates are negligible in E/S0 galaxies and very uncertain in Irr galaxies. Only the statistical errors are used to derive the ratios.

The ratio of the SN Ia to the CC SN rates shows a marginal ($\sim 1.5\sigma$) trend from the least to the most massive galaxies. The SN Ia rate is about 25% of the CC SN rate when the galaxy mass is smaller than $\sim 3 \times 10^{10} L_\odot$, and about 40% for the large galaxies. There are two likely causes for this trend. (a) The result of the different RSSs in the rate-size relation for the SNe Ia and the CC SNe. As $\text{SNuM(Ia)} \propto M^{-0.50}$ and $\text{SNuM(CC)} \propto M^{-0.55}$, the ratio $\text{SNuM(Ia)}/\text{SNuM(CC)}$ should increase with mass in proportion to $M^{0.05}$. (b) More massive galaxies have, on average, an earlier spiral Hubble type. As SNuM(Ia) is nearly constant in different galaxy Hubble types, and SNuM(CC) decreases significantly in earlier spiral galaxies, the $\text{SNuM(Ia)}/\text{SNuM(CC)}$ ratio should increase in earlier spiral or higher mass galaxies. Because of the uncertainties of the ratios, it is difficult to disentangle the relative contributions of these two causes.

The ratio of the SN Ibc to the overall CC SN rates is $\sim 35\%$ for galaxies with $M > 1.0 \times 10^{10} L_\odot$, and then declines to $\sim 10\%$ at $M = 0.15 \times 10^{10} L_\odot$. In other words, for the least massive galaxies, there are fewer SNe Ibc relative to the total population of CC SNe. This is consistent with the host-galaxy properties of the LF SNe as discussed in Paper II, where we found that the SN Ibc hosts are skewed toward more massive galaxies than the SN II hosts, possibly indicating a metallicity effect. However, we note again that the trend is of low significance ($\sim 2\sigma$). Arcavi et al. (2010) re-

ported that the SN Ibc fraction among the CC SNe does not change in dwarf galaxies, though with small-number statistics.

5 CONCLUSIONS AND FUTURE IMPROVEMENTS

This is the third installment of a series of papers aiming to derive the SN rates in the local Universe from the Lick Observatory SN Search (LOSS). The goal of this paper is to put together all of the ingredients from Papers I (Leaman et al. 2011) and II (Li et al. 2011) to derive the final rates for the most common types of SNe: Ia, Ibc, and II. We refer readers to Paper I for an outline of the series, and a detailed list of improvements of our rate calculation over past work. Section 1.1 of the current paper also has a short summary of the first two papers in the series. The conclusions that are specific to this paper are as follows.

(i) The control-time calculations for the galaxies are done numerically due to the combined complexity of the SN light curves, the limiting magnitudes, and the detection-efficiency curves. For each SN type, the luminosity functions are considered separately for two broad Hubble-type bins.

(ii) SN rates are traditionally expressed in units which are linearly normalised by the host-galaxy mass or luminosity (SNuM/SNuB/SNuK), but we find this to be an inadequate description of the data. The rates calculated in SNu units all demonstrate a correlation with galaxy sizes such that galaxies of smaller mass or luminosity have higher SN rates. As the result of this rate-size relation, our rates are derived for galaxies having a fiducial size, and correction factors with a rate-size power-law slope (RSS) are used to evaluate the rates for any given galaxy size. Another implication is that the SN frequency (SNe per year) for a galaxy is not linearly proportional to its size, but rather to size $^{1+{\rm RSS}}$.

(iii) The RSSs are found to have a strong dependence on the normalisation, the SN types, and the galaxy grouping methods. The RSSs for the two types of core-collapse SNe (Ibc and II) are in general consistent with each other. No apparent dependence on the galaxy Hubble types or colours is found, but this may be due to the limitation of the precision of our RSS measurements.

(iv) We have tested the robustness of our rate-calculation pipeline in several ways. The SN rates using different SN subsamples are in general consistent with each other. No systematic trend is found for the rates in different distance bins, or in galaxies of different angular sizes. The SN Ia rates are insensitive to the input SN luminosity function, but the core-collapse SNe are. When the SNe in the highly inclined galaxies ($i > 75^\circ$) are excluded from the rate calculations, the SN Ia and SN Ibc rates do not show a significant difference in the different inclination bins. The SNe II, however, exhibit a potential difference in the late-type spiral galaxies or galaxies having different $B - K$ colours. No inclination correction factor is used in our calculation, and the implication on the uncertainty is discussed.

(v) We use Poisson statistics to calculate the statistical uncertainty in the rates. For the systematic uncertainty, we consider several sources: the different SN samples, the different SN input luminosity functions, the uncertainties of the RSSs, the uncertainty caused by the treatment of the

inclination correction factors, and a universal miscellaneous uncertainty. The systematic uncertainty is comparable to the statistical uncertainty in most cases ($\sim 20\%$), but can be as high as 80% of the measurements for the SN II rates in late-type spiral galaxies due to the uncertain inclination corrections.

(vi) The SN Ia rate in a galaxy of the fiducial size with the B -band luminosity normalisation (SNuB) declines from the early- to the late-type galaxies, and from the red to the blue galaxies, likely due to the increasing influence of very massive stars in the total B -band luminosity in the blue, late-type galaxies. The core-collapse SN rates are small in the early-type (E-S0) and red galaxies, and increase toward late-type and blue galaxies.

(vii) For the rates in a galaxy of the fiducial size with the K -band luminosity or the mass as the normalisation (SNuK or SNuM), the SN Ia rate is nearly constant among different Hubble types. The core-collapse SN rates in general have an increasing trend from early-type to late-type, and red to blue, galaxies. However, the SN Ibc rate may decline for the bluest galaxy bins or from Sc to Irr galaxies.

(viii) Our average SN rates for galaxies of different Hubble types or colours agree with the published results to within uncertainties when the rates are calculated in the same manner (in particular, without adopting the rate-size relation in our rate calculations).

(ix) While the rate-size relation for the core-collapse SNe may be linked to the connection between the specific star-formation rate and the galaxy sizes, it is not clear that such a link can be established for the SNe Ia. It is important to investigate whether the RSSs are universal in galaxies of different properties such as Hubble type, colours, and specific star-formation rates. Numerically, the rate-size relation indicates that the SN rates cannot be adequately parameterised by a single parameter using galaxy Hubble types or $B - K$ colours.

(x) We attempt to fit the SN Ia rates with the two-component model of Mannucci et al. (2005) and Scannapieco & Bildsten (2005). We find that the model is affected by the choice of the normalisation for the rates, the rate-size relation, and the way the galaxies are grouped (Hubble type or colour). There may not be a one-to-one correlation or physical connection between the SN Ia and the core-collapse SN rates. The SN Ia rates in young stellar populations may have a strong correlation with the core-collapse SN rates.

(xi) We derive a local volumetric rate of 0.301 ± 0.062 , 0.258 ± 0.072 , and 0.447 ± 0.139 for SNe Ia, Ibc, and II, respectively (in units of 10^{-4} SN Mpc $^{-3}$ yr $^{-1}$). The uncertainties of these rates are dominated by the uncertainties in the galaxy luminosity density used to convert our per-galaxy rates to volumetric rates.

(xii) We derive a SN rate of 2.84 ± 0.60 per century for the Milky Way (to within a systematic factor of ~ 2 , dominated by the uncertainty in the properties of the Galaxy), consistent with previous estimates.

(xiii) The ratio of the SN Ibc rate to the total core-collapse SN rate declines for the least massive galaxies, perhaps indicating a metallicity effect on the binary evolution of massive stars.

While the first three papers in this series conclude our investigation for the rates of the most common SN types

(Ia, Ibc, and II) in galaxies of different Hubble types and $B - K$ colours, more analysis is underway to determine our rates for the “known unknowns” — the rare and peculiar transients and SNe in our search. We also plan to investigate the SN rates in additional categories of galaxies, such as radio and other active galaxies, interacting galaxies, and cluster versus field galaxies. In addition, we are in the process of deriving more physical parameters for our sample galaxies, such as the star-formation rates. One important study, for example, is to check whether there is a rate-size relation when the galaxies are grouped among different (specific) star-formation rates.

We are continuing our SN search in order to decrease the statistical uncertainties. As discussed throughout this series, even though we have a large number of SNe in the rate calculations, the measurements of the rates and certain parameters will benefit from a even larger sample of SNe. In particular, improved precision on the RSSs will provide information on whether they are insensitive to the galaxy properties and thus are universal, which in turn will constrain the origin of the rate-size relation; improved precision on the rates will help determine their dependence on the galaxy inclinations; more SNe discovered in the Irr galaxies will improve the precision of the rather poor measurements reported in this series. We plan to improve our rate-calculation pipeline so that the rates may be easily updated with new SN discoveries and monitoring history information.

ACKNOWLEDGMENTS

We thank the referee, Enrico Cappellaro, for useful comments and suggestions which helped improve the paper. We are grateful to the many students, postdocs, and other collaborators who have contributed to the Katzman Automatic Imaging Telescope and the Lick Observatory Supernova Search over the past two decades, and to discussions concerning the determination of supernova rates — especially Ryan Foley, Saurabh Jha, Maryam Modjaz, Frank Serduke, Jeffrey Silverman, Nathan Smith, Thea Steele, and Richard Treffers. Assaf Horesh helped make Figure 21. We thank the Lick Observatory staff for their assistance with the operation of KAIT. LOSS, conducted by A.V.F.’s group, has been supported by many grants from the US National Science Foundation (NSF; most recently AST-0607485 and AST-0908886), the TABASGO Foundation, US Department of Energy SciDAC grant DE-FC02-06ER41453, and US Department of Energy grant DE-FG02-08ER41563. KAIT and its ongoing operation were made possible by donations from Sun Microsystems, Inc., the Hewlett-Packard Company, AutoScope Corporation, Lick Observatory, the NSF, the University of California, the Sylvia & Jim Katzman Foundation, and the TABASGO Foundation. We give particular thanks to Russell M. Genet, who made KAIT possible with his initial special gift; former Lick Director Joseph S. Miller, who allowed KAIT to be placed at Lick Observatory and provided staff support; and the TABASGO Foundation, without which this work would not have been completed. J.L. is grateful for a fellowship from the NASA Postdoctoral Program. D.P. is supported by an Einstein Fellowship. X.W. acknowledges NSFC grants (10673007, 11073013) and the China-973 Program 2009CB824800. We made use of the

NASA/IPAC Extragalactic Database (NED), which is operated by the Jet Propulsion Laboratory, California Institute of Technology, under contract with NASA. We acknowledge use of the HyperLeda database (<http://leda.univ-lyon1.fr>).

REFERENCES

- Arcavi I., et al. 2010, ApJ, 721, 777
 Barris B. J., Tonry J. L. 2006, ApJ, 637, 427
 Bartunov O. S., Tsvetkov D. Yu., Filimonova I. V 1994, PASP, 106, 1276
 Bazin G., et al. 2009, A&A, 499, 653
 Blanc G., et al. 2004, A&A, 423, 881
 Botticella M. T., et al. 2008, A&A, 479, 49
 Bottinelli L., Gouguenheim L., Paturel G., Teerikorpi P. 1995, A&A, 296, 64
 Brandt T. D., Tojeiro R., Aubourg É., Heavens A., Jimenez R., Strauss M. A. 2010, AJ, 140, 804
 Cappellaro E., Turatto M., Benetti S., Tsvetkov D. Yu., Bartunov O. S., Makarova I. N. 1993, A&A, 273, 383
 Cappellaro E., Turatto M., Tsvetkov D. Yu., Bartunov O. S., Pollas C., Evans R., Hamuy M. 1997, A&A, 322, 431 (C97)
 Cappellaro E., Evans R., Turatto M. 1999, A&A, 351, 459 (C99)
 Cappellaro E., et al. 2005, A&A, 430, 83
 Dahlen T., et al. 2004, ApJ, 613, 189
 Dahlen T., Strolger L.-G., Riess A. G. 2008, ApJ, 681, 462
 Dallaporta N. 1973, A&A, 29, 393
 Diehl R., et al. 2006, Nature, 439, 45
 Dilday B., et al. 2008, ApJ, 682, 262
 Filippenko A. V., Li W., Treffers R. R. 2011, in prep.
 Filippenko A. V., Li W., Treffers R. R., Modjaz M. 2001, in Small-Telescope Astronomy on Global Scales, ed. W. P. Chen, C. Lemme, & B. Paczyński (San Francisco: ASP), 121
 Gehrels N. 1986, ApJ, 303, 336
 Greggio L. 2005, A&A, 441, 1055
 Hachisu I., Kato M., Nomoto K. 2008, ApJ, 683, L127
 Hardin D., et al. 2000, A&A, 362, 419
 Hopkins A. M., Beacom J. F. 2006, ApJ, 651, 142
 Horesh A., Poznanski D., Ofek E. O., Maoz D. 2008, MNRAS, 389, 1871
 Kochanek C. S., et al. 2001, ApJ, 560, 566
 Leaman J., et al. 2011, MNRAS, submitted (Paper I)
 Li W., et al. 2000, in Cosmic Explosions, ed. S. S. Holt & W. W. Zhang (New York: AIP), 103
 Li W., et al. 2011, MNRAS, submitted (Paper II)
 Lipunov V. M., Panchenko I. E., Pruzhinskaya M. V. 2010, New Astronomy, in press (arXiv:1005.4134)
 Madgwick D. S., Hewett P. C., Mortlock D. J., Wang L. 2003, ApJ, 599, L33
 Mannucci F., Buttery H., Maiolino R., Marconi A., Pozzetti L. 2007, A&A, 461, 423
 Mannucci F., Della Valle M., Panagia N. 2006, MNRAS, 370, 773
 Mannucci F., Della Valle M., Panagia N., Cappellaro E., Cresci G., Maiolino R., Petrosian A., Turatto M. 2005, A&A, 433, 807 (M05)
 Mannucci, F. 2008, Chinese Journal of Astronomy and Astrophysics Supplement, 8, 143
 Mannucci F., Maoz D., Sharon K., Botticella M. T., Della Valle M., Gal-Yam A., Panagia N. 2008, MNRAS, 383, 1121
 Maoz D., Mannucci F., Li W., Filippenko A. V., Della Valle M., Panagia N. 2011, MNRAS, in press (arXiv:1002.3056)
 Neill J. D., et al. 2006, AJ, 132, 1126
 Neill J. D., et al. 2007, in The Multicoloured Landscape of Compact Objects and Their Explosive Origins, ed. T. Di Salvo, et al. (New York: AIP), 421
 Neill J. D., et al. 2009, ApJ, 707, 1449
 Noeske K. G., et al. 2007a, ApJ, 660, L43
 Noeske K. G., et al. 2007b, ApJ, 660, L47
 Oemler A., Jr., Tinsley, B. M. 1979, AJ, 84, 985
 Perets H. B., et al. 2010, Nature, 465, 322
 Pritchett C. J., Howell D. A., Sullivan M. 2008, ApJ, 683, L25
 Riess A. G., et al. 2009, ApJ, 699, 539
 Salim S., et al. 2007, ApJS, 173, 267

- Scannapieco E., Bildsten L. 2005, ApJ, 629, L85
Schiminovich D., et al. 2007, ApJS, 173, 315
Smith N., et al. 2011, MNRAS, in press
Spergel D. N., et al. 2007, ApJS, 170, 377
Sullivan M., et al. 2006, ApJ, 648, 868
Tammann G. A. 1974, in Supernovae and Supernova Remnants,
ed. C. B. Cosmovici (Dordrecht: Reidel), 155
Timmes F. X., Diehl R., Hartmann D. H. 1997, ApJ, 479, 760
Tonry J. L., et al. 2003, ApJ, 594, 1
van den Bergh S. 1988, Comments on Astrophysics, 12, 131
van den Bergh S. 1991, Physics Reports, 204, 385
van den Bergh S., Tammann G. A. 1991, ARAA, 29, 363
van den Bergh S., McClure R. D. 1994, ApJ, 425, 205
van der Kruit P. C. 1987, NATO ASIC Proc. 207: The Galaxy,

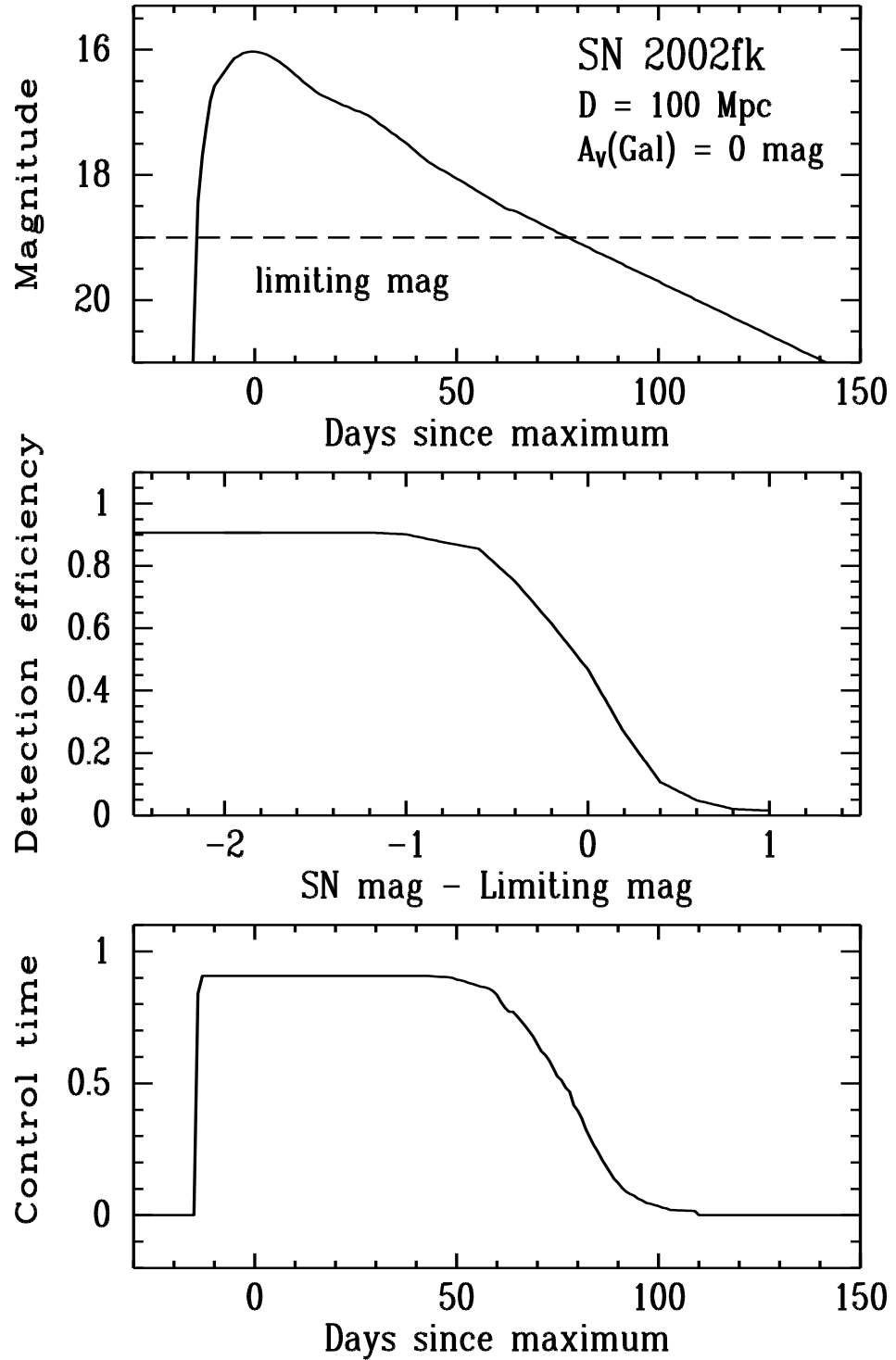


Figure 1. An example of the control-time calculation. *Top panel:* The apparent light curve of SN 2002fk in a galaxy at 100 Mpc, with no Milky Way extinction. The limiting magnitude (19) is marked by the dashed line. *Middle panel:* The detection-efficiency curve for the galaxy (assumed to be of type Sb–Sbc), as adopted from Paper I. *Bottom panel:* The control-time curve. The curve generally has a rising, a constant, and a declining portion.

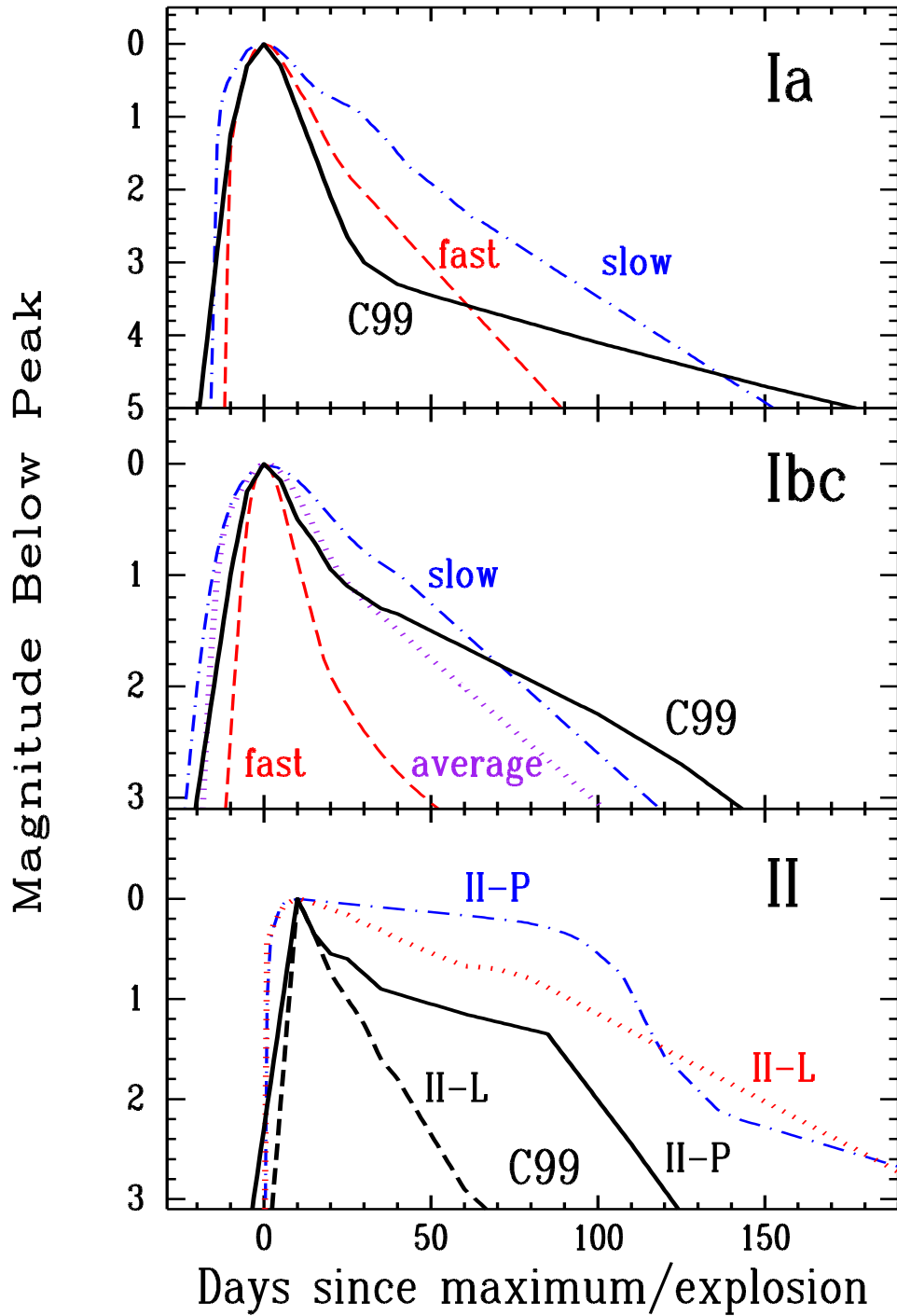


Figure 2. A comparison of the light curves adopted in our rate calculation and those used by C99. The C99 light curves are the thick solid or dashed lines. There is a dramatic difference between the two light-curve sets due to the different passbands used in the surveys, and a direct comparison is not very meaningful.

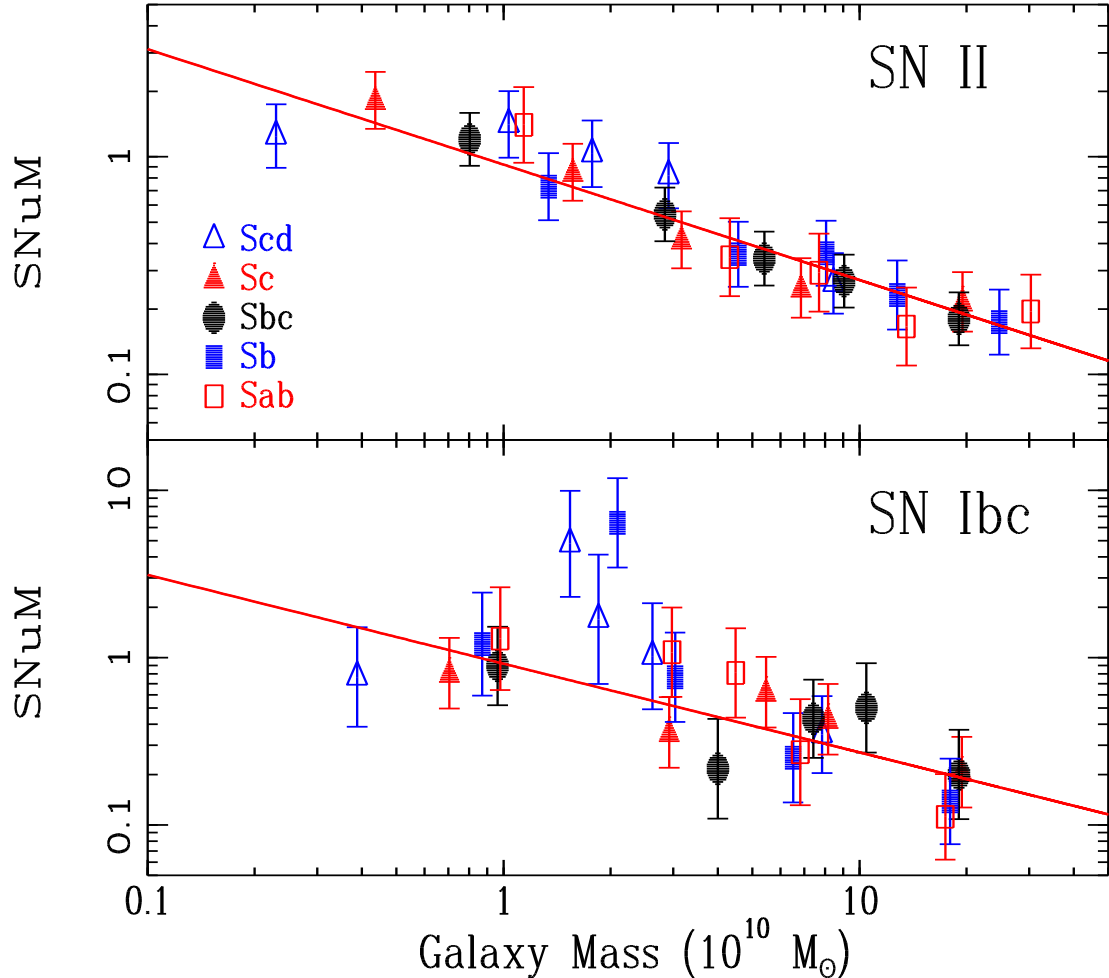


Figure 3. The core-collapse SN rates (in SNUM) in galaxies of different masses. *Top panel:* The SNe II in Sab–Scd galaxies are split into 7 bins according to the mass of their host galaxies, and the rates (SNUM) are calculated for each mass bin. A χ^2 -minimizing technique is used to scale and fit the rates with the solid curve (using the rates in the Sbc galaxy bins as the anchor points), which has a power-law index of -0.55 . *Bottom panel:* The same as the top panel, but for the rates of SNe Ibc. The rates in different galaxy Hubble types are scaled to be fit by the linear curve derived from the SN II rates as shown in the top panel. A similar relation exists between the SNUK rates and galaxy L_K , and the SNUB rates and galaxy L_B , but it is not shown here for clarity.

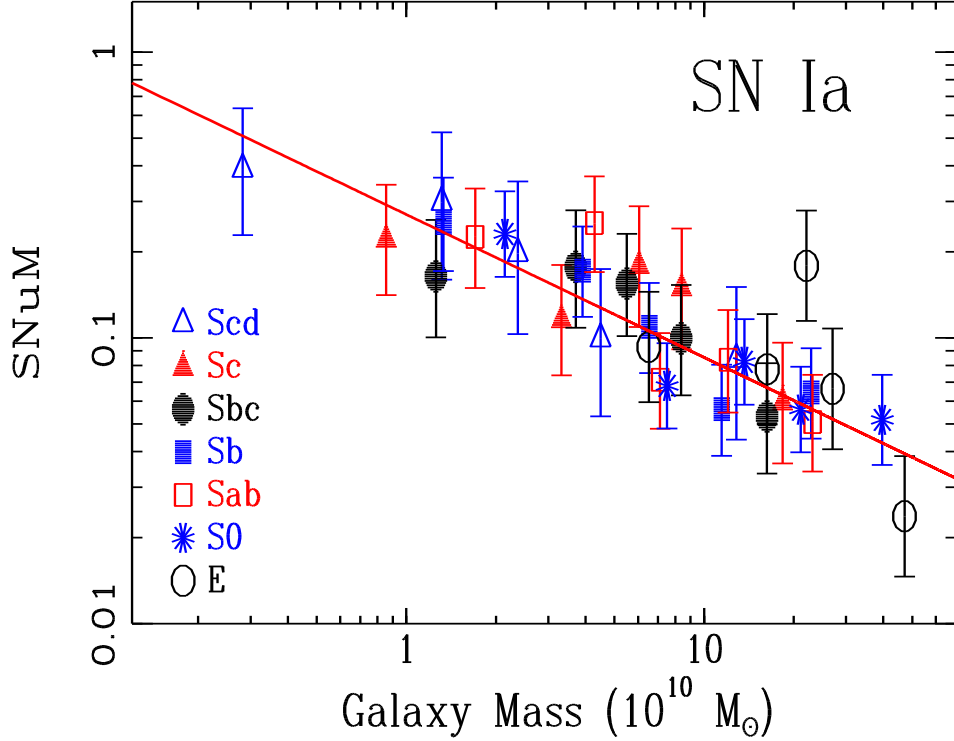


Figure 4. Same as the top panel of Figure 3, but for the SNuM rates of SNe Ia. The rates for the different Hubble types have been scaled up and down to match the normalisation for the Sb galaxies, which have been used as anchor points for the fit. The solid curve has a power-law index of -0.50 . The SNuK and SNuB rates have similar dependences on galaxy L_K and L_B , respectively, but are not shown here for clarity.

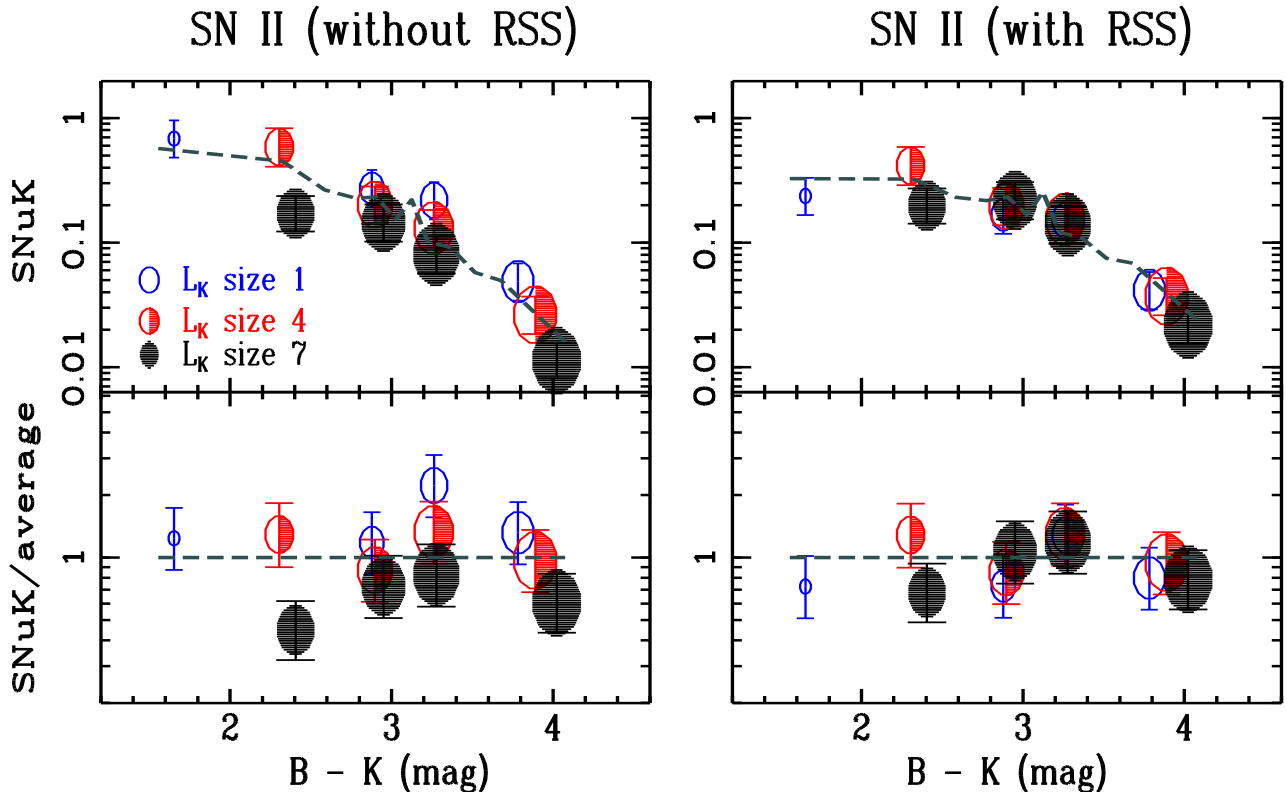


Figure 5. The rate-size relation for the SN rates with different galaxy $B - K$ colours. The SNuK rates of SNe II are used as an example (the SNuB and SNuM rates of SNe II, and the SN Ia rates, all exhibit a similar relation). The left and right panels show the SNuK rates as a function of galaxy $B - K$ colour without and after considering the rate-size relation, respectively, while the top and bottom panels display the original rates and the rates after being normalised by the average measurements (the dashed lines), respectively. For each panel, the galaxies are first divided into 4 $B - K$ colour groups (same symbol, left to right). For each colour group, the galaxies are then divided into 7 L_K bins (different symbols). For clarity, only 3 size bins are shown from the smallest (i.e., size bin 1, open circles) to the intermediate (size bin 4, half-solid circles) to the largest (size bin 7, solid circles). The size of the symbol is proportional to the logarithm of the average L_K value of each bin. The left panels exhibit a systematic trend in which the less massive galaxy bins have higher rates (for the same colour group). After considering the rate-size relation (with RSS = -0.38), this trend is gone (the right panels).

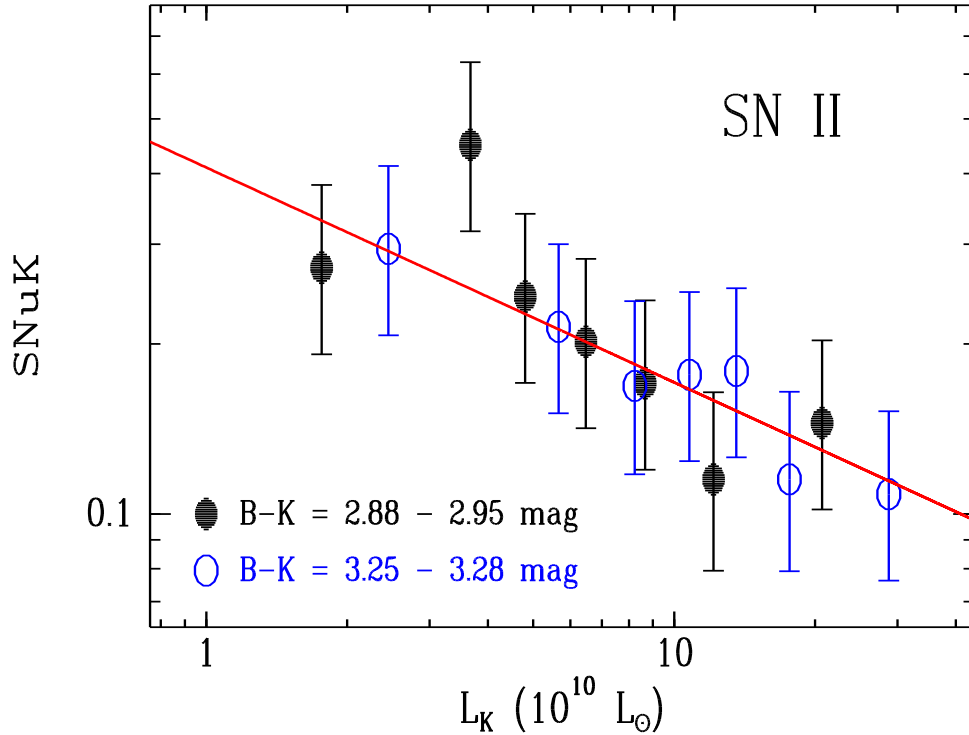


Figure 6. A further demonstration of the rate-size relation for the SNuK rates of SNe II in two narrow ranges of galaxy $B - K$ colour: the solid circles are for the galaxies with average $B - K$ colour of 2.88–2.95 mag (used as the anchor points), and the open circles are for $B - K = 3.25 - 3.28$ mag. Since there are only minimal differences in the $B - K$ colours within the same colour group, the correlation between SNuK and L_K is close to the intrinsic rate-size relation, shown as the solid line (with RSS = −0.38).

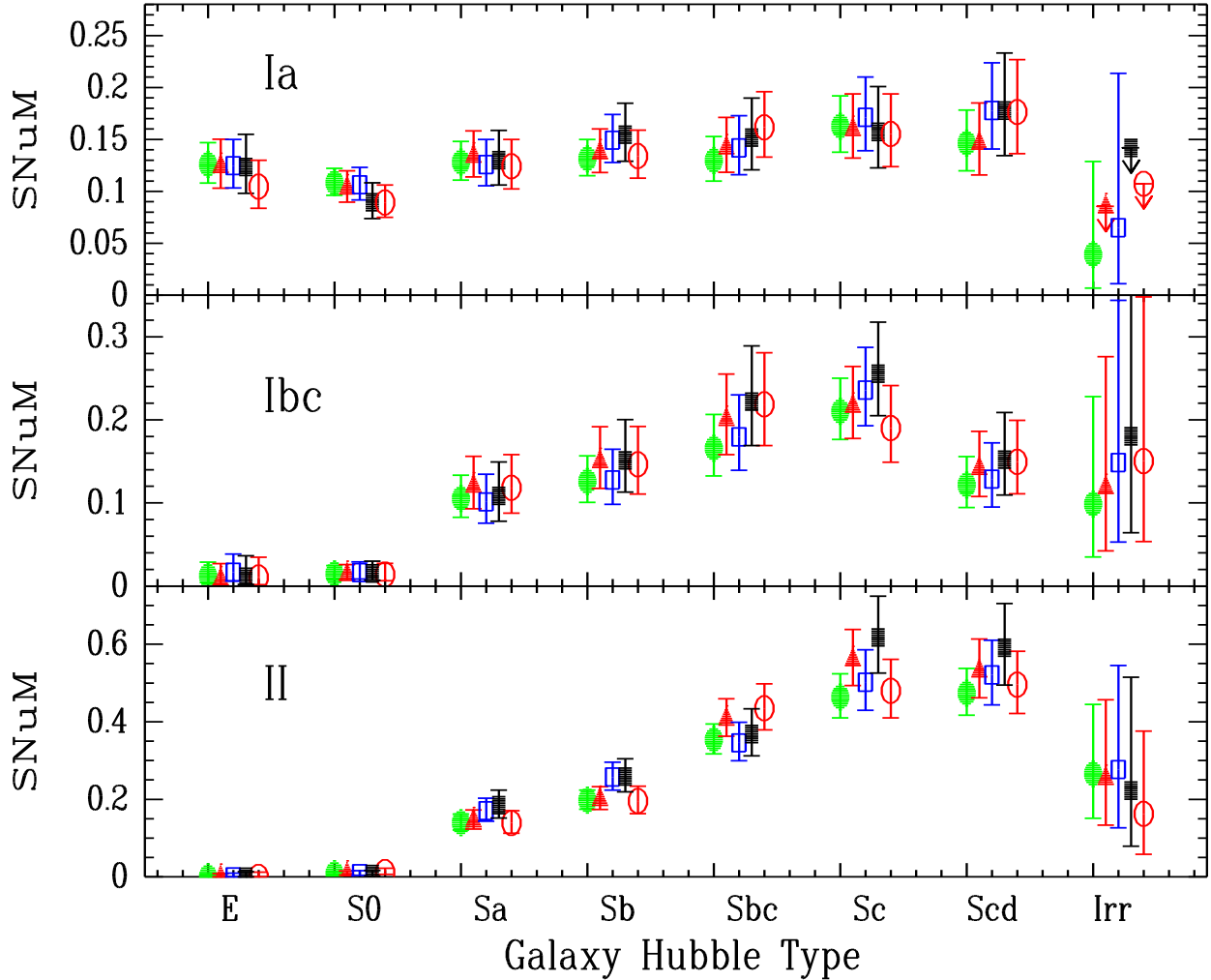


Figure 7. The SN rates (for a galaxy of the fiducial size) from different SN samples. Solid dots: the “full” sample (total number of SNe = 929). Triangles: the “full-optimal” sample (total = 726). Open squares: the “season” sample (total = 656). Solid squares: the “season-optimal” sample (total = 499). Open circles: same as the “full-optimal” sample but only with SNe discovered before the end of 2006.

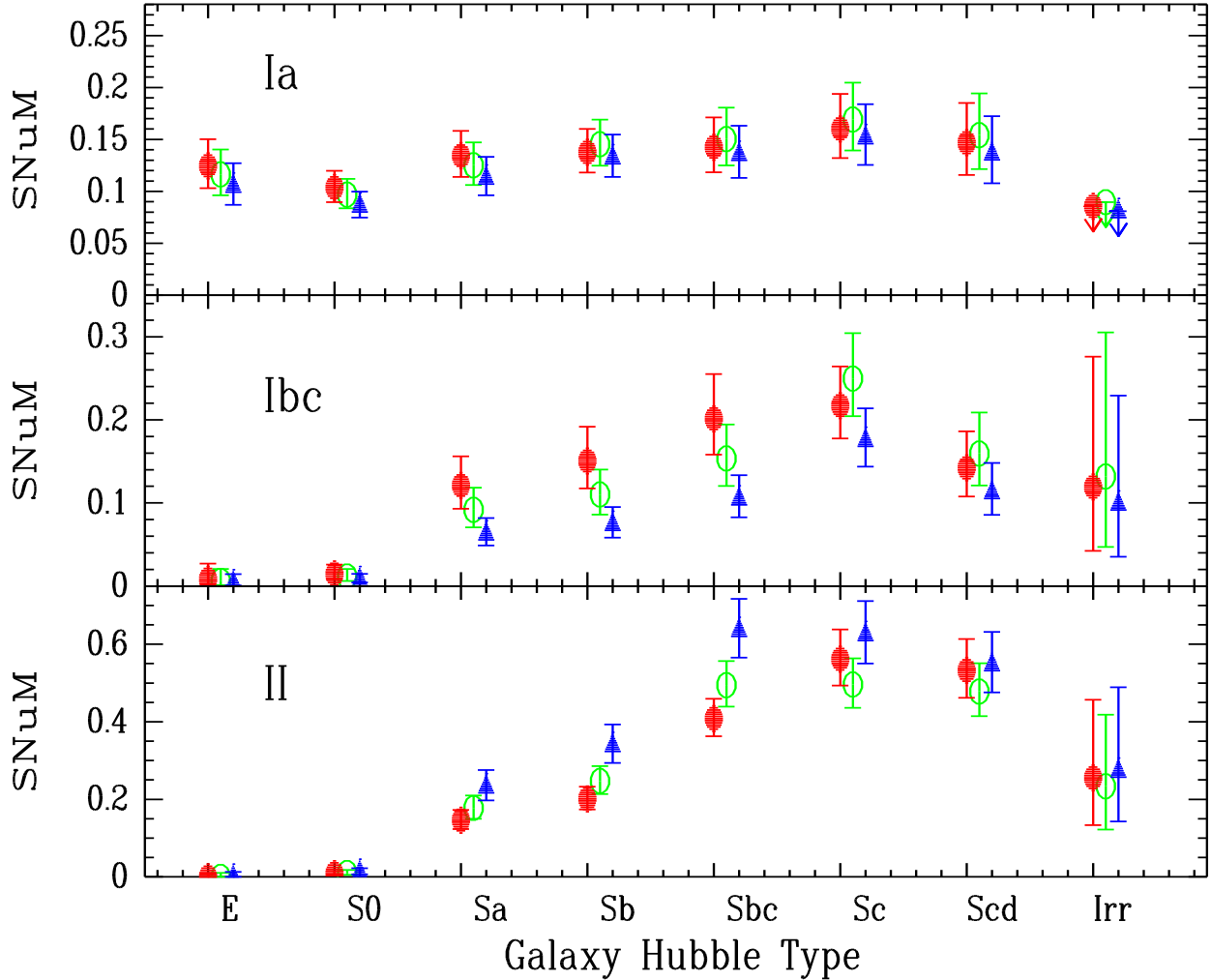


Figure 8. The SN rates (for a galaxy of the fiducial size) using different input LFs and light-curve shapes. Solid dots: two LFs are used for each type of SN. Open circles: a single LF is used for each SN type. Triangles: the C99 light curves (i.e., no LF) are used.

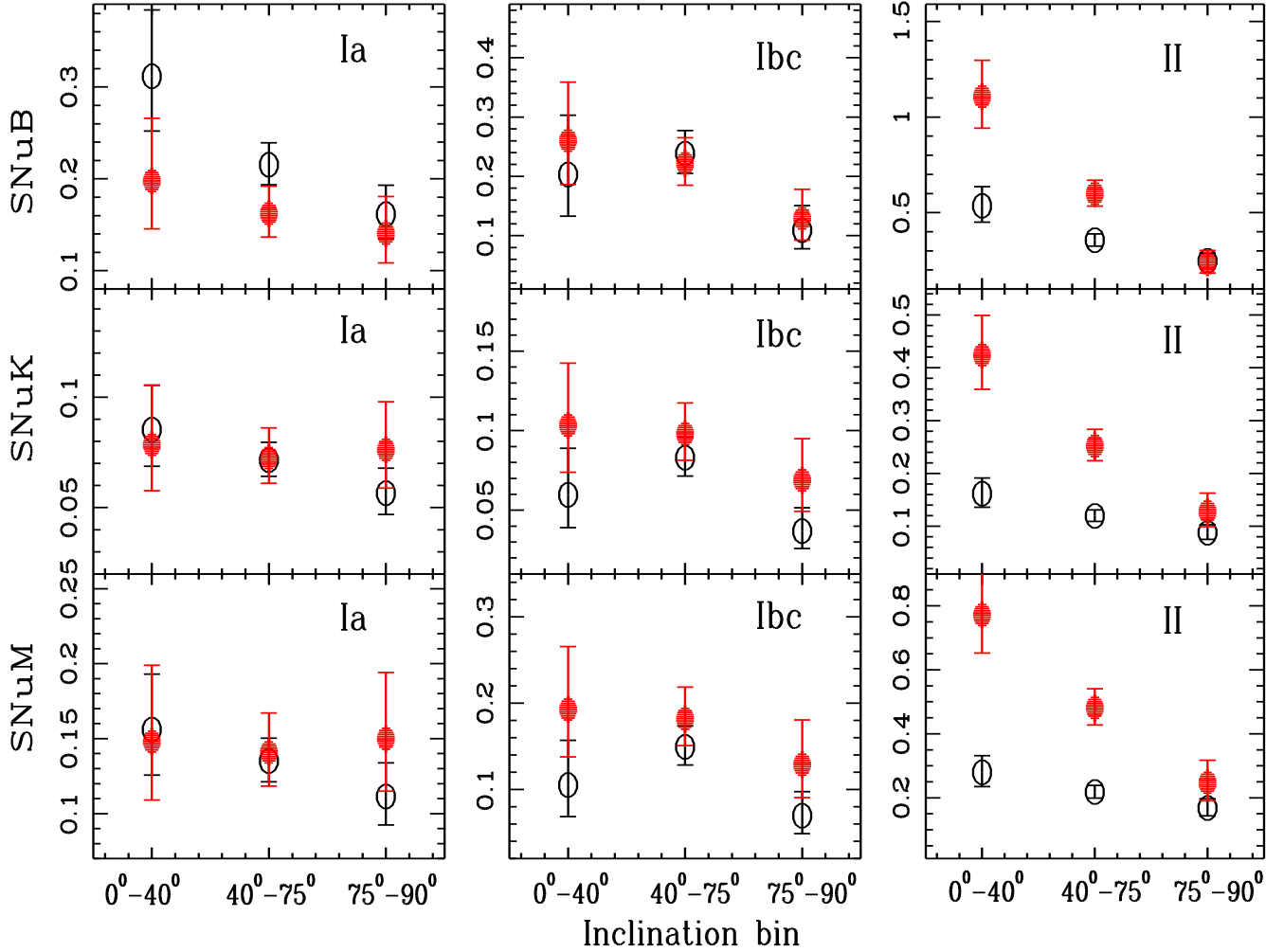


Figure 9. The SN rates (for a galaxy of the fiducial size) in different inclination bins. The solid dots are for the rates in late-type spiral galaxies (Sc–Scd), while the open circles are for the early-type spirals (Sa–Sbc). From left to right are the rates for the SNe Ia, Ibc, and II, respectively. From top to bottom are the rates using different normalisations.

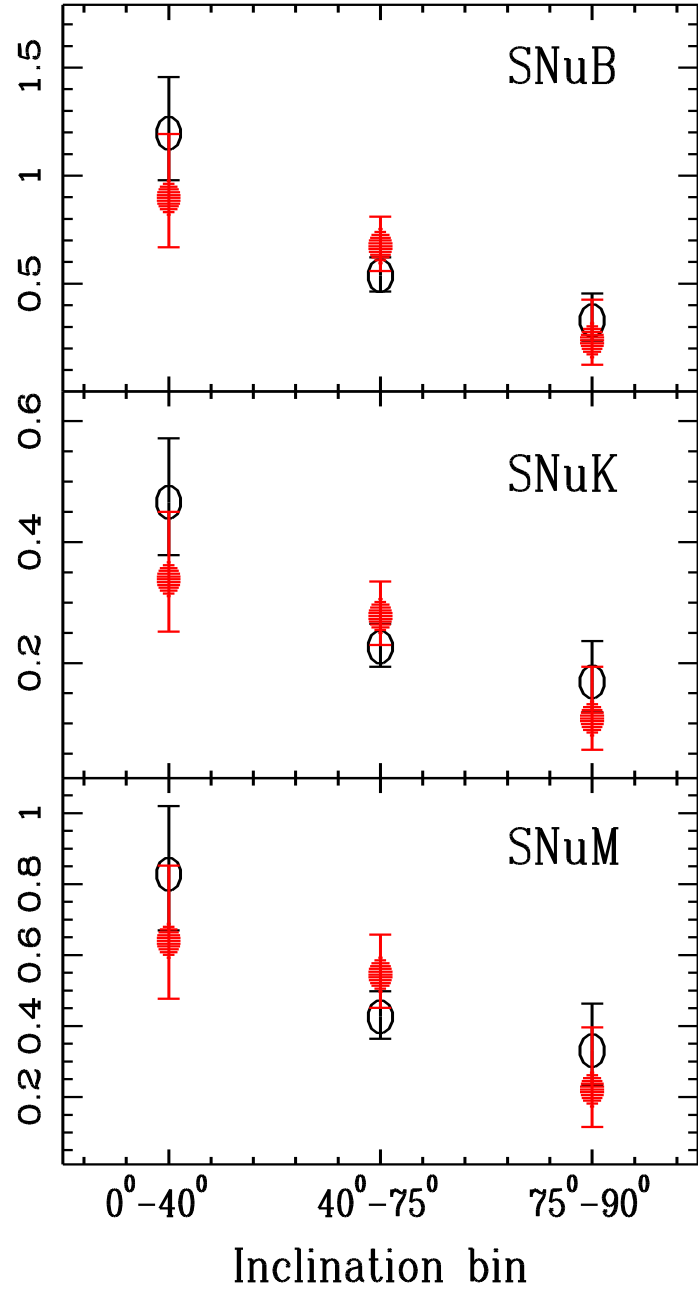


Figure 10. The SN II rates (for a galaxy of the fiducial size) in the late-type spirals (Sc–Scd) in different inclination bins. The open circles are for the rates in the galaxies within 75 Mpc, while the solid dots are for the rates in the galaxies more distant than 75 Mpc.

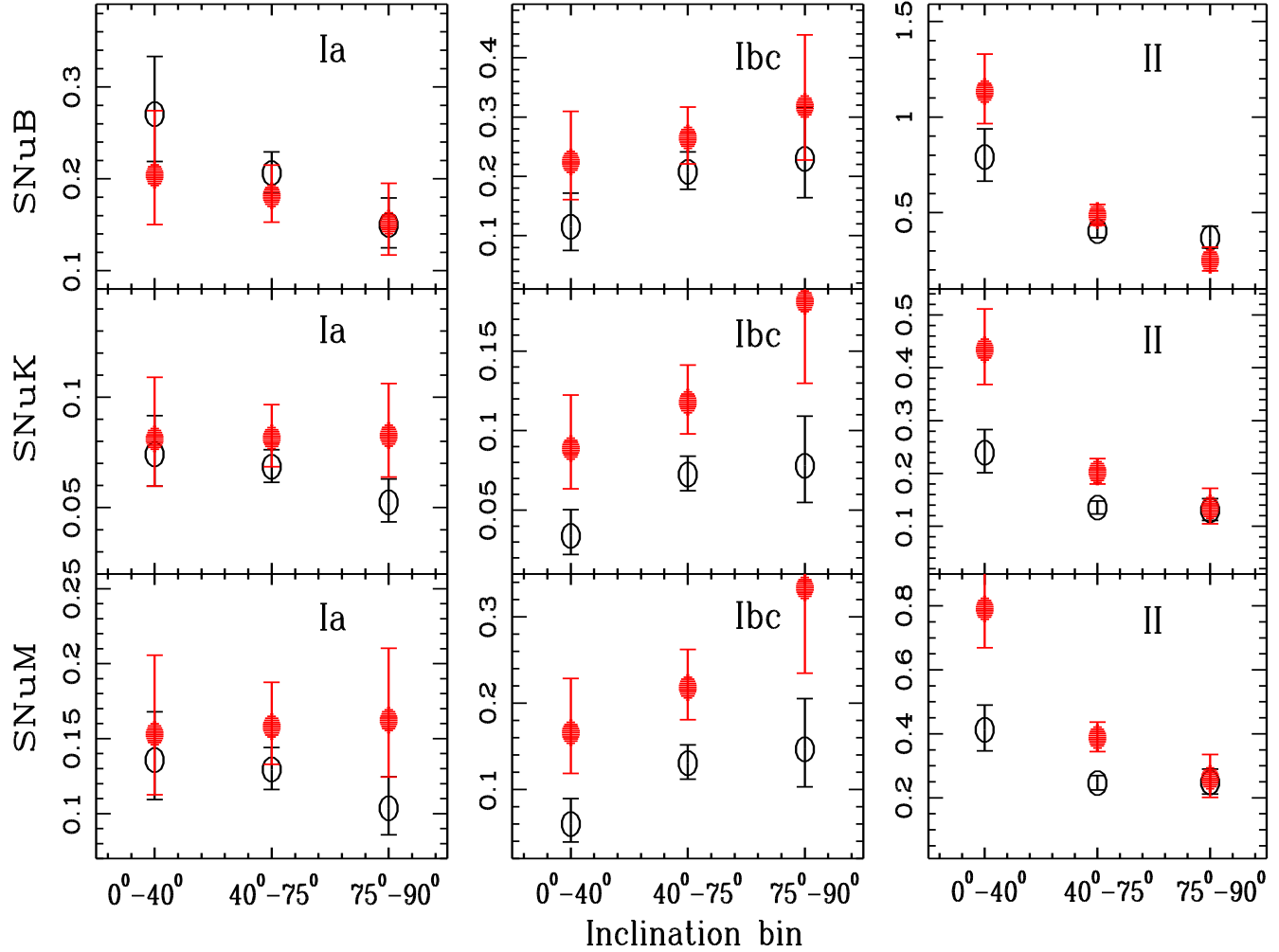


Figure 11. The same as Figure 9, but with the LF SNe divided into different inclination bins when the control time is calculated. In other words, the LF is constructed separately for each inclination bin, using the SNe in the LF sample whose host-galaxy inclinations fall into the same inclination bin.

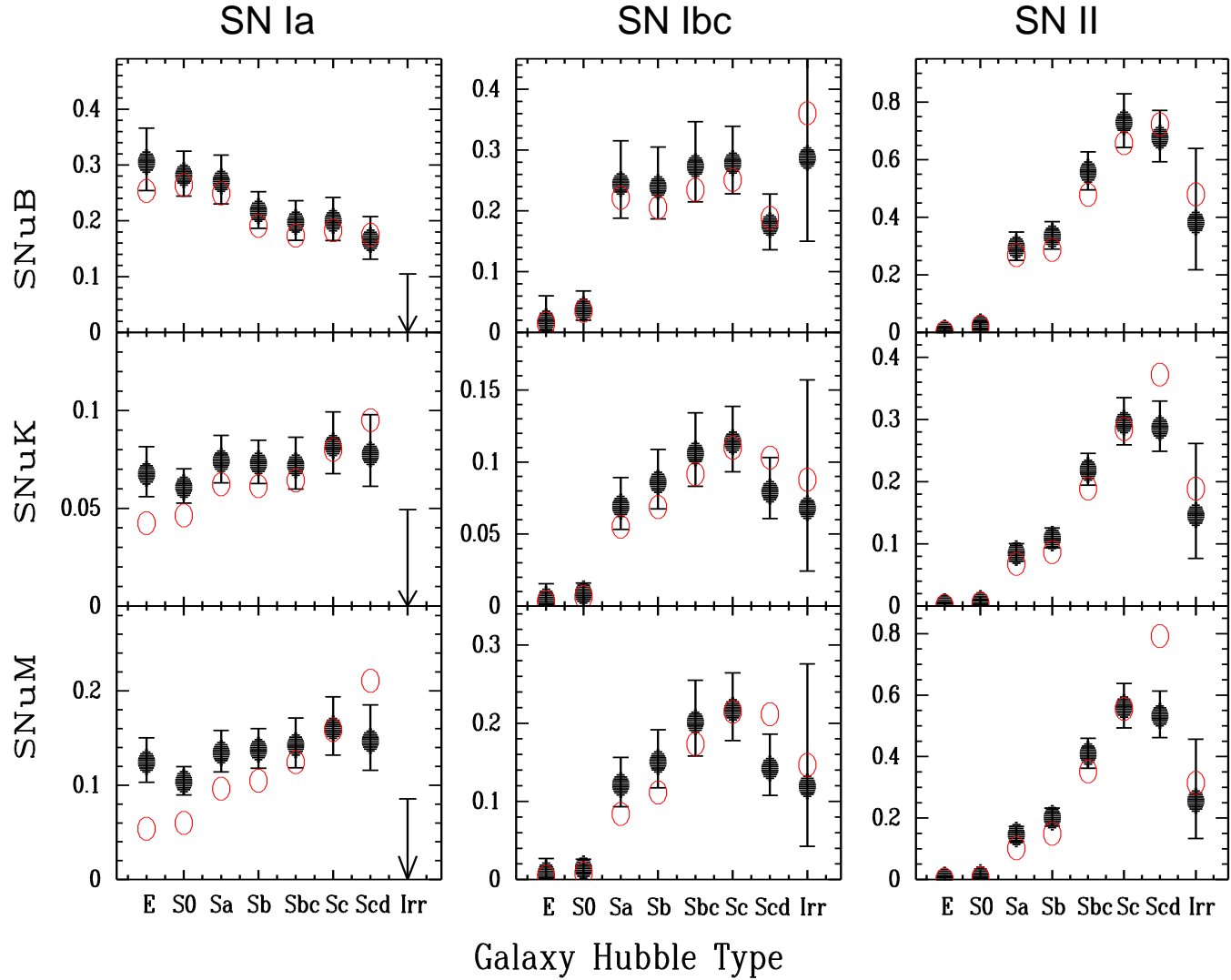


Figure 12. The SN rates (for a galaxy of the fiducial size) for galaxies of different Hubble types (solid circles). The open circles without error bars are the rates evaluated at the median galaxy size in each Hubble-type bin.

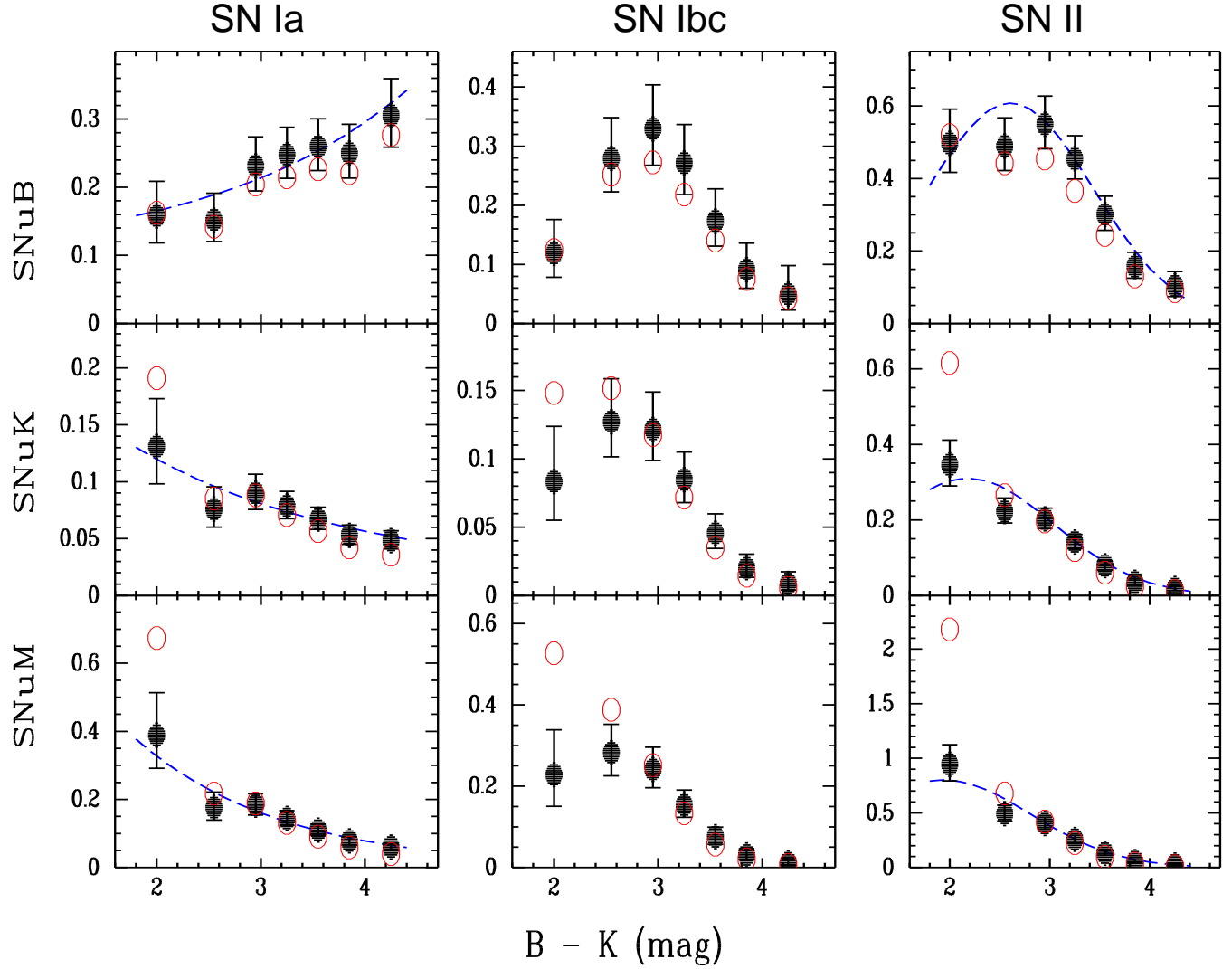


Figure 13. Same as Figure 12, but for galaxies having different $B - K$ colours (solid circles). The open circles without error bars are the rates evaluated at the median galaxy size in each colour bin. The dashed lines represent the second-order polynomial fits (as a function of $B - K$ colour) for the logarithm of the rates as determined during the multivariate linear regression model analysis in §2.2.

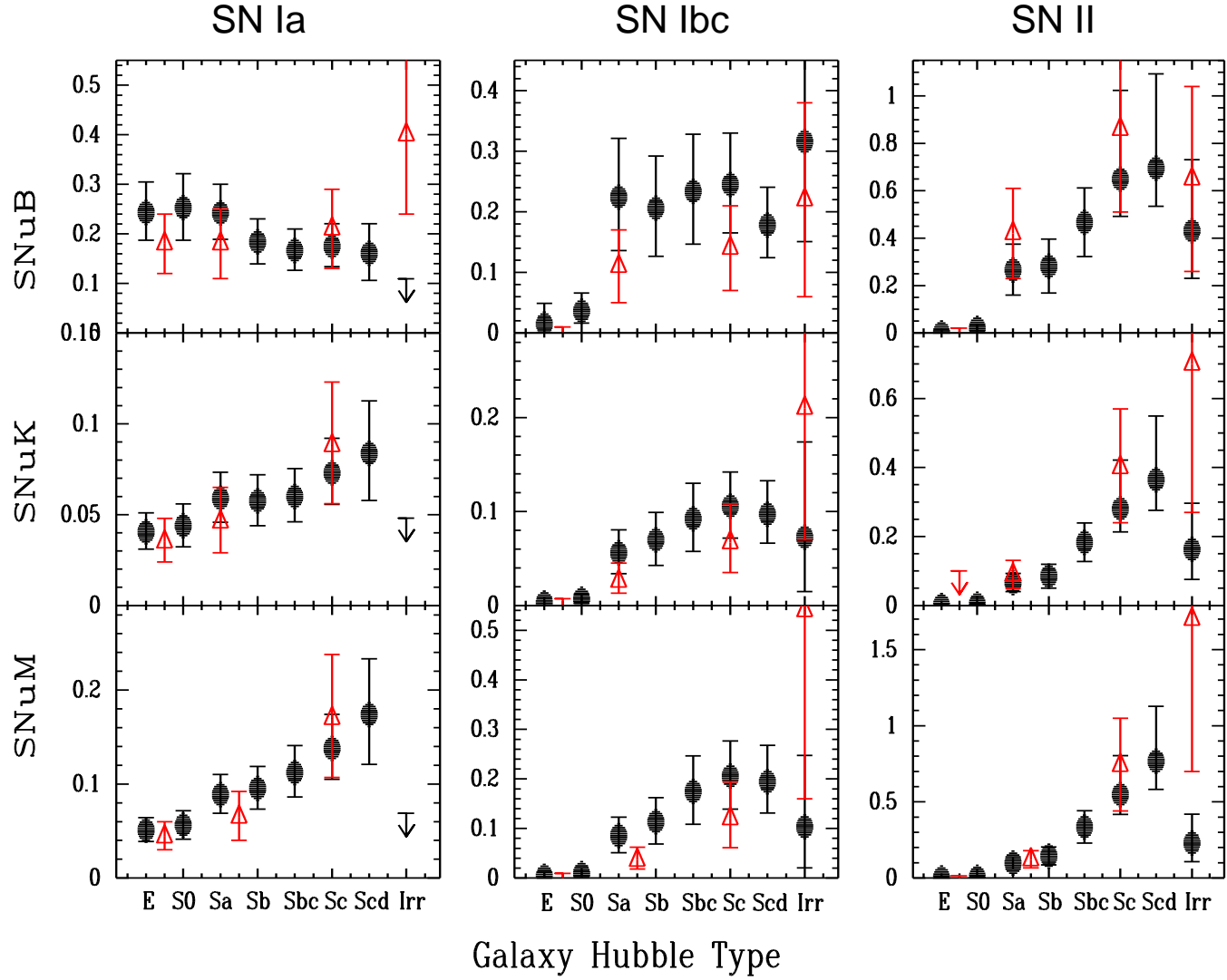


Figure 14. Comparison with published results. To mimic the past calculations, our rates (the solid dots) are calculated without using RSSs, so they are the average for the galaxies with different sizes. The published results (open triangles) come from C99 (SNuB) and M05 (SNuK and SNuM). The M05 SNuK and SNuM rates for SNe Ia in Irr galaxies are off the scale of the plot (higher than the ordinate limit).

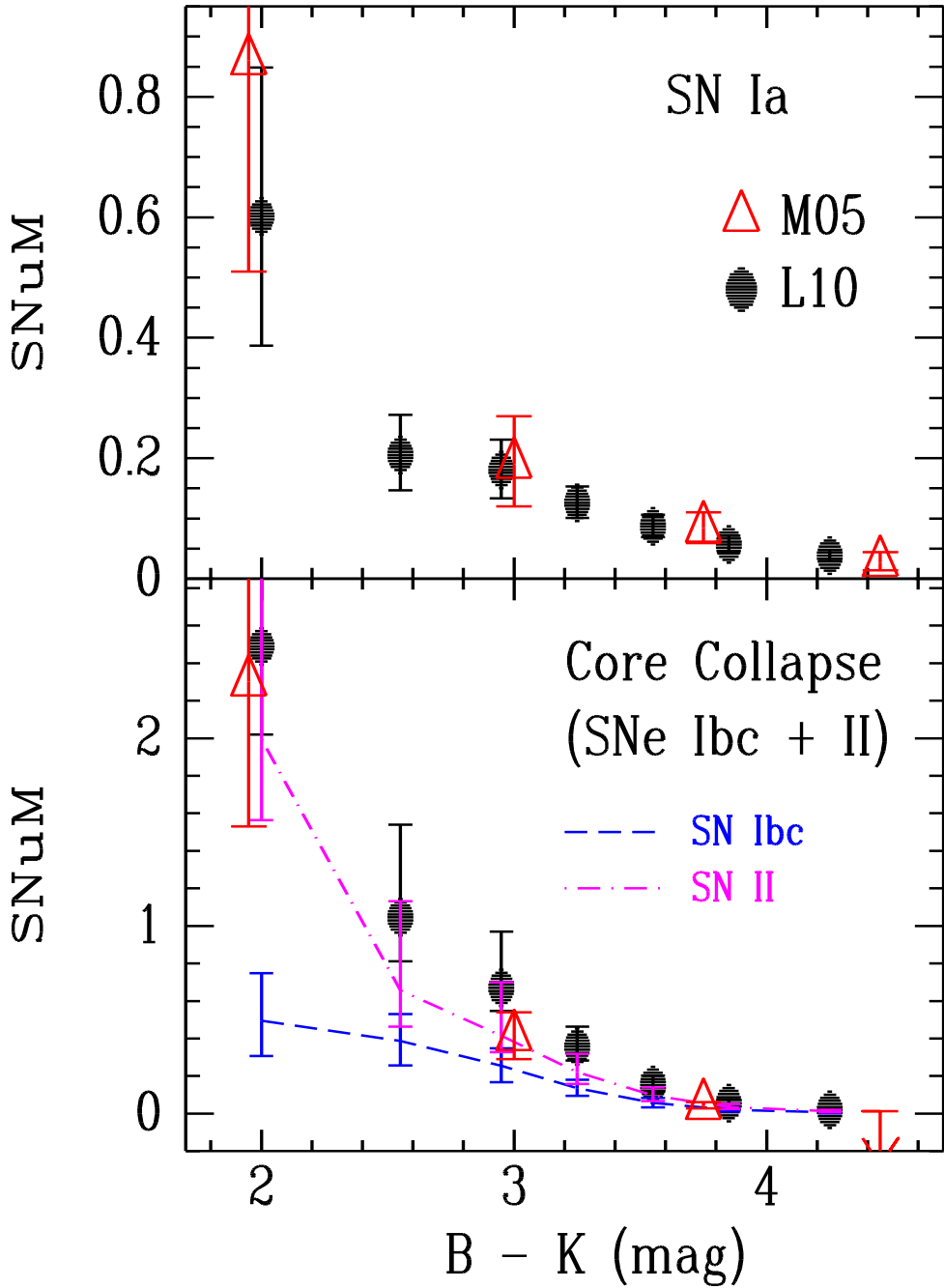


Figure 15. The same as Figure 14, but for the SNUm rates in galaxies having different $B - K$ colours. The dashed and the dash-dotted lines in the bottom panel show the contribution of the SN Ibc and SN II rates to the total core-collapse SN rates, respectively.

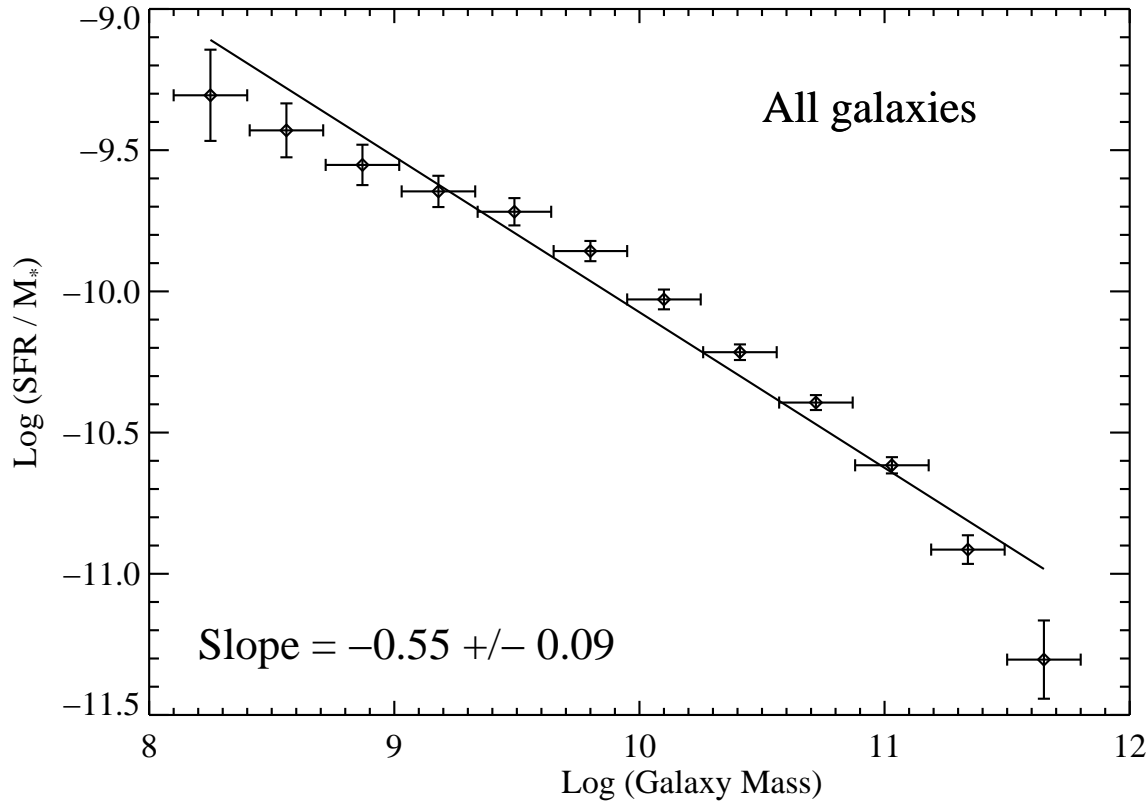


Figure 16. The correlation between the specific star-formation rate and the galaxy stellar mass. This is an integration of the published contour map in Figure 7 of Schiminovich et al. (2007). The linear fit (the solid line) gives a power-law index of -0.55 ± 0.09 , similar to that of the rate-size relation for the core-collapse SNe.

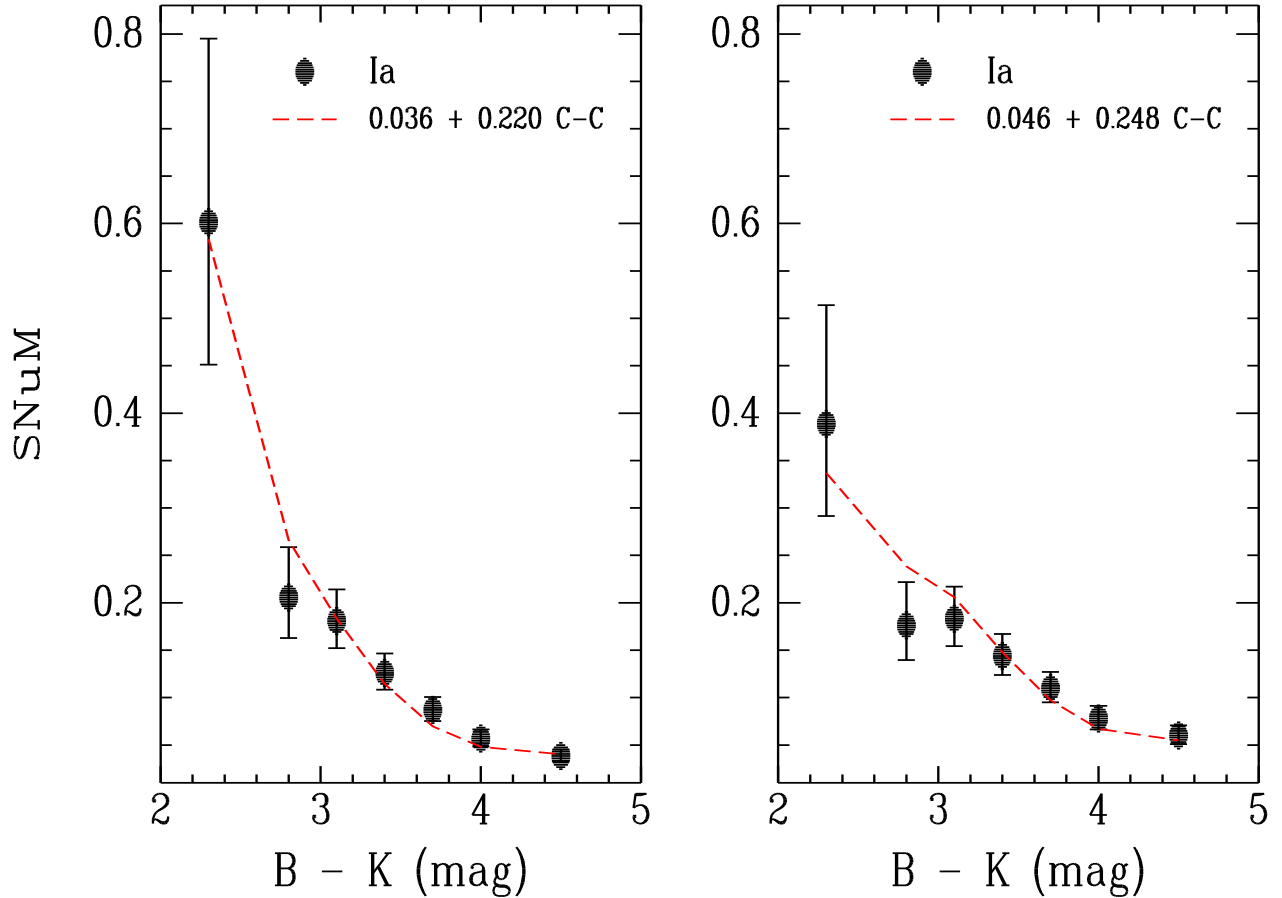


Figure 17. The two-component model fits for the SN Ia rates when SNUM versus galaxy $B - K$ colour are considered. The left panel shows the model fit for the average galaxy size (i.e., no RSSs are used), while the right panel shows the fit for the fiducial galaxy size (i.e., RSSs are used). Both fits have $\chi^2/\text{DOF} < 1.0$.

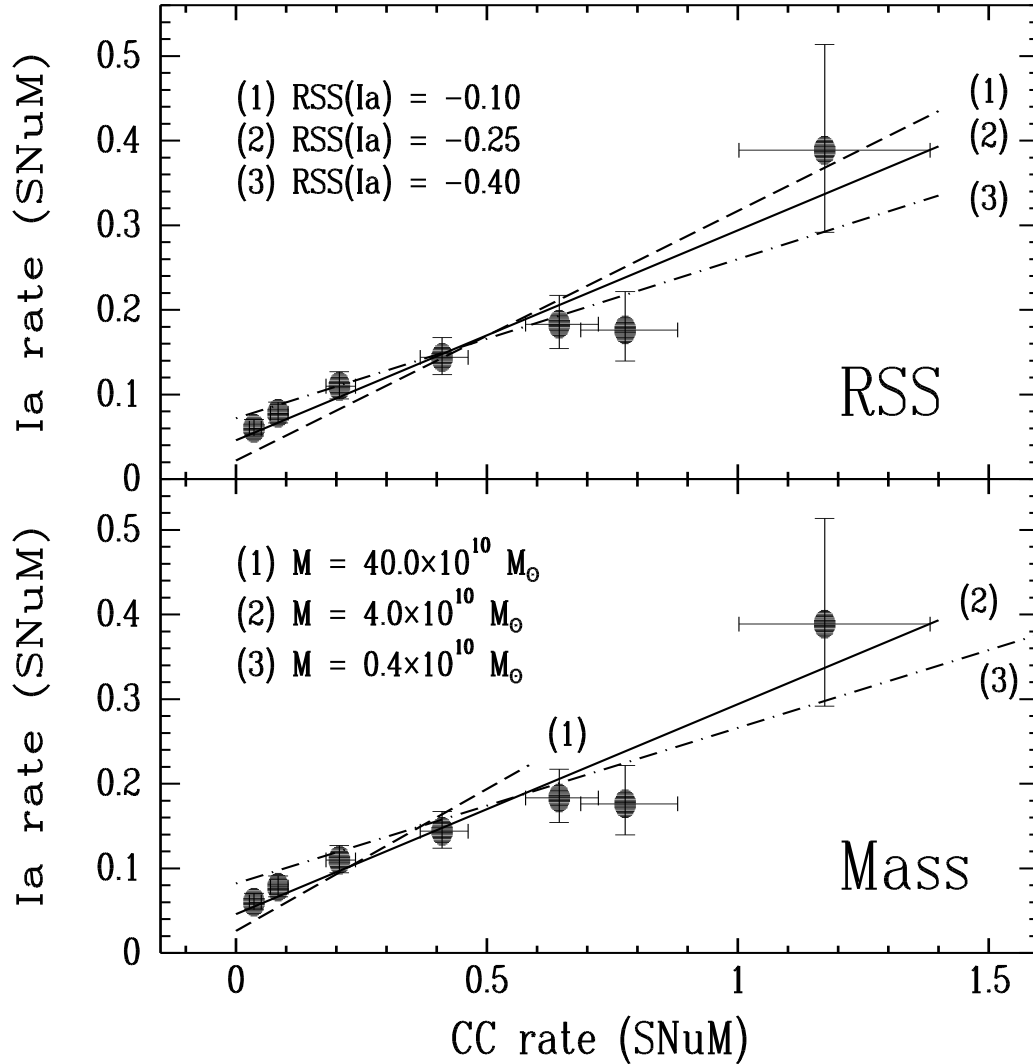


Figure 18. The effect of different RSSs (top panel) and galaxy masses (bottom panel) for the two-component model fits for the SN Ia rates. For clarity, only the data points (and their error bars) for fit (1) (top panel) and fit (2) (bottom panel) are shown, respectively. All fits have reduced $\chi^2 < 1.0$.

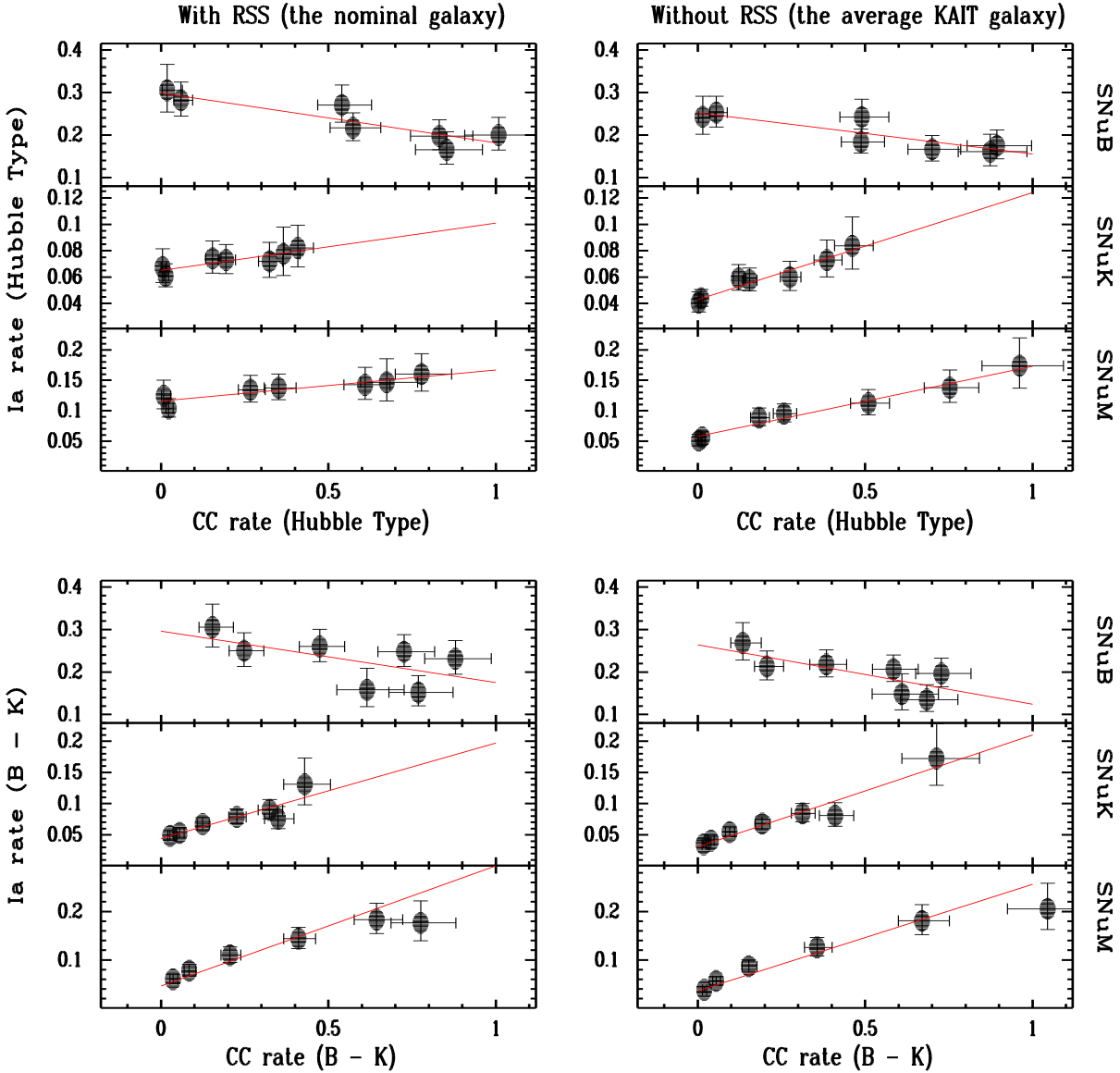


Figure 19. The two-component model fits for the SN Ia rates are affected by several factors: different normalisations (marked to the right), with or without the use of RSSs (left and right panels, respectively), and different grouping methods for the galaxies (top panel, using galaxy Hubble types; bottom panel, using galaxy $B - K$ colour).

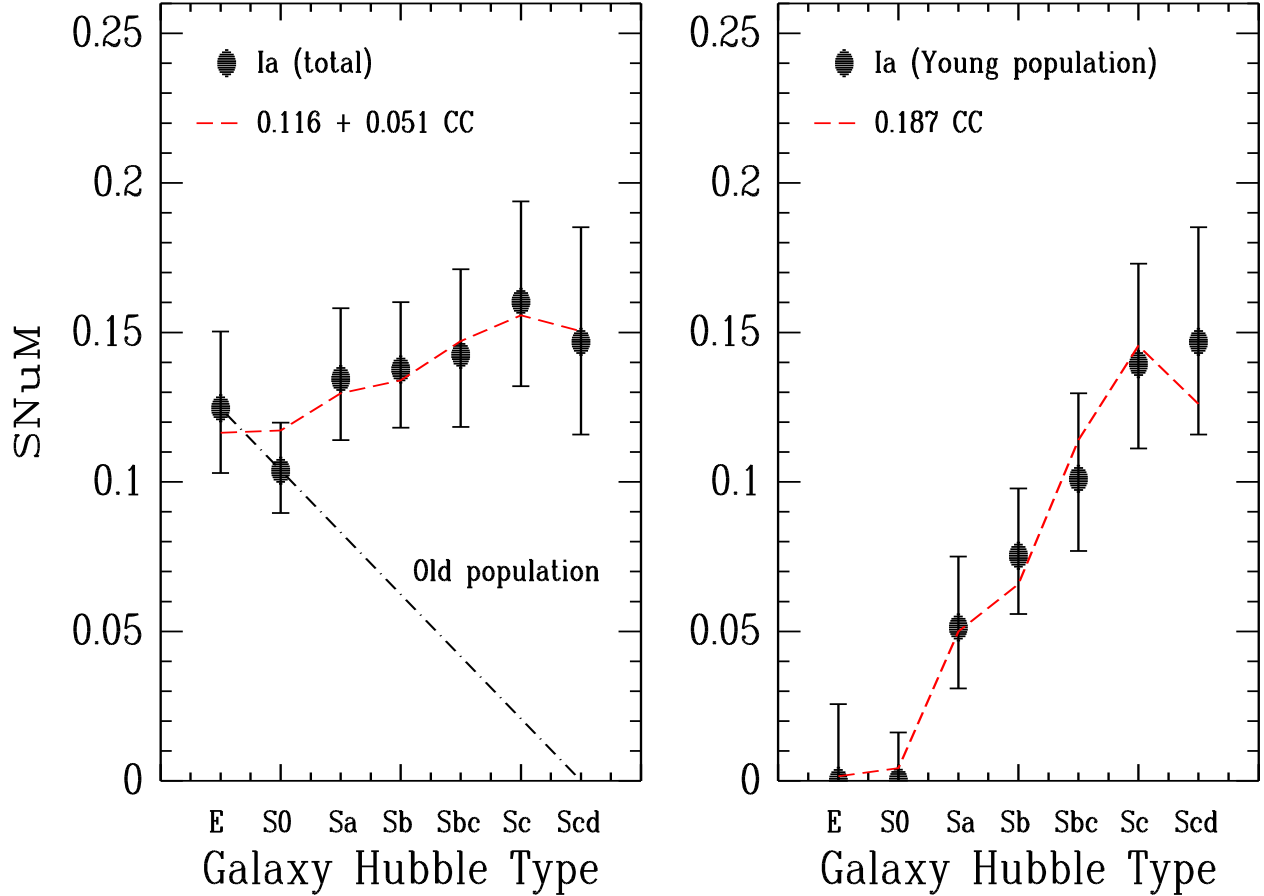


Figure 20. The effect of considering old and young populations for the two-component model for the SN Ia rates. Here the SNuM rates for a fiducial galaxy size are considered for different Hubble types. *Left panel:* The total SN Ia rates (solid dots) are fit with the two-component model (dashed line). The dash-dotted line shows a toy model for the SN Ia rates in old populations. *Right panel:* After subtracting the contribution from old populations, the SN Ia rates in young populations (solid dots) are fit with the two-component model (dashed line).

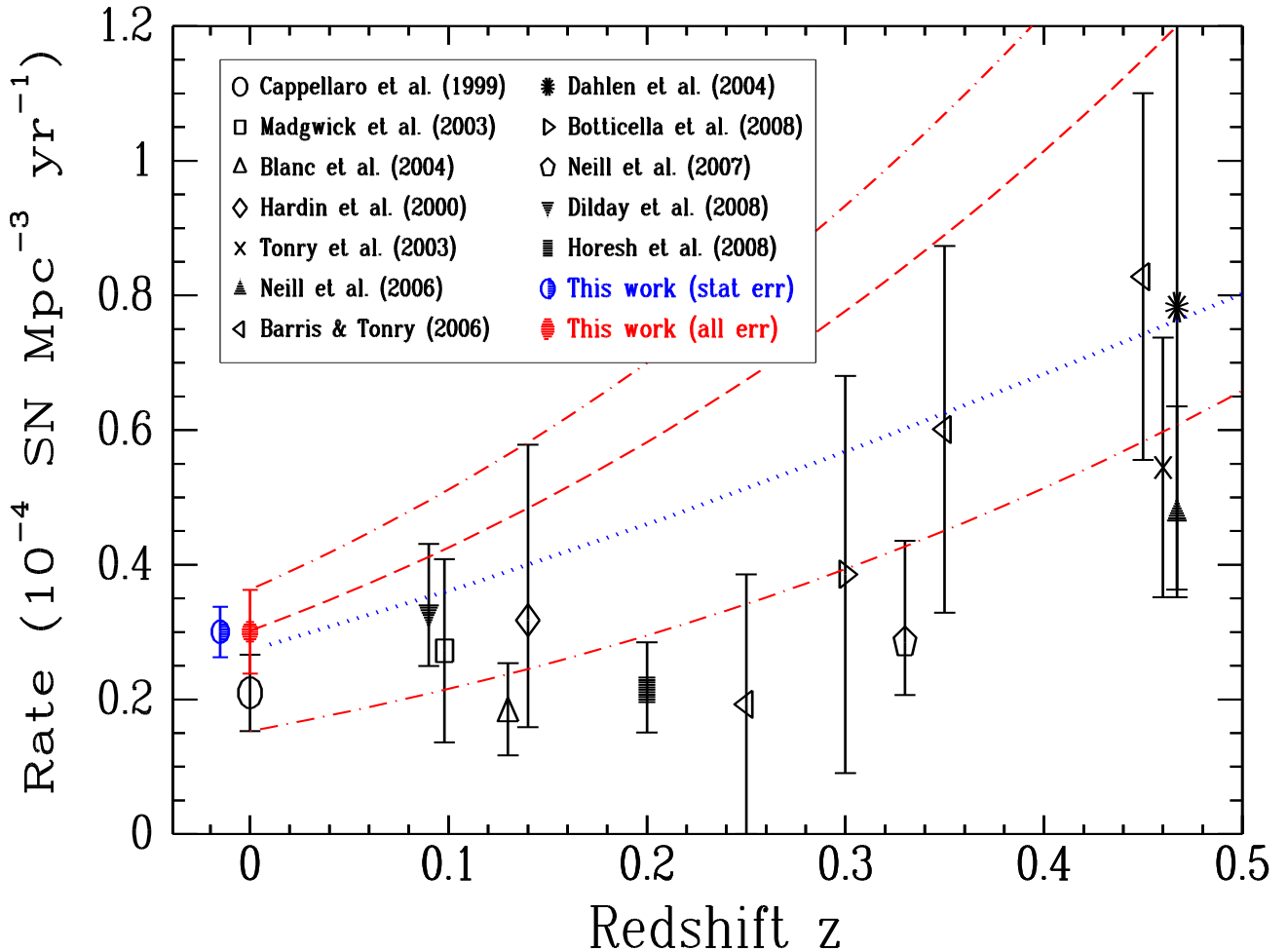


Figure 21. The volumetric rate of SNe Ia at different redshifts. Our rate is marked with only the statistical uncertainty (half-filled circle), and with the total uncertainty (solid circle). The rest of the rates are adopted from Horesh et al. (2008). The dashed line is evaluated at our rate with a functional form of $(1 + z)^{3.6}$, and is the star-formation rate history from Hopkins & Beacom (2006). The upper and lower dash-dotted lines follow the same functional form and are evaluated at the 1σ upper error bar of our measurement, and the 1σ lower error bar of the C99 measurement, respectively. The dotted line is the expected SN Ia rate from the SFR history study by Mannucci et al. (2007).

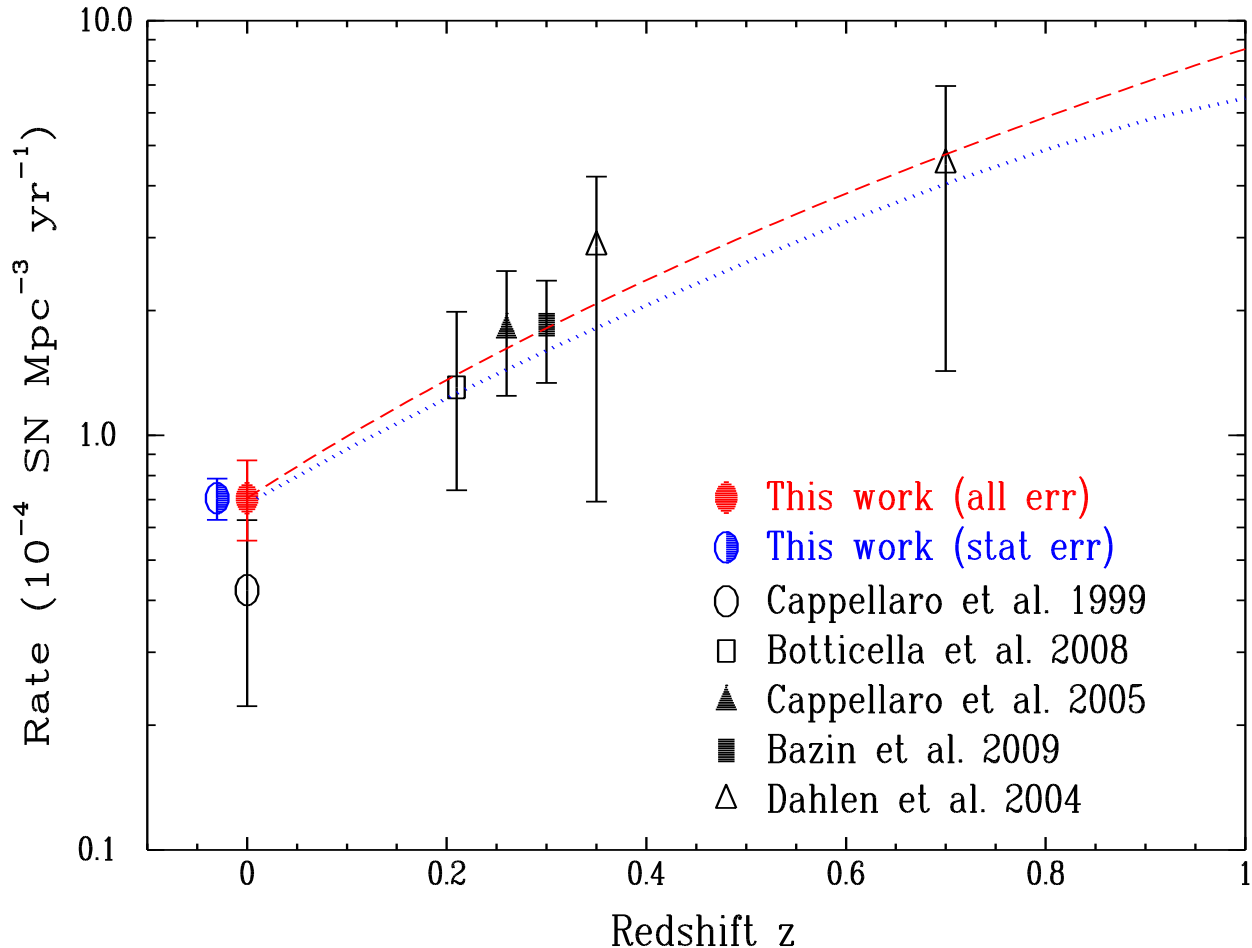


Figure 22. The same as Figure 21, but for the core-collapse SN rates.

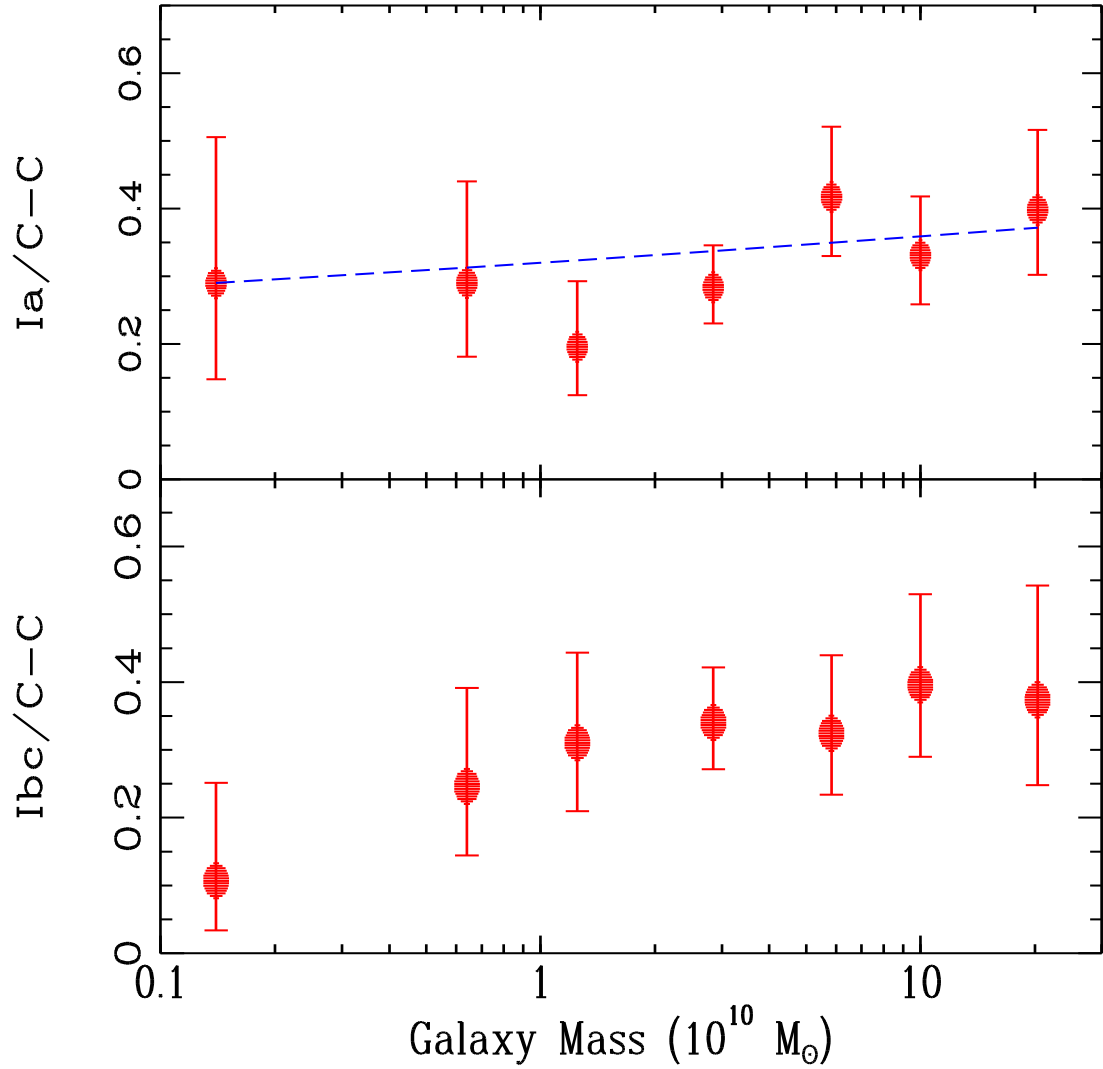


Figure 23. The rate ratios for different galaxy masses. The top panel shows the ratio of the SN Ia rate to the core-collapse SN rate, while the bottom panel gives the ratio of the SN Ibc rate to the core-collapse SN rate. The dashed line in the top panel follows $M^{0.05}$, which is the expected SN Ia to CC SN rate ratio due to different RSSs in the rate-size relations.

Table 1. The rate-size correction factors.^a

Hubble Type	RSS(SN Ia)	RSS(SN II)
E	-0.513 ± 0.316	—
S0	-0.503 ± 0.158	—
Sa	-0.637 ± 0.199	-0.653 ± 0.167
Sb	-0.555 ± 0.171	-0.498 ± 0.165
Sbc	-0.443 ± 0.241	-0.628 ± 0.121
Sc	-0.329 ± 0.201	-0.626 ± 0.111
Scd	-0.435 ± 0.195	-0.437 ± 0.128

^aSNuM rates for SNe Ia and II in the “full-optimal” sample are used.

Table 2. Adopted correction factors and fiducial galaxy sizes.

Rate	Galaxy groups	RSS(Ia)	RSS(Ibc, II)	Fiducial size
SNuB	Hubble type	$\text{RSS}_B = -0.23 \pm 0.20$	$\text{RSS}_B = -0.27 \pm 0.10$	$L_{B0} = 2 \times 10^{10} L_\odot$
SNuK	Hubble type	$\text{RSS}_K = -0.35 \pm 0.10$	$\text{RSS}_K = -0.45 \pm 0.10$	$L_{K0} = 7 \times 10^{10} L_\odot$
SNuM	Hubble type	$\text{RSS}_M = -0.50 \pm 0.10$	$\text{RSS}_M = -0.55 \pm 0.10$	$M_0 = 4 \times 10^{10} M_\odot$
SNuB	$B - K$	$\text{RSS}_B = -0.25 \pm 0.15$	$\text{RSS}_B = -0.38 \pm 0.10$	$L_{B0} = 2 \times 10^{10} L_\odot$
SNuK	$B - K$	$\text{RSS}_K = -0.25 \pm 0.15$	$\text{RSS}_K = -0.38 \pm 0.10$	$L_{K0} = 7 \times 10^{10} L_\odot$
SNuM	$B - K$	$\text{RSS}_M = -0.25 \pm 0.15$	$\text{RSS}_M = -0.38 \pm 0.10$	$M_0 = 4 \times 10^{10} M_\odot$

Table 3. SN rates in different galaxy inclination bins.

Rate	Gal	SN	$r0(0-40)^a$	$r1(40-75)^a$	$r2(75-90)^a$	$r3(0-75)^a$	$r0/r1 - 1$	$r0/r2 - 1$	$r0/r3 - 1$
SNuB	Sa-Sbc	Ia	0.312(0.066)	0.215(0.023)	0.162(0.029)	0.231(0.022)	0.45(0.34)	0.93(0.54)	0.35(0.31)
SNuB	Sc-Scd	Ia	0.198(0.060)	0.162(0.028)	0.140(0.036)	0.170(0.025)	0.22(0.43)	0.41(0.56)	0.16(0.39)
SNuB	Sa-Sbc	Ibc	0.203(0.085)	0.238(0.036)	0.109(0.036)	0.233(0.033)	-0.15(0.38)	0.86(0.99)	-0.13(0.39)
SNuB	Sc-Scd	Ibc	0.260(0.086)	0.222(0.040)	0.129(0.043)	0.230(0.036)	0.17(0.44)	1.02(0.95)	0.13(0.41)
SNuB	Sa-Sbc	II	0.535(0.093)	0.356(0.032)	0.247(0.038)	0.385(0.030)	0.51(0.29)	1.17(0.50)	0.39(0.26)
SNuB	Sc-Scd	II	1.107(0.177)	0.599(0.068)	0.236(0.059)	0.710(0.065)	0.85(0.36)	3.68(1.39)	0.56(0.29)
SNuK	Sa-Sbc	Ia	0.085(0.018)	0.072(0.008)	0.056(0.011)	0.074(0.007)	0.19(0.29)	0.51(0.43)	0.15(0.27)
SNuK	Sc-Scd	Ia	0.078(0.024)	0.072(0.013)	0.076(0.020)	0.074(0.011)	0.08(0.38)	0.03(0.41)	0.06(0.36)
SNuK	Sa-Sbc	Ibc	0.060(0.025)	0.083(0.012)	0.037(0.013)	0.079(0.011)	-0.28(0.32)	0.62(0.88)	-0.24(0.33)
SNuK	Sc-Scd	Ibc	0.103(0.034)	0.098(0.018)	0.069(0.023)	0.099(0.016)	0.06(0.40)	0.50(0.70)	0.04(0.38)
SNuK	Sa-Sbc	II	0.162(0.028)	0.120(0.011)	0.088(0.014)	0.127(0.010)	0.35(0.26)	0.84(0.43)	0.27(0.24)
SNuK	Sc-Scd	II	0.424(0.070)	0.252(0.030)	0.128(0.032)	0.294(0.028)	0.68(0.34)	2.32(0.99)	0.44(0.27)
SNuM	Sa-Sbc	Ia	0.156(0.034)	0.135(0.015)	0.111(0.021)	0.139(0.013)	0.16(0.28)	0.40(0.40)	0.12(0.26)
SNuM	Sc-Scd	Ia	0.148(0.045)	0.141(0.024)	0.150(0.040)	0.143(0.021)	0.05(0.37)	-0.01(0.40)	0.04(0.35)
SNuM	Sa-Sbc	Ibc	0.105(0.044)	0.149(0.023)	0.070(0.024)	0.141(0.020)	-0.30(0.31)	0.51(0.82)	-0.26(0.33)
SNuM	Sc-Scd	Ibc	0.193(0.064)	0.182(0.034)	0.129(0.045)	0.184(0.029)	0.06(0.40)	0.49(0.72)	0.04(0.38)
SNuM	Sa-Sbc	II	0.280(0.048)	0.218(0.020)	0.168(0.027)	0.229(0.018)	0.28(0.25)	0.66(0.39)	0.22(0.23)
SNuM	Sc-Scd	II	0.771(0.128)	0.481(0.057)	0.247(0.063)	0.553(0.052)	0.60(0.33)	2.12(0.96)	0.40(0.27)

^aSN rates for the galaxies with inclination in the range $0^\circ - 40^\circ$, $40^\circ - 75^\circ$, $75^\circ - 90^\circ$, and $0^\circ - 75^\circ$, respectively.

Landscape Table 4 to go here.

Table 4. SN rates in fiducial galaxies of different Hubble types.

Landscape Table 5 to go here.

Table 5. SN rates in fiducial galaxies of different $B - K$ colours.

Table 6. SN rates in average galaxies of different Hubble types.^a

Hub.	SN	SNuB ^b	N_B^c	SNuK ^b	N_K^c	SNuM ^b	N_M^c
E	SN Ia	$0.243^{+0.048}_{-0.041}(0.038)$	35.0	$0.041^{+0.008}_{-0.007}(0.006)$	33.0	$0.051^{+0.010}_{-0.009}(0.008)$	33.0
S0	SN Ia	$0.253^{+0.038}_{-0.034}(0.057)$	56.0	$0.044^{+0.007}_{-0.006}(0.010)$	54.0	$0.056^{+0.009}_{-0.008}(0.013)$	54.0
Sab	SN Ia	$0.242^{+0.042}_{-0.036}(0.039)$	44.3	$0.059^{+0.010}_{-0.009}(0.010)$	43.3	$0.089^{+0.016}_{-0.013}(0.015)$	43.3
Sb	SN Ia	$0.184^{+0.030}_{-0.026}(0.036)$	50.2	$0.058^{+0.009}_{-0.008}(0.011)$	50.2	$0.095^{+0.016}_{-0.014}(0.018)$	49.2
Sbc	SN Ia	$0.166^{+0.032}_{-0.027}(0.029)$	36.6	$0.060^{+0.012}_{-0.010}(0.010)$	34.6	$0.112^{+0.023}_{-0.019}(0.018)$	34.6
Sc	SN Ia	$0.175^{+0.037}_{-0.031}(0.027)$	32.0	$0.073^{+0.015}_{-0.013}(0.012)$	32.0	$0.138^{+0.029}_{-0.024}(0.022)$	32.0
Scd	SN Ia	$0.161^{+0.041}_{-0.033}(0.043)$	23.0	$0.084^{+0.022}_{-0.018}(0.019)$	22.0	$0.174^{+0.045}_{-0.037}(0.038)$	22.0
Irr	SN Ia	$0.000^{+0.109}_{-0.000}(-)$	0.0	$0.000^{+0.048}_{-0.000}(-)$	0.0	$0.000^{+0.069}_{-0.000}(-)$	0.0
E	SN Ibc	$0.015^{+0.034}_{-0.012}(0.007)$	1.0	$0.003^{+0.006}_{-0.002}(0.001)$	1.0	$0.004^{+0.008}_{-0.003}(0.002)$	1.0
S0	SN Ibc	$0.036^{+0.028}_{-0.017}(0.010)$	4.0	$0.007^{+0.005}_{-0.003}(0.002)$	4.0	$0.009^{+0.007}_{-0.004}(0.003)$	4.0
Sab	SN Ibc	$0.224^{+0.065}_{-0.052}(0.072)$	18.5	$0.056^{+0.016}_{-0.013}(0.018)$	18.5	$0.086^{+0.025}_{-0.020}(0.028)$	18.5
Sb	SN Ibc	$0.206^{+0.056}_{-0.045}(0.065)$	20.5	$0.070^{+0.019}_{-0.015}(0.023)$	21.5	$0.113^{+0.031}_{-0.025}(0.037)$	20.5
Sbc	SN Ibc	$0.234^{+0.062}_{-0.050}(0.071)$	21.3	$0.092^{+0.025}_{-0.020}(0.029)$	21.3	$0.175^{+0.047}_{-0.038}(0.055)$	21.3
Sc	SN Ibc	$0.245^{+0.053}_{-0.045}(0.066)$	30.0	$0.106^{+0.023}_{-0.019}(0.028)$	30.0	$0.206^{+0.045}_{-0.037}(0.055)$	30.0
Scd	SN Ibc	$0.178^{+0.052}_{-0.041}(0.035)$	18.7	$0.097^{+0.029}_{-0.023}(0.021)$	17.7	$0.194^{+0.060}_{-0.047}(0.042)$	16.7
Irr	SN Ibc	$0.316^{+0.249}_{-0.151}(0.068)$	4.0	$0.073^{+0.093}_{-0.047}(0.034)$	2.0	$0.103^{+0.136}_{-0.067}(0.049)$	2.0
E	SN II	$0.000^{+0.014}_{-0.000}(-)$	0.0	$0.000^{+0.003}_{-0.000}(-)$	0.0	$0.000^{+0.003}_{-0.000}(-)$	0.0
S0	SN II	$0.020^{+0.015}_{-0.009}(0.006)$	4.0	$0.004^{+0.003}_{-0.002}(0.001)$	4.0	$0.005^{+0.004}_{-0.002}(0.001)$	4.0
Sab	SN II	$0.266^{+0.047}_{-0.041}(0.098)$	42.2	$0.066^{+0.012}_{-0.010}(0.024)$	42.2	$0.098^{+0.018}_{-0.015}(0.035)$	41.2
Sb	SN II	$0.282^{+0.043}_{-0.037}(0.106)$	56.3	$0.085^{+0.013}_{-0.012}(0.032)$	53.3	$0.144^{+0.023}_{-0.020}(0.055)$	53.3
Sbc	SN II	$0.466^{+0.058}_{-0.052}(0.134)$	80.1	$0.183^{+0.023}_{-0.020}(0.052)$	81.1	$0.335^{+0.042}_{-0.038}(0.098)$	79.1
Sc	SN II	$0.649^{+0.088}_{-0.078}(+0.364)$	69.0	$0.280^{+0.038}_{-0.034}(+0.136)$	68.0	$0.547^{+0.075}_{-0.066}(+0.245)$	68.0
Scd	SN II	$0.695^{+0.097}_{-0.086}(-0.135)$	65.3	$0.364^{+0.055}_{-0.048}(+0.176)$	57.3	$0.767^{+0.116}_{-0.102}(+0.342)$	56.3
Irr	SN II	$0.431^{+0.291}_{-0.186}(0.074)$	5.0	$0.162^{+0.128}_{-0.078}(0.039)$	4.0	$0.230^{+0.181}_{-0.110}(0.054)$	4.0

^aUncertainties are ordered as statistical and systematic (in parentheses).^bThe rate for the average galaxy size.^cThe number of SNe used in the rate calculation.

Table 7. SN rates in average galaxies of different $B - K$ colours.^a

$B - K$	SN	SNuB ^b	N_B^c	SNuK ^b	N_K^c	SNuM ^b	N_M^c
<2.3	SN Ia	$0.148^{+0.048}_{-0.037}(0.038)$	15.6	$0.172^{+0.056}_{-0.043}(0.044)$	15.6	$0.601^{+0.194}_{-0.150}(0.153)$	15.6
2.3–2.8	SN Ia	$0.135^{+0.035}_{-0.028}(0.026)$	22.6	$0.081^{+0.021}_{-0.017}(0.016)$	22.6	$0.206^{+0.053}_{-0.043}(0.040)$	22.6
2.8–3.1	SN Ia	$0.196^{+0.036}_{-0.031}(0.041)$	39.8	$0.084^{+0.016}_{-0.013}(0.018)$	39.8	$0.181^{+0.033}_{-0.029}(0.038)$	39.8
3.1–3.4	SN Ia	$0.206^{+0.034}_{-0.029}(0.030)$	50.2	$0.068^{+0.011}_{-0.010}(0.010)$	50.2	$0.126^{+0.020}_{-0.018}(0.018)$	50.2
3.4–3.7	SN Ia	$0.218^{+0.034}_{-0.030}(0.034)$	53.6	$0.054^{+0.009}_{-0.007}(0.008)$	53.6	$0.087^{+0.014}_{-0.012}(0.014)$	53.6
3.7–4.0	SN Ia	$0.213^{+0.036}_{-0.031}(0.041)$	46.0	$0.041^{+0.007}_{-0.006}(0.008)$	46.0	$0.057^{+0.010}_{-0.008}(0.011)$	46.0
>4.0	SN Ia	$0.269^{+0.047}_{-0.041}(0.045)$	43.0	$0.035^{+0.006}_{-0.005}(0.006)$	43.0	$0.038^{+0.007}_{-0.006}(0.006)$	43.0
<2.3	SN Ibc	$0.120^{+0.058}_{-0.041}(0.020)$	8.2	$0.141^{+0.068}_{-0.048}(0.024)$	8.2	$0.495^{+0.239}_{-0.169}(0.084)$	8.2
2.3–2.8	SN Ibc	$0.253^{+0.063}_{-0.051}(0.069)$	24.1	$0.152^{+0.038}_{-0.031}(0.041)$	24.1	$0.388^{+0.096}_{-0.078}(0.105)$	24.1
2.8–3.1	SN Ibc	$0.277^{+0.062}_{-0.052}(0.079)$	28.3	$0.119^{+0.027}_{-0.022}(0.034)$	28.3	$0.255^{+0.057}_{-0.048}(0.073)$	28.3
3.1–3.4	SN Ibc	$0.222^{+0.053}_{-0.044}(0.051)$	25.5	$0.073^{+0.018}_{-0.014}(0.017)$	25.5	$0.135^{+0.032}_{-0.027}(0.031)$	25.5
3.4–3.7	SN Ibc	$0.143^{+0.045}_{-0.035}(0.050)$	16.3	$0.036^{+0.011}_{-0.009}(0.013)$	16.3	$0.057^{+0.018}_{-0.014}(0.020)$	16.3
3.7–4.0	SN Ibc	$0.078^{+0.038}_{-0.027}(0.025)$	8.0	$0.015^{+0.007}_{-0.005}(0.005)$	8.0	$0.021^{+0.010}_{-0.007}(0.007)$	8.0
>4.0	SN Ibc	$0.045^{+0.043}_{-0.024}(0.019)$	3.0	$0.006^{+0.006}_{-0.003}(0.002)$	3.0	$0.006^{+0.006}_{-0.004}(0.003)$	3.0
<2.3	SN II	$0.490^{+0.093}_{-0.079}(+0.376)$	38.1	$0.572^{+0.108}_{-0.092}(+0.422)$	38.1	$1.994^{+0.378}_{-0.321}(+1.332)$	38.1
2.3–2.8	SN II	$0.432^{+0.068}_{-0.060}(+0.344)$	52.3	$0.258^{+0.041}_{-0.039}(+0.199)$	52.3	$0.657^{+0.104}_{-0.090}(+0.462)$	52.3
2.8–3.1	SN II	$0.451^{+0.063}_{-0.056}(+0.348)$	64.8	$0.194^{+0.039}_{-0.024}(+0.144)$	64.8	$0.415^{+0.058}_{-0.051}(+0.280)$	64.8
3.1–3.4	SN II	$0.363^{+0.051}_{-0.045}(+0.174)$	65.3	$0.119^{+0.017}_{-0.015}(+0.051)$	65.3	$0.221^{+0.031}_{-0.027}(+0.091)$	65.3
3.4–3.7	SN II	$0.241^{+0.041}_{-0.035}(+0.117)$	47.1	$0.060^{+0.010}_{-0.009}(+0.026)$	47.1	$0.096^{+0.016}_{-0.014}(+0.040)$	47.1
3.7–4.0	SN II	$0.129^{+0.032}_{-0.026}(+0.062)$	24.0	$0.025^{+0.006}_{-0.005}(+0.011)$	24.0	$0.034^{+0.009}_{-0.007}(+0.014)$	24.0
>4.0	SN II	$0.090^{+0.034}_{-0.025}(+0.045)$	12.0	$0.012^{+0.004}_{-0.003}(+0.005)$	12.0	$0.013^{+0.005}_{-0.004}(+0.006)$	12.0

^aUncertainties are ordered as statistical and systematic (in parentheses).^bThe rate for the average galaxy size.^cThe number of SNe used in the rate calculation.

Table 8. Two-component model fits to the SN Ia rates.^a

Mass ^b	RSS	<i>a</i>	<i>b</i>	$\chi^2(c)^c$
4.0	-0.10	0.022(0.023)	0.295(0.083)	10.06
4.0	-0.25	0.046(0.019)	0.248(0.071)	7.13
4.0	-0.40	0.072(0.016)	0.188(0.058)	4.31
0.4	-0.25	0.082(0.034)	0.184(0.053)	7.13
4.0	-0.25	0.046(0.019)	0.248(0.071)	7.13
40.0	-0.25	0.026(0.011)	0.335(0.096)	7.13

^aThe rates for galaxies of different $B - K$ colours are used in the analysis.

^bGalaxy mass, in units of $10^{10} L_\odot$.

^c χ^2/DOF for a constant fit to the SN Ia rates.

Table 9. More two-component model fits to the SN Ia rates.^a

Src	Rate	a_1 (with RSS)	b_1 (with RSS)	$\chi^2(c)_1^b$	a_2 (no RSS)	b_2 (no RSS)	$\chi^2(c)_2^b$
H-type	SNuB	0.299(0.031)	-0.117(0.044)	1.465	0.252(0.025)	-0.097(0.041)	1.277
H-type	SNuK	0.065(0.007)	0.036(0.032)	0.353	0.043(0.005)	0.081(0.030)	1.787
H-type	SNuM	0.116(0.012)	0.051(0.032)	0.770	0.058(0.008)	0.115(0.030)	5.184
$B - K$	SNuB	0.296(0.039)	-0.121(0.063)	1.641	0.264(0.033)	-0.140(0.062)	1.339
$B - K$	SNuK	0.044(0.008)	0.153(0.054)	2.477	0.031(0.009)	0.179(0.058)	4.983
$B - K$	SNuM	0.046(0.019)	0.248(0.071)	7.128	0.036(0.022)	0.220(0.067)	11.960

^aThe correlation is fit as rate(SN Ia) = $a + b \times \text{rate(SN CC)}$.

^b χ^2/DOF for a constant fit to the SN Ia rates.

Table 10. Volumetric rate.

Rate	SN Ia	SN Ibc	SN II
Early(fiducial; SNuK)	$0.064^{+0.008}_{-0.007} (+0.013)$	$0.008^{+0.006}_{-0.004} (+0.002)$	$0.004^{+0.003}_{-0.002} (+0.001)$
Late(fiducial; SNuK)	$0.074^{+0.006}_{-0.006} (+0.012)$	$0.096^{+0.010}_{-0.009} (-0.018)$	$0.172^{+0.011}_{-0.011} (+0.045)$
Early(LF-average; SNuK)	$0.048^{+0.006}_{-0.005} (+0.010)$	$0.006^{+0.004}_{-0.003} (+0.002)$	$0.003^{+0.002}_{-0.001} (+0.001)$
Late(LF-average; SNuK)	$0.065^{+0.006}_{-0.005} (+0.010)$	$0.083^{+0.009}_{-0.008} (+0.016)$	$0.149^{+0.010}_{-0.009} (+0.039)$
Vol-rate ($10^{-4} \text{ SN Mpc}^{-3} \text{ yr}^{-1}$)	$0.301^{+0.038}_{-0.037} (+0.049)$	$0.258^{+0.044}_{-0.042} (+0.058)$	$0.447^{+0.068}_{-0.068} (+0.131)$

Table 11. Milky Way rate (per century).

Normalisation	Size ^a	SN Ia	SN Ibc	SN II	CC SNe	Total SNe	Comments
L_B	2.0	0.40	0.55	1.11	1.66	2.06	Galaxy size from van der Kruit (1987)
L_B	2.3	0.44	0.61	1.23	1.84	2.28	Galaxy size from van den Bergh (1988)
L_B	4.3	0.71	0.96	1.95	2.91	3.62	M31 size
L_K	6.3	0.47	0.70	1.44	2.14	2.61	M31 size
Mass	2.3	0.43	0.63	1.27	1.90	2.33	M31 size
L_B	3.5	0.61	0.82	1.68	2.50	3.11	Average Sbc galaxy size
L_K	9.7	0.62	0.89	1.83	2.72	3.34	Average Sbc galaxy size
Mass	5.2	0.65	0.91	1.84	2.75	3.40	Average Sbc galaxy size
		0.54 ± 0.12	0.76 ± 0.16	1.54 ± 0.32	2.30 ± 0.48	2.84 ± 0.60	

^aFor L_B and L_K , the units are $10^{10} L_\odot$; for mass, the units are $10^{10} M_\odot$.

APPENDIX A: DISCOVERY OF THE RATE-SIZE RELATION

As in §2, for the discussion in this Appendix, we use the “full-optimal” SN sample with 726 objects that occurred in the “optimal” galaxy sample to compute the SN rates.

We have performed various tests to check the robustness of our rate-calculation pipeline. One such test yielded an unexpected result, as shown in Figure A1. Here the SNe are combined in different Hubble-type bins, and the rates in SNuM are calculated for the galaxies in different distance bins (with a bin size of 30 Mpc). Only the statistical uncertainties are shown (see §3.4 for more discussion of how the errors are calculated). In principle, the rate for each SN type should remain constant (i.e., no evolution) in the small redshift range we considered. However, Figure A1 shows a strong declining trend for the SNe Ia in E–S0 galaxies, as well as for SNe Ibc and SNe II in Sb–Irr galaxies: the rate in the 0–30 Mpc bin is a factor of 2–3 higher than that in the 120–150 Mpc bin. The SN Ia rates in Sb–Irr galaxies are also consistent with a declining trend, though with a lower significance.

The search for the possible causes of this trend fundamentally changed our rate calculations. First, we suspected that the trend could be caused by a bottom-heavy LF for the SNe — the LF has many faint objects that can only be detected in the very nearby galaxies. One main reason we chose to construct a complete SN sample with the nearby SNe in Paper II is to quantify the fraction of subluminous SNe after correction for their incompleteness in our search. As it turns out, the LF does not solve this problem; the rates shown in Figure A1 have made use of the LFs derived from Paper II.

Another possible cause is the missing fraction of SNe in the nuclei of galaxies. As we go to larger distances, the average *angular* size of the galaxies becomes smaller, and the central area (with a fixed radius of a few pixels) which we avoid in the SN search would become a larger fraction of the total galaxy. This could potentially lead to a larger missing fraction of SNe in more distant galaxies, resulting in a lower apparent SN rate. To check this, we divide the galaxies into bins with different angular sizes and calculate their rates. The results are shown in Figure A2. Only SNe in Sb–Irr galaxies are considered, since the early-type galaxies with small angular sizes are not considered in the final rate calculations. There is no strong correlation between the SN rates and the angular galaxy sizes: the rate is consistent with a constant for all of the three SN types. As described in §4.2.3 of Paper I, the missing fraction of SNe from the radial distribution and Monte Carlo simulation studies is $\sim 10\%$ of all SNe, not enough to explain the big difference (a factor of 2–3) shown in Figure A1. The lack of a correlation between the SN rates and the angular sizes of the galaxies is probably due to two competing factors: while the SN rate can be depressed in galaxies having smaller angular sizes due to a larger fraction of the missed SNe in the nuclei, it can also be enhanced if these galaxies have a smaller average *size* (luminosity or mass) as discussed below, although we note that a smaller angular size does not necessarily translate into a smaller luminosity or mass.

We also considered whether the trend could be caused by a change of Hubble-type distribution of the LOSS sample galaxies with distance, as described in §4.1.4 of Paper I. Since the SN rates for galaxies of different Hubble types are different, a declining trend could be observed if the more nearby distance bin mainly consists of galaxies with higher SN rates (i.e., late-type spirals), while the more distant bin is dominated by galaxies with lower rates (i.e., early-type spirals). We have calculated the average SN rate for each distance bin after weighting the SN rate for each galaxy by

its total normalised control time and its average SN rate for its Hubble-type (as discussed in §4.1), and find that the effect of changing Hubble-type distribution over distance is $\lesssim 5\%$ for SNe Ia, $\lesssim 10\%$ for SNe Ibc, and $\lesssim 20\%$ for SNe II. Again, this is not enough to explain the strong rate-distance trend shown in Figure A1.

As discussed in §4.1.4 and Figure 5 of Paper I, there are important changes in the galaxy properties over the 0 to 200 Mpc distance range of the LOSS sample galaxies due to selection biases. In particular, the average luminosity of the galaxies increases monotonically with increasing distance due to a strong Malmquist bias in the current astronomical databases. If there is a correlation between the galaxy size (luminosity or mass) and the SN rates, it may explain the observed declining trend of the SN rates with increasing distance.

At first thought, this may seem unlikely, since the SN rates have already been *linearly* normalised by the galaxy size, as indicated by Equations (A3) and (A4) of Paper I. However, as shown in §2, a strong correlation between the SN rates and the galaxy size is found. Consequently, our SN rates are calculated for a fiducial galaxy size, and the rates for other galaxy sizes are derived using a rate-size relation, as discussed in more detail in §2.

The effect of adopting the rate-size relation in the rate calculations for the galaxies in different distance bins is illustrated in Figure A3. Here all of the rates are converted to the fiducial galaxy size. The rates are consistent with being a constant in different distance bins for each SN type, suggesting that the rate-size relation is the main reason for the declining trend in the SN rates over distance.

An alternative way to demonstrate our solution to the rate-distance trend is shown by the dashed lines in Figure A1. Here, we adopt the final SNuM for the fiducial galaxy size in each Hubble-type bin (§3.5), and calculate the average SNuM for each distance bin. To calculate this average, the rate for each galaxy is corrected by its Hubble type and galaxy size, and weighted by its total control time. In other words, the dashed lines are what we would expect for the change of the average SNuM for the LOSS galaxies over distance, after considering the change in the galaxy Hubble-type and size distribution over distance, and the monitoring history of the galaxies. The dashed lines provide an excellent fit to the observed rate-distance trend.

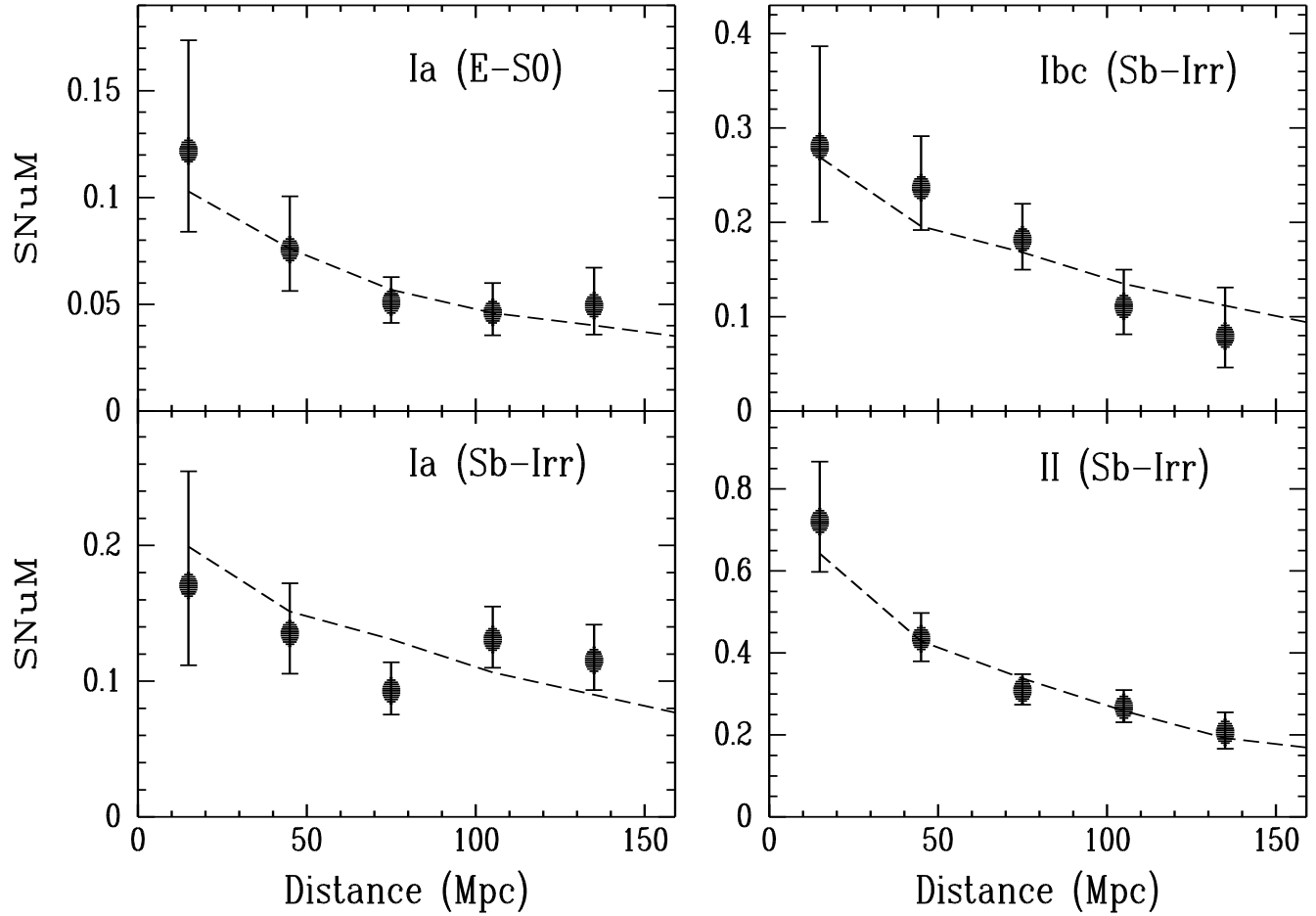


Figure A1. The SN rates in various Hubble types in different distance bins. There is a significant declining trend for the rates. The dashed lines are fits to the trend after considering the rate-size relation and the control times of the galaxies. See text in the Appendix for more details.

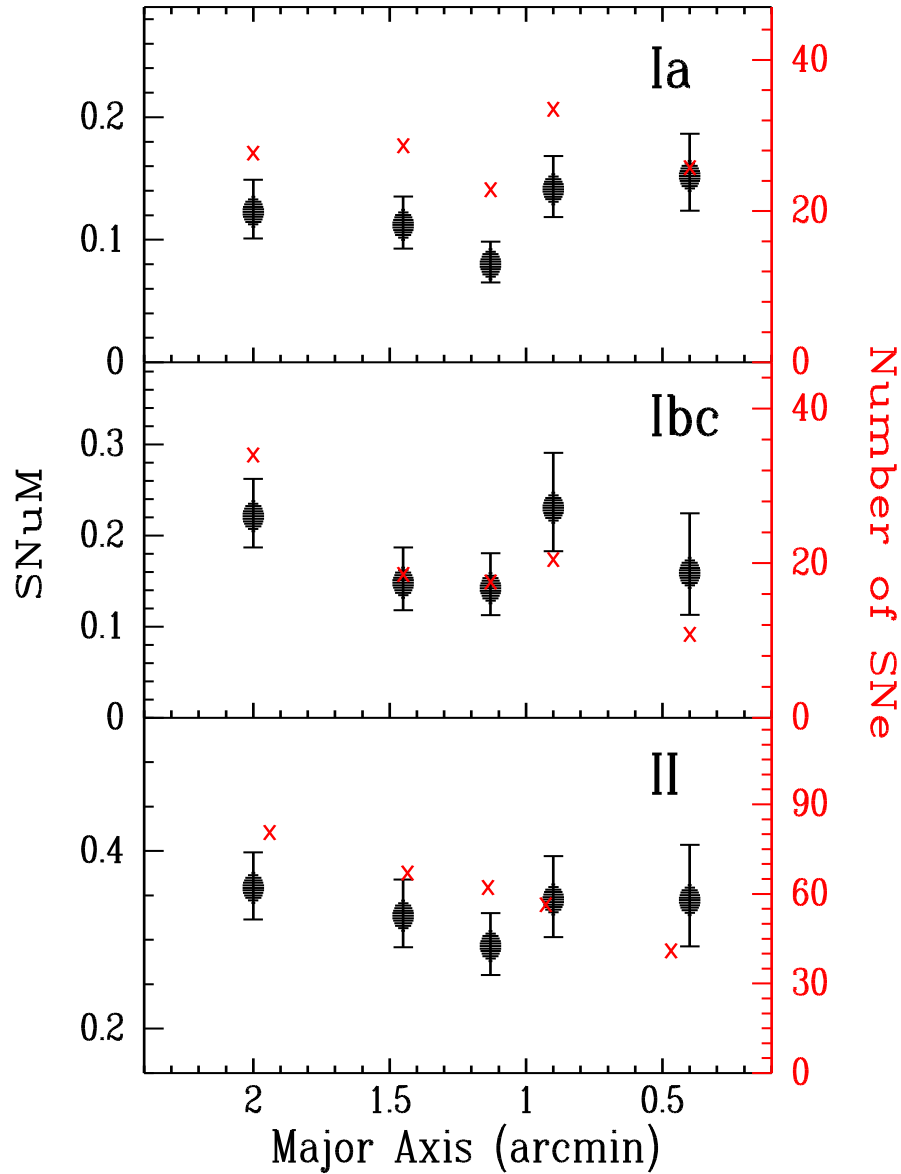


Figure A2. The SN rates (solid dots) in galaxies of different angular sizes. The number of SNe used to calculate each rate is also shown (crosses) with the scale to the right of the plot. No obvious trend is found.

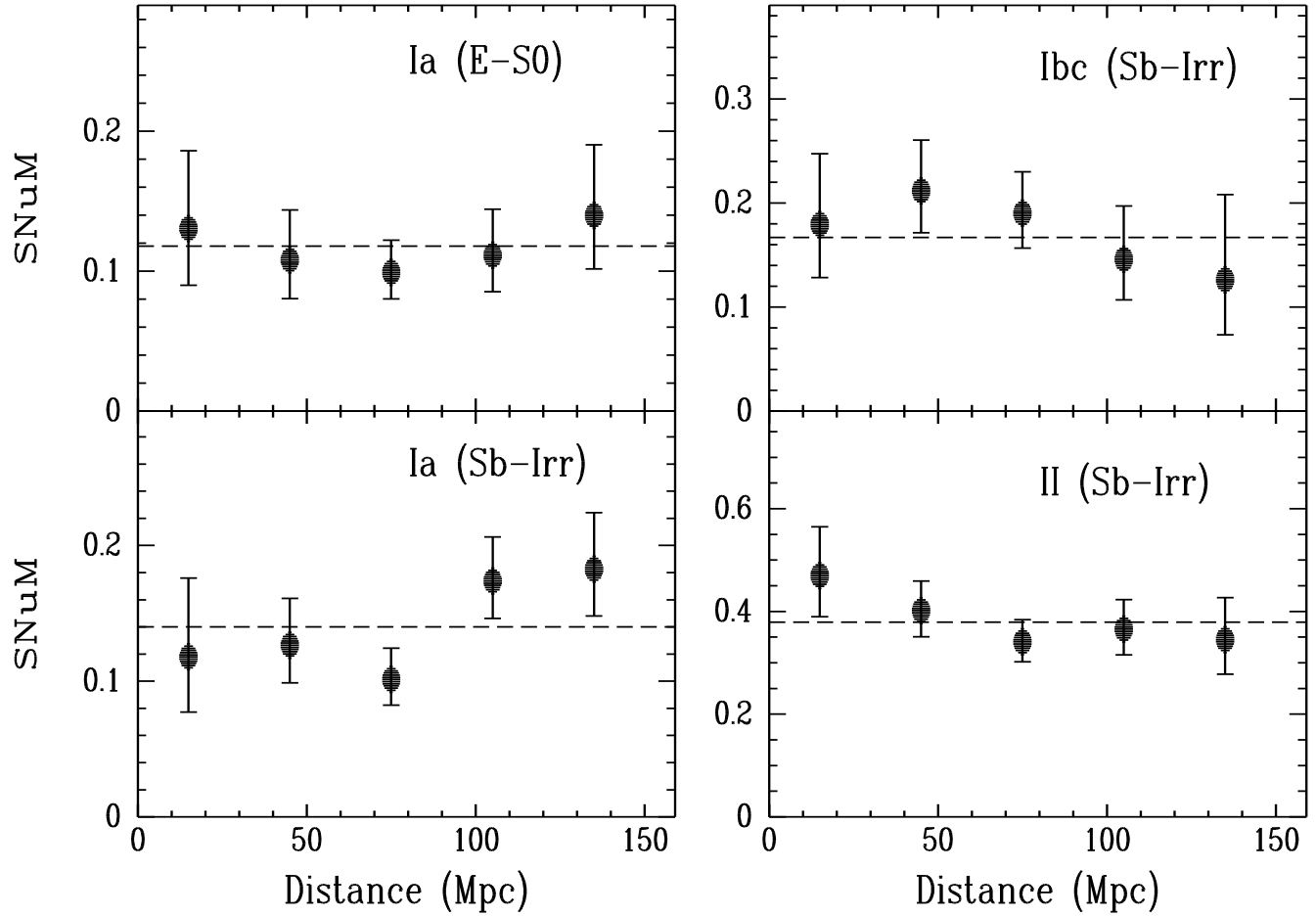


Figure A3. The SN rates for the same mass ($M = 4.0 \times 10^{10} M_{\odot}$) in different distance bins. The rates are consistent with being a constant in different distance bins, suggesting that the rate-size relation, combined with the increasing Malmquist bias of the galaxy sample, is responsible for the declining trend seen in Figure A1.

APPENDIX B: SUPERNOVA RATE AS A FUNCTION OF HOST-GALAXY PROPERTIES

As discussed in §4.2, the existence of the rate-size relation indicates that numerically, the rates cannot be adequately described by a single parameter using either galaxy Hubble type or $B - K$ colour, and the galaxy size (L_B , L_K , mass) is used as a second parameter to quantify the rates (in the form of the rate-size relation). We have considered other combinations of parameters to describe the rates. In particular, here we discuss how the rates can be parameterised as a function of both galaxy Hubble type and $B - K$ colour. It is generally accepted that there is a correlation between galaxy size and colour, with smaller galaxies having bluer colours. Consequently, the empirical rate-size relation can be converted to a rate-colour relation.

We first investigate the galaxy size and colour correlation using our own galaxy sample. Figure B1 shows the results for the “optimal” sample. A strong correlation between the galaxy L_K (or mass) and $B - K$ colour is confirmed. The galaxy L_B value shows a relatively weak (but significant) correlation with $B - K$ colour as well. We divide the galaxies into ten $B - K$ colour bins and calculate their average galaxy sizes and $B - K$ colours; the results are plotted as the dashed lines. A linear regression fit yields the following correlations:

$$\log(L_B) = \text{constant} + (1.20 \pm 0.27)\log(B - K), \quad (\text{B1})$$

$$\log(L_K) = \text{constant} + (3.99 \pm 0.17)\log(B - K), \text{ and} \quad (\text{B2})$$

$$\log(\text{Mass}) = \text{constant} + (5.43 \pm 0.11)\log(B - K). \quad (\text{B3})$$

In principle, the rate-size relation given by Eqs. (1)–(3) in §2.1 can then be written as (using SNuB as an example)

$$\begin{aligned} \log\text{SNuB}(L_B) &= \text{constant} + \text{RSS}_B \times \log(L_B) \\ &= \text{constant}' + \text{RSS}_B \times (1.20 \pm 0.27)\log(B - K). \end{aligned} \quad (\text{B4})$$

In other words, the rate-size relation can be converted to a rate-colour relation,

$$\text{SNuB}(B - K) = \text{SNuB}[(B - K)_0] \left[\frac{B - K}{(B - K)_0} \right]^{\text{RCS}_B}, \quad (\text{B5})$$

where “RCS” stands for rate-colour slope, and $\text{RCS}_B = \text{RSS}_B \times (1.20 \pm 0.27)$. For completeness, the equations for SNuK and SNuM are as follows:

$$\text{SNuK}(B - K) = \text{SNuK}[(B - K)_0] \left[\frac{B - K}{(B - K)_0} \right]^{\text{RCS}_K}, \text{ and} \quad (\text{B6})$$

$$\text{SNuM}(B - K) = \text{SNuM}[(B - K)_0] \left[\frac{B - K}{(B - K)_0} \right]^{\text{RCS}_M}, \quad (\text{B7})$$

where $\text{RCS}_K = \text{RSS}_K \times (3.99 \pm 0.17)$, and $\text{RCS}_M = \text{RSS}_M \times (5.43 \pm 0.11)$. These RCS values are listed in the last two columns of Table B1 when the RSS_B , RSS_K , and RSS_M values in Table 2 are adopted.

The above analysis applies the galaxy size-colour correlation to the rate-size relation to derive the rate-colour relation. Numerically, the rate-colour relation can be directly derived from the data, as shown in Figure B2. The left and right panels illustrate the results for SNe Ia and SNe II, respectively, while the top to bottom panels show the results for the different normalisations. Consider the SNuB rate of SNe Ia (the top-left panel) as an example. For each Hubble type, the galaxies are sorted according to their $B - K$ colours and then divided into 5 bins from the bluest to the reddest, and the rates are calculated for each bin. The rates in Sb galaxies are used as the anchor points, and those in the other Hubble types are scaled by a multiplicative constant, so the ensemble of data can be fit by the dashed

line. For the SN II rates in the right panels, the rates in Sbc galaxies are used as the anchor points.

The dashed lines in Figure B2 provide good fits to the data, with $\chi^2/\text{DOF} < 1.0$ for all of the cases. This indicates that a power-law correlation between the rates and $B - K$ colours — that is, the rate-colour relation as expressed by Eqs. (B5)–(B7) — is a reasonable choice. The power-law indexes (i.e., the RCS values derived directly from the data) are reported in the second and third columns of Table B1.

A comparison between the two sets of RCS values for the rate-colour relation indicates that for the SNuK and SNuM rates, the RCSs are consistent with each other to within the uncertainties. For the SNuB rates, however, the rate-colour relation derived directly from the data shows a trend that is contrary to the expectation from the galaxy size-colour correlation: galaxies with bluer colours have smaller SNuB rates. We emphasise that this trend is only marginal: $\sim 2.0\sigma$ for the SN Ia rates, and $\sim 1.4\sigma$ for SN II rates. As the RCS values derived from the galaxy size-colour correlation also have rather large uncertainties, the two sets of RCSs are only different at the $\sim 2\sigma$ level. For our final rate-colour relations, we adopt the RCS values derived directly from the data (Columns 2 and 3 in Table B1).

The existence of the rate-colour relation implies that the galaxy Hubble-type rates should be evaluated at a fiducial $B - K$ colour, so the rates at any given colour can be calculated using Eqs. (B5)–(B7). We adopt $(B - K)_0 = 3.0$ mag in our analysis, a value that is close to the average colour of the “optimal” galaxy sample.

The rates for the fiducial $B - K$ colour can be calculated by scaling the control time of each galaxy by a factor of $[(B - K)/(B - K)_0]^{\text{RCS}}$, where RCS is listed in Table B1 and is different for different normalisations¹². This is similar to the treatment of the rate-size relation as described in §2.3. These rates are listed in Table B2.

An interesting question is whether the rate for a galaxy with the fiducial $B - K$ colour is consistent with the rate for a galaxy with the fiducial size. In Figure B3, we compare the rates for the fiducial $B - K$ colour (open circles, from Table B2) to those for the fiducial sizes (solid circles, from Table 4). As the values for the fiducial $B - K$ colour and size (L_B , L_K , and mass) are chosen quite arbitrarily, the rates can be scaled by a multiplicative constant (which simply means adopting a different fiducial value). Nevertheless, because the fiducial values are chosen to be close to the average of the KAIT sample galaxies, the two sets of rates are in good agreement for SNuK and SNuM. The SNuB rates for the fiducial $B - K$ colours need to be scaled by a factor of 0.91 to achieve better agreement with those for the fiducial sizes.

The rate-colour relation discussed in this section offers an alternative to the rate-size relation employed in our rate calculations. There are advantages and disadvantages to adopting either relation: while it may be easier to physically understand a correlation between the rates and colours (which are often tied to the star-formation rate), the two relations likely share the same physical origin because of the tight correlation between galaxy sizes and colours discussed here. Numerically, both relations are empirically derived from the data, so either relation can be used to parameterise the rates. We do not adopt the rate-colour relation in our rate calculations for

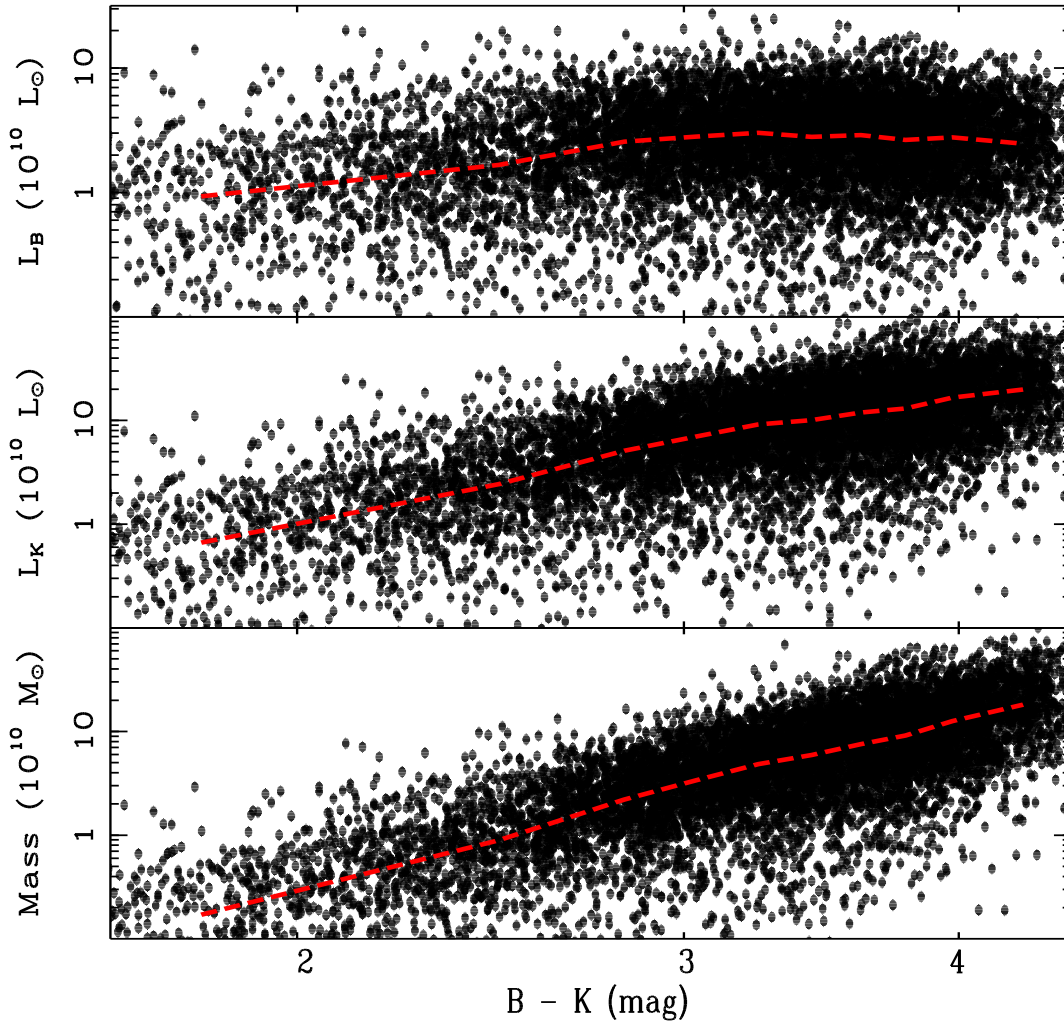
¹² When performing this calculation, we need to reject ~ 50 galaxies with negative $B - K$ colours (i.e., very blue galaxies) because otherwise it is numerically impossible to calculate the power-law value.

the following reasons: (a) the relation for the SNuB rates is contrary to expectations, though with a low significance; (b) numerically, it is impossible to calculate rates for galaxies with $B - K < 0$ mag for SNuK and SNuM; and (c) it is difficult to publish the rates in galaxies of different $B - K$ colours using the rate-colour relation, which requires the rates to be described by a single $B - K$ colour parameter (and we have demonstrated in §2.2 that this is not the case).

Table B1. Correction factors using $B - K$ colours for the Hubble-type rates.

Rate	RCS(Ia)	RCS(Ibc, II)	Fiducial $B - K$	RCS(Ia)(exp) ^a	RCS(Ibc, II)(exp) ^a
SNuB	0.73 ± 0.36	0.38 ± 0.28	3.0	-0.28 ± 0.25	-0.32 ± 0.14
SNuK	-1.46 ± 0.36	-1.55 ± 0.26	3.0	-1.40 ± 0.40	-1.80 ± 0.41
SNuM	-2.96 ± 0.36	-2.77 ± 0.28	3.0	-2.72 ± 0.55	-2.99 ± 0.55

^aThese RCS values are derived from the RSS values in the rate-size relation (as reported in Table 2) and the correlation between size and $B - K$ colour (Eqs. B1–B3).

**Figure B1.** The correlation between the galaxy size (L_B , top panel; L_K , middle panel; mass, bottom panel) and $B - K$ colour.

Landscape Table B2 to go here.

Table B2. SN rates in galaxies of different Hubble type.

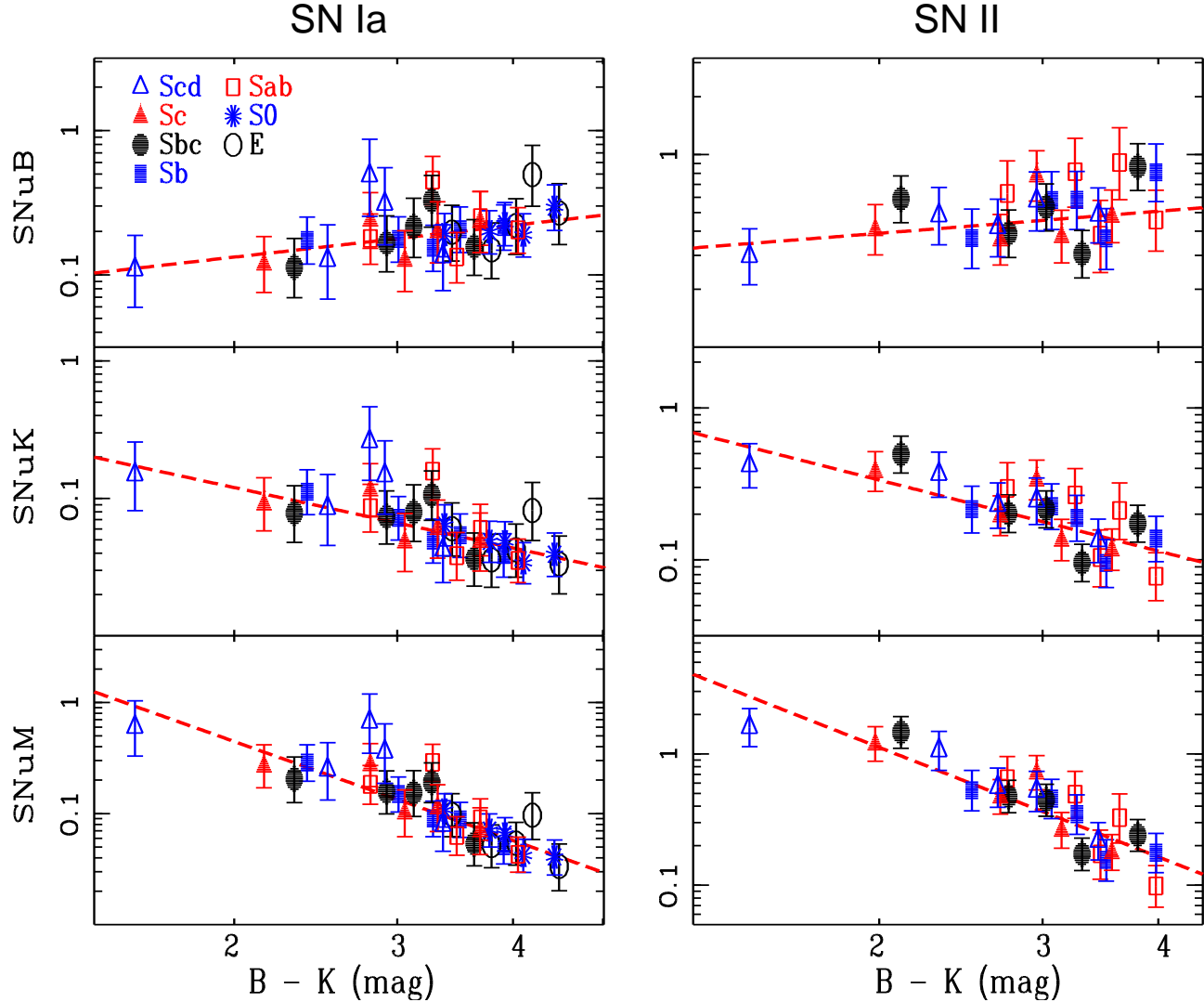


Figure B2. The Hubble-type SN rates in galaxies of different $B - K$ colours. For each Hubble type, the galaxies are divided into five $B - K$ colour bins, and their rates are derived. The left panels show the results for SNe Ia, where the rates for the Sb galaxies are used as the anchor points and the rates in other Hubble types are scaled by a multiplicative constant, so the ensemble of data points can be fit by the dashed lines. The right panels show the results for SNe II, where the rates for the Sbc galaxies are used as the anchor points.

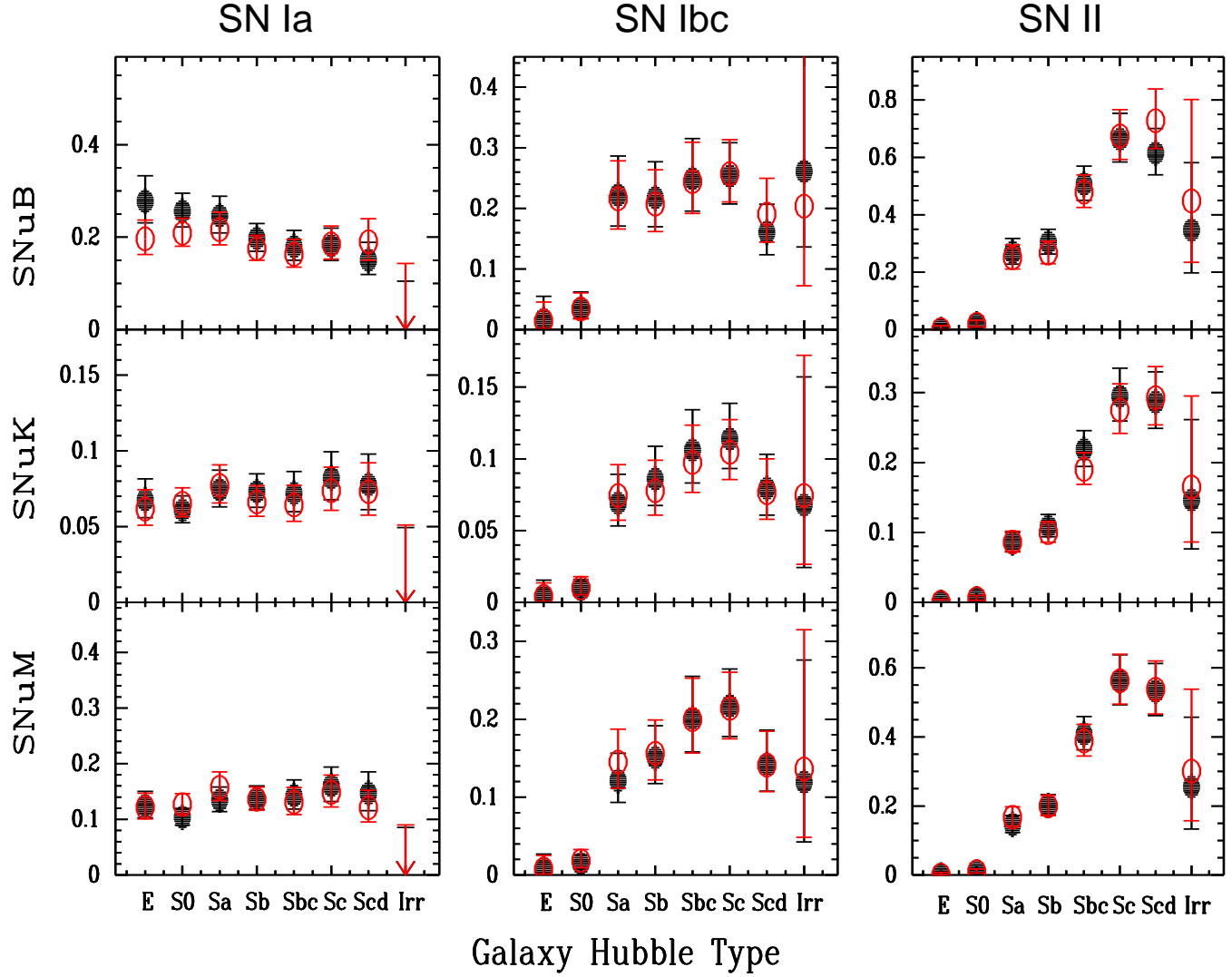


Figure B3. The SN rates for galaxies of different Hubble types. The open circles indicate rates for a galaxy with the fiducial $B - K$ colour, while the solid circles give rates for a galaxy with the fiducial size. The SNUB rates for the fiducial $B - K$ colour are scaled by a factor of 0.91. See text in the Appendix (§B) for more details.

Table 4. SN rates in fiducial galaxies of different Hubble types.^a

Hub.	SN	SNuB(L_{B0}) ^b	N_B^c	RSS _B	L_{B0}^d	SNuK(L_{K0}) ^b	N_K^c	RSS _K	L_{K0}^d	SNuM(M_0) ^b	N_M^c	RSS _M	M_0^d
E	Ia	$0.305^{+0.061}_{-0.051}(0.074)$	35.0	-0.23(0.20)	2.0	$0.068^{+0.014}_{-0.012}(0.014)$	33.0	-0.35(0.10)	7.0	$0.125^{+0.026}_{-0.022}(0.028)$	33.0	-0.50(0.10)	4.0
S0	Ia	$0.282^{+0.043}_{-0.038}(0.065)$	56.0	-0.23(0.20)	2.0	$0.061^{+0.009}_{-0.008}(0.014)$	54.0	-0.35(0.10)	7.0	$0.104^{+0.016}_{-0.014}(0.024)$	54.0	-0.50(0.10)	4.0
Sab	Ia	$0.271^{+0.047}_{-0.041}(0.049)$	44.3	-0.23(0.20)	2.0	$0.074^{+0.013}_{-0.011}(0.013)$	43.3	-0.35(0.10)	7.0	$0.134^{+0.024}_{-0.020}(0.023)$	43.3	-0.50(0.10)	4.0
Sb	Ia	$0.217^{+0.035}_{-0.031}(0.052)$	50.2	-0.23(0.20)	2.0	$0.073^{+0.012}_{-0.010}(0.015)$	50.2	-0.35(0.10)	7.0	$0.138^{+0.023}_{-0.020}(0.028)$	49.2	-0.50(0.10)	4.0
Sbc	Ia	$0.198^{+0.038}_{-0.032}(0.044)$	36.6	-0.23(0.20)	2.0	$0.072^{+0.014}_{-0.012}(0.012)$	34.6	-0.35(0.10)	7.0	$0.142^{+0.029}_{-0.024}(0.024)$	34.6	-0.50(0.10)	4.0
Sc	Ia	$0.200^{+0.042}_{-0.035}(0.037)$	32.0	-0.23(0.20)	2.0	$0.082^{+0.017}_{-0.014}(0.013)$	32.0	-0.35(0.10)	7.0	$0.160^{+0.034}_{-0.028}(0.025)$	32.0	-0.50(0.10)	4.0
Scd	Ia	$0.165^{+0.042}_{-0.034}(0.047)$	23.0	-0.23(0.20)	2.0	$0.078^{+0.020}_{-0.016}(0.020)$	22.0	-0.35(0.10)	7.0	$0.147^{+0.038}_{-0.031}(0.040)$	22.0	-0.50(0.10)	4.0
Irr	Ia	$0.000^{+0.105}_{-0.000}(-)$	0.0	-0.23(0.20)	2.0	$0.000^{+0.049}_{-0.000}(-)$	0.0	-0.35(0.10)	7.0	$0.000^{+0.086}_{-0.000}(-)$	0.0	-0.50(0.10)	4.0
E	Ibc	$0.018^{+0.042}_{-0.015}(0.008)$	1.0	-0.27(0.10)	2.0	$0.005^{+0.011}_{-0.004}(0.002)$	1.0	-0.45(0.10)	7.0	$0.008^{+0.019}_{-0.007}(0.004)$	1.0	-0.55(0.10)	4.0
S0	Ibc	$0.038^{+0.030}_{-0.018}(0.010)$	4.0	-0.27(0.10)	2.0	$0.009^{+0.007}_{-0.004}(0.002)$	4.0	-0.45(0.10)	7.0	$0.014^{+0.011}_{-0.007}(0.004)$	4.0	-0.55(0.10)	4.0
Sab	Ibc	$0.244^{+0.071}_{-0.056}(0.075)$	18.5	-0.27(0.10)	2.0	$0.069^{+0.020}_{-0.016}(0.021)$	18.5	-0.45(0.10)	7.0	$0.121^{+0.035}_{-0.028}(0.036)$	18.5	-0.55(0.10)	4.0
Sb	Ibc	$0.239^{+0.073}_{-0.052}(0.075)$	20.5	-0.27(0.10)	2.0	$0.086^{+0.028}_{-0.018}(0.027)$	21.5	-0.45(0.10)	7.0	$0.150^{+0.041}_{-0.033}(0.046)$	20.5	-0.55(0.10)	4.0
Sbc	Ibc	$0.274^{+0.059}_{-0.059}(0.083)$	21.3	-0.27(0.10)	2.0	$0.106^{+0.028}_{-0.023}(0.031)$	21.3	-0.45(0.10)	7.0	$0.201^{+0.054}_{-0.043}(0.059)$	21.3	-0.55(0.10)	4.0
Sc	Ibc	$0.279^{+0.061}_{-0.051}(0.077)$	30.0	-0.27(0.10)	2.0	$0.114^{+0.025}_{-0.021}(0.031)$	30.0	-0.45(0.10)	7.0	$0.217^{+0.047}_{-0.039}(0.059)$	30.0	-0.55(0.10)	4.0
Scd	Ibc	$0.177^{+0.051}_{-0.041}(0.033)$	18.7	-0.27(0.10)	2.0	$0.079^{+0.024}_{-0.019}(0.016)$	17.7	-0.45(0.10)	7.0	$0.142^{+0.044}_{-0.034}(0.032)$	16.7	-0.55(0.10)	4.0
Irr	Ibc	$0.287^{+0.226}_{-0.137}(0.068)$	4.0	-0.27(0.10)	2.0	$0.068^{+0.089}_{-0.044}(0.036)$	2.0	-0.45(0.10)	7.0	$0.119^{+0.157}_{-0.077}(0.065)$	2.0	-0.55(0.10)	4.0
E	II	$0.000^{+0.018}_{-0.009}(-)$	0.0	-0.27(0.10)	2.0	$0.000^{+0.005}_{-0.000}(-)$	0.0	-0.45(0.10)	7.0	$0.000^{+0.008}_{-0.000}(-)$	0.0	-0.55(0.10)	4.0
S0	II	$0.022^{+0.017}_{-0.010}(0.006)$	4.0	-0.27(0.10)	2.0	$0.005^{+0.004}_{-0.002}(0.002)$	4.0	-0.45(0.10)	7.0	$0.008^{+0.007}_{-0.004}(0.002)$	4.0	-0.55(0.10)	4.0
Sab	II	$0.296^{+0.053}_{-0.045}(0.111)$	42.2	-0.27(0.10)	2.0	$0.085^{+0.015}_{-0.013}(0.032)$	42.2	-0.45(0.10)	7.0	$0.146^{+0.026}_{-0.023}(0.054)$	41.2	-0.55(0.10)	4.0
Sb	II	$0.334^{+0.051}_{-0.044}(0.129)$	56.3	-0.27(0.10)	2.0	$0.108^{+0.017}_{-0.015}(0.043)$	53.3	-0.45(0.10)	7.0	$0.201^{+0.032}_{-0.027}(0.079)$	53.3	-0.55(0.10)	4.0
Sbc	II	$0.557^{+0.069}_{-0.062}(0.159)$	80.1	-0.27(0.10)	2.0	$0.219^{+0.027}_{-0.024}(0.059)$	81.1	-0.45(0.10)	7.0	$0.408^{+0.051}_{-0.046}(0.111)$	79.1	-0.55(0.10)	4.0
Sc	II	$0.730^{+0.099}_{-0.088}(+0.432)$	69.0	-0.27(0.10)	2.0	$0.295^{+0.040}_{-0.036}(+0.140)$	68.0	-0.45(0.10)	7.0	$0.561^{+0.077}_{-0.068}(+0.248)$	68.0	-0.55(0.10)	4.0
Scd	II	$0.677^{+0.094}_{-0.083}(+0.396)$	65.3	-0.27(0.10)	2.0	$0.287^{+0.043}_{-0.038}(+0.139)$	57.3	-0.45(0.10)	7.0	$0.532^{+0.081}_{-0.071}(+0.242)$	56.3	-0.55(0.10)	4.0
Irr	II	$0.382^{+0.258}_{-0.164}(0.071)$	5.0	-0.27(0.10)	2.0	$0.146^{+0.115}_{-0.070}(0.033)$	4.0	-0.45(0.10)	7.0	$0.255^{+0.201}_{-0.122}(0.057)$	4.0	-0.55(0.10)	4.0

^aUncertainties are ordered as statistical and systematic (in parentheses).^bThe rate for the fiducial galaxy size. For any given galaxy size, use Eqs. (1)–(3), reproduced here, to calculate the rates: SNuB(L_B) = SNuB(L_{B0}) $(L_B/L_{B0})^{\text{RSS}_B}$, SNuB(L_K) = SNuK(L_{K0}) $(L_K/L_{K0})^{\text{RSS}_K}$, and SNuM(M) = SNuM(M_0) $(M/M_0)^{\text{RSS}_M}$.^cThe number of SNe used in the rate calculation.^dFor L_{B0} and L_{K0} , the units are 10^{10} L_\odot ; for M_0 , the units are 10^{10} M_\odot .

Table 5. SN rates in fiducial galaxies of different $B - K$ colours.^a

$B - K$	SN	$\text{SNuB}(L_{B0})^b$	N_B^c	RSS_B	L_{B0}^d	$\text{SNuK}(L_{K0})^b$	N_K^c	RSS_K	L_{K0}^d	$\text{SNuM}(M_0)^b$	N_M^c	RSS_M	M_0^d
<2.3	Ia	$0.158^{+0.051}_{-0.040}(0.043)$	15.6	-0.25(0.15)	2.0	$0.131^{+0.042}_{-0.033}(0.043)$	15.6	-0.25(0.15)	7.0	$0.389^{+0.125}_{-0.097}(0.154)$	15.6	-0.25(0.15)	4.0
2.3–2.8	Ia	$0.152^{+0.039}_{-0.032}(0.030)$	22.6	-0.25(0.15)	2.0	$0.076^{+0.020}_{-0.016}(0.015)$	22.6	-0.25(0.15)	7.0	$0.176^{+0.045}_{-0.037}(0.038)$	22.6	-0.25(0.15)	4.0
2.8–3.1	Ia	$0.231^{+0.043}_{-0.036}(0.054)$	39.8	-0.25(0.15)	2.0	$0.090^{+0.017}_{-0.014}(0.020)$	39.8	-0.25(0.15)	7.0	$0.183^{+0.034}_{-0.029}(0.040)$	39.8	-0.25(0.15)	4.0
3.1–3.4	Ia	$0.248^{+0.040}_{-0.035}(0.043)$	50.2	-0.25(0.15)	2.0	$0.079^{+0.013}_{-0.011}(0.013)$	50.2	-0.25(0.15)	7.0	$0.144^{+0.023}_{-0.020}(0.023)$	50.2	-0.25(0.15)	4.0
3.4–3.7	Ia	$0.260^{+0.041}_{-0.035}(0.047)$	53.6	-0.25(0.15)	2.0	$0.067^{+0.010}_{-0.009}(0.013)$	53.6	-0.25(0.15)	7.0	$0.110^{+0.017}_{-0.015}(0.022)$	53.6	-0.25(0.15)	4.0
3.7–4.0	Ia	$0.250^{+0.043}_{-0.037}(0.052)$	46.0	-0.25(0.15)	2.0	$0.053^{+0.009}_{-0.008}(0.013)$	46.0	-0.25(0.15)	7.0	$0.078^{+0.013}_{-0.011}(0.020)$	46.0	-0.25(0.15)	4.0
>4.0	Ia	$0.305^{+0.054}_{-0.046}(0.056)$	43.0	-0.25(0.15)	2.0	$0.048^{+0.009}_{-0.007}(0.012)$	43.0	-0.25(0.15)	7.0	$0.060^{+0.011}_{-0.009}(0.019)$	43.0	-0.25(0.15)	4.0
<2.3	Ibc	$0.119^{+0.057}_{-0.040}(0.019)$	8.2	-0.38(0.10)	2.0	$0.083^{+0.040}_{-0.028}(0.019)$	8.2	-0.38(0.10)	7.0	$0.228^{+0.110}_{-0.078}(0.064)$	8.2	-0.38(0.10)	4.0
2.3–2.8	Ibc	$0.279^{+0.069}_{-0.056}(0.081)$	24.1	-0.38(0.10)	2.0	$0.127^{+0.032}_{-0.026}(0.037)$	24.1	-0.38(0.10)	7.0	$0.282^{+0.070}_{-0.057}(0.086)$	24.1	-0.38(0.10)	4.0
2.8–3.1	Ibc	$0.329^{+0.074}_{-0.062}(0.091)$	28.3	-0.38(0.10)	2.0	$0.122^{+0.027}_{-0.023}(0.033)$	28.3	-0.38(0.10)	7.0	$0.241^{+0.054}_{-0.045}(0.066)$	28.3	-0.38(0.10)	4.0
3.1–3.4	Ibc	$0.271^{+0.065}_{-0.053}(0.063)$	25.5	-0.38(0.10)	2.0	$0.085^{+0.020}_{-0.017}(0.020)$	25.5	-0.38(0.10)	7.0	$0.154^{+0.037}_{-0.030}(0.035)$	25.5	-0.38(0.10)	4.0
3.4–3.7	Ibc	$0.173^{+0.045}_{-0.042}(0.062)$	16.3	-0.38(0.10)	2.0	$0.045^{+0.014}_{-0.011}(0.016)$	16.3	-0.38(0.10)	7.0	$0.075^{+0.024}_{-0.019}(0.027)$	16.3	-0.38(0.10)	4.0
3.7–4.0	Ibc	$0.091^{+0.045}_{-0.032}(0.030)$	8.0	-0.38(0.10)	2.0	$0.020^{+0.010}_{-0.007}(0.007)$	8.0	-0.38(0.10)	7.0	$0.031^{+0.015}_{-0.011}(0.011)$	8.0	-0.38(0.10)	4.0
>4.0	Ibc	$0.050^{+0.048}_{-0.027}(0.021)$	3.0	-0.38(0.10)	2.0	$0.009^{+0.009}_{-0.005}(0.004)$	3.0	-0.38(0.10)	7.0	$0.012^{+0.011}_{-0.006}(0.005)$	3.0	-0.38(0.10)	4.0
<2.3	II	$0.497^{+0.094}_{-0.080}(+0.377)$	38.1	-0.38(0.10)	2.0	$0.346^{+0.066}_{-0.056}(+0.268)$	38.1	-0.38(0.10)	7.0	$0.945^{+0.179}_{-0.152}(+0.702)$	38.1	-0.38(0.10)	4.0
2.3–2.8	II	$0.490^{+0.077}_{-0.067}(+0.388)$	52.3	-0.38(0.10)	2.0	$0.223^{+0.035}_{-0.031}(+0.177)$	52.3	-0.38(0.10)	7.0	$0.493^{+0.078}_{-0.068}(+0.370)$	52.3	-0.38(0.10)	4.0
2.8–3.1	II	$0.550^{+0.077}_{-0.068}(+0.419)$	64.8	-0.38(0.10)	2.0	$0.203^{+0.028}_{-0.025}(+0.154)$	64.8	-0.38(0.10)	7.0	$0.403^{+0.056}_{-0.050}(+0.287)$	64.8	-0.38(0.10)	4.0
3.1–3.4	II	$0.455^{+0.064}_{-0.056}(+0.217)$	65.3	-0.38(0.10)	2.0	$0.142^{+0.020}_{-0.018}(+0.037)$	65.3	-0.38(0.10)	7.0	$0.257^{+0.036}_{-0.032}(+0.105)$	65.3	-0.38(0.10)	4.0
3.4–3.7	II	$0.301^{+0.051}_{-0.044}(+0.144)$	47.1	-0.38(0.10)	2.0	$0.079^{+0.013}_{-0.012}(+0.035)$	47.1	-0.38(0.10)	7.0	$0.131^{+0.022}_{-0.019}(+0.055)$	47.1	-0.38(0.10)	4.0
3.7–4.0	II	$0.157^{+0.039}_{-0.032}(+0.073)$	24.0	-0.38(0.10)	2.0	$0.035^{+0.009}_{-0.007}(+0.015)$	24.0	-0.38(0.10)	7.0	$0.053^{+0.013}_{-0.011}(+0.022)$	24.0	-0.38(0.10)	4.0
>4.0	II	$0.104^{+0.040}_{-0.030}(+0.050)$	12.0	-0.38(0.10)	2.0	$0.018^{+0.007}_{-0.005}(+0.008)$	12.0	-0.38(0.10)	7.0	$0.024^{+0.009}_{-0.007}(-0.008)$	12.0	-0.38(0.10)	4.0

^aUncertainties are ordered as statistical and systematic (in parentheses).

^bThe rate for the fiducial galaxy size. For any given galaxy size, use Eqs. (1)–(3), reproduced here, to calculate the rates: $\text{SNuB}(L_B) = \text{SNuB}(L_{B0})(L_B/L_{B0})^{\text{RSS}_B}$, $\text{SNuK}(L_K) = \text{SNuK}(L_{K0})(L_K/L_{K0})^{\text{RSS}_K}$, and $\text{SNuM}(M) = \text{SNuM}(M_0)(M/M_0)^{\text{RSS}_M}$.

^cThe number of SNe used in the rate calculation.

^dFor L_{B0} and L_{K0} , the units are 10^{10} L_\odot ; for M_0 , the units are 10^{10} M_\odot .

APPENDIX A:

APPENDIX B:

Table B2. SN rates in galaxies of different Hubble type.^a

Hub.	SN	SNuB[$(B - K)_0$] ^b	N_B^c	RCS _B	$(B - K)_0$	SNuK[$(B - K)_0$] ^b	N_K^c	RCS _K	$(B - K)_0$	SNuM[$(B - K)_0$] ^b	N_M^c	RCS _M	$(B - K)_0$
E	Ia	$0.196^{+0.041}_{-0.034}(0.033)$	33.0	0.73(0.36)	3.0	$0.062^{+0.013}_{-0.010}(0.019)$	33.0	-1.46(0.36)	3.0	$0.122^{+0.025}_{-0.021}(0.060)$	33.0	-2.96(0.36)	3.0
S0	Ia	$0.209^{+0.032}_{-0.028}(0.039)$	54.0	0.73(0.36)	3.0	$0.065^{+0.010}_{-0.009}(0.025)$	54.0	-1.46(0.36)	3.0	$0.127^{+0.020}_{-0.017}(0.070)$	54.0	-2.96(0.36)	3.0
Sab	Ia	$0.216^{+0.038}_{-0.033}(0.035)$	43.3	0.73(0.36)	3.0	$0.077^{+0.014}_{-0.012}(0.025)$	43.3	-1.46(0.36)	3.0	$0.157^{+0.028}_{-0.024}(0.079)$	43.3	-2.96(0.36)	3.0
Sb	Ia	$0.175^{+0.029}_{-0.027}(0.049)$	49.2	0.73(0.36)	3.0	$0.066^{+0.011}_{-0.009}(0.014)$	49.2	-1.46(0.36)	3.0	$0.136^{+0.022}_{-0.019}(0.052)$	49.2	-2.96(0.36)	3.0
Sbc	Ia	$0.163^{+0.033}_{-0.027}(0.040)$	34.6	0.73(0.36)	3.0	$0.064^{+0.013}_{-0.011}(0.015)$	34.6	-1.46(0.36)	3.0	$0.131^{+0.026}_{-0.022}(0.053)$	34.6	-2.96(0.36)	3.0
Sc	Ia	$0.185^{+0.039}_{-0.033}(0.039)$	32.0	0.73(0.36)	3.0	$0.074^{+0.015}_{-0.013}(0.019)$	32.0	-1.46(0.36)	3.0	$0.148^{+0.031}_{-0.026}(0.066)$	32.0	-2.96(0.36)	3.0
Scd	Ia	$0.190^{+0.050}_{-0.040}(0.065)$	22.0	0.73(0.36)	3.0	$0.073^{+0.019}_{-0.015}(0.016)$	22.0	-1.46(0.36)	3.0	$0.121^{+0.032}_{-0.026}(0.045)$	22.0	-2.96(0.36)	3.0
Irr	Ia	$0.000^{+0.143}_{-0.000}(-)$	0.0	0.73(0.36)	3.0	$0.000^{+0.051}_{-0.000}(-)$	0.0	-1.46(0.36)	3.0	$0.000^{+0.090}_{-0.000}(-)$	0.0	-2.96(0.36)	3.0
E	Ibc	$0.014^{+0.032}_{-0.012}(0.007)$	1.0	0.38(0.28)	3.0	$0.004^{+0.009}_{-0.003}(0.002)$	1.0	-1.55(0.26)	3.0	$0.008^{+0.018}_{-0.006}(0.004)$	1.0	-2.77(0.28)	3.0
S0	Ibc	$0.034^{+0.027}_{-0.016}(0.009)$	4.0	0.38(0.28)	3.0	$0.010^{+0.008}_{-0.005}(0.004)$	4.0	-1.55(0.26)	3.0	$0.018^{+0.014}_{-0.009}(0.010)$	4.0	-2.77(0.28)	3.0
Sab	Ibc	$0.216^{+0.063}_{-0.050}(0.062)$	18.5	0.38(0.28)	3.0	$0.074^{+0.022}_{-0.017}(0.036)$	18.5	-1.55(0.26)	3.0	$0.145^{+0.042}_{-0.033}(0.088)$	18.5	-2.77(0.28)	3.0
Sb	Ibc	$0.207^{+0.057}_{-0.045}(0.062)$	20.5	0.38(0.28)	3.0	$0.078^{+0.021}_{-0.017}(0.036)$	20.5	-1.55(0.26)	3.0	$0.156^{+0.043}_{-0.034}(0.091)$	20.5	-2.77(0.28)	3.0
Sbc	Ibc	$0.244^{+0.065}_{-0.052}(0.073)$	21.3	0.38(0.28)	3.0	$0.097^{+0.026}_{-0.021}(0.040)$	21.3	-1.55(0.26)	3.0	$0.199^{+0.053}_{-0.043}(0.107)$	21.3	-2.77(0.28)	3.0
Sc	Ibc	$0.257^{+0.056}_{-0.047}(0.084)$	30.0	0.38(0.28)	3.0	$0.105^{+0.023}_{-0.019}(0.021)$	30.0	-1.55(0.26)	3.0	$0.214^{+0.047}_{-0.039}(0.067)$	30.0	-2.77(0.28)	3.0
Scd	Ibc	$0.191^{+0.059}_{-0.046}(0.049)$	16.7	0.38(0.28)	3.0	$0.076^{+0.024}_{-0.019}(0.017)$	16.7	-1.55(0.26)	3.0	$0.141^{+0.044}_{-0.034}(0.051)$	16.7	-2.77(0.28)	3.0
Irr	Ibc	$0.204^{+0.268}_{-0.131}(0.115)$	2.0	0.38(0.28)	3.0	$0.074^{+0.024}_{-0.048}(0.024)$	2.0	-1.55(0.26)	3.0	$0.136^{+0.179}_{-0.088}(0.046)$	2.0	-2.77(0.28)	3.0
E	II	$0.000^{+0.014}_{-0.000}(-)$	0.0	0.38(0.28)	3.0	$0.000^{+0.004}_{-0.000}(-)$	0.0	-1.55(0.26)	3.0	$0.000^{+0.007}_{-0.000}(-)$	0.0	-2.77(0.28)	3.0
S0	II	$0.018^{+0.014}_{-0.009}(0.006)$	4.0	0.38(0.28)	3.0	$0.005^{+0.004}_{-0.003}(0.002)$	4.0	-1.55(0.26)	3.0	$0.010^{+0.008}_{-0.005}(0.005)$	4.0	-2.77(0.28)	3.0
Sab	II	$0.250^{+0.043}_{-0.039}(0.106)$	41.2	0.38(0.28)	3.0	$0.086^{+0.016}_{-0.013}(0.019)$	41.2	-1.55(0.26)	3.0	$0.168^{+0.030}_{-0.026}(0.047)$	41.2	-2.77(0.28)	3.0
Sb	II	$0.266^{+0.042}_{-0.036}(0.119)$	53.3	0.38(0.28)	3.0	$0.100^{+0.016}_{-0.014}(0.023)$	53.3	-1.55(0.26)	3.0	$0.200^{+0.031}_{-0.027}(0.056)$	53.3	-2.77(0.28)	3.0
Sbc	II	$0.479^{+0.066}_{-0.054}(0.150)$	79.1	0.38(0.28)	3.0	$0.190^{+0.024}_{-0.021}(0.059)$	79.1	-1.55(0.26)	3.0	$0.388^{+0.049}_{-0.043}(0.165)$	79.1	-2.77(0.28)	3.0
Sc	II	$0.675^{+0.092}_{-0.082}(+0.399)$	68.0	0.38(0.28)	3.0	$0.275^{+0.038}_{-0.033}(+0.147)$	68.0	-1.55(0.26)	3.0	$0.563^{+0.077}_{-0.068}(+0.338)$	68.0	-2.77(0.28)	3.0
Sed	II	$0.728^{+0.111}_{-0.097}(+0.434)$	56.3	0.38(0.28)	3.0	$0.293^{+0.044}_{-0.039}(+0.156)$	56.3	-1.55(0.26)	3.0	$0.538^{+0.082}_{-0.072}(+0.321)$	56.3	-2.77(0.28)	3.0
Irr	II	$0.448^{+0.354}_{-0.214}(0.092)$	4.0	0.38(0.28)	3.0	$0.165^{+0.130}_{-0.079}(0.066)$	4.0	-1.55(0.26)	3.0	$0.301^{+0.237}_{-0.144}(0.162)$	4.0	-2.77(0.28)	3.0

^aUncertainties are ordered as statistical and systematic (in parentheses).

^bThe rates for the fiducial galaxy $B - K$ colour. For any given galaxy colour, use Eqs. (B5)–(B7) in the Appendix to calculate the rates.

^cNumber of SNe used in the rate calculations.